UNIVERSITY OF TWENTE.

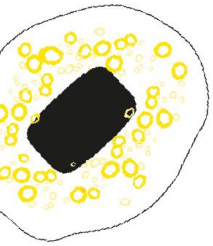

Extending the Applicability of the Floating Frame Formulation in Global Coordinates

The Generalised Superelement Formulation and the Nonlinear Floating Frame Formulation

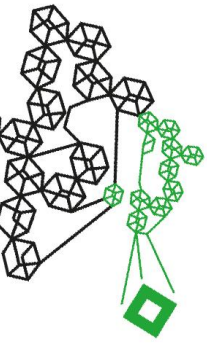

Name: M.L. Wevers
University: University of Twente
Degree programme: Mechanical Engineering
Chair: Applied Mechanics and Data Analysis

Date: 24 April 2024

Summary

The superelement floating frame formulation models the motion of a flexible body by making a distinction between its overall rigid-body motion and its local deformations and expresses its equations of motion in terms of the global nodal degrees of freedom of its interface points. Limitations of this formulation are that it requires the linear finite element model describing the local flexible behaviour to be reduced using a reduction basis that only contains boundary modes and it can only be applied to problems in which the local deformations remain small. Two generalisations are therefore proposed: the generalised superelement formulation and the nonlinear floating frame formulation.

The generalised superelement formulation allows for the use of an arbitrary reduction basis that is able to (1) describe rigid-body motion and (2) describe the local nodal degrees of freedom of the interface points independently. It expresses the governing equations in terms of the global nodal degrees of freedom of the interface points as well as a set of internal flexible coordinates.

The nonlinear floating frame formulation makes a distinction between the overall rigid-body motion and local deformations of a body or its individual elements and models the local flexible behaviour using a geometrically nonlinear model to allow for arbitrarily large local deformations. It expresses the governing equations in terms of all global nodal degrees of freedom and can be considered an alternative to the total and updated Lagrangian nonlinear finite element formulations.

The reduction bases obtained with the most commonly used component mode synthesis methods that can be used in the generalised superelement formulation are presented. The equations of motion of a single flexible body and the coupling method to obtain the constrained equations of motion of a flexible multibody system are formulated for the generalised superelement formulation. The global internal load vector and tangent stiffness matrix that can be used in incremental solution procedures are formulated for the nonlinear floating frame formulation using continuum elements. Both methods are implemented and validated using a benchmark problem. The superelement floating frame formulation and the co-rotational nonlinear finite element formulation are illustrated as simplifications of the nonlinear floating frame formulation.

The validation results indicate the successful implementation of the generalised superelement formulation and the nonlinear floating frame formulation. Recommendations for further research and further extensions of both methods are provided.

Nomenclature

A	total transformation matrix in the generalised superelement formulation
$\mathbf{B}_a$	a^{th} linear strain discretisation matrix
$\boldsymbol{c}_R$	arbitrary constants
$C\left(\boldsymbol{q}_{FF}\right)$	traditional floating frame constraint functions
$C_{\boldsymbol{q}}$	Jacobian of the traditional floating frame constraint functions
C_{FF}^{j}	traditional floating frame local matrix of fictitious forces of a single flexible body
C_{FF}	traditional floating frame system matrix of fictitious forces
C_{GS}^{o}	generalised superelement global matrix of fictitious forces of a single flexible body
C_{GS}	generalised superelement system matrix of fictitious forces
d	normalised midpoint deflection
D_a	a^{th} quadratic strain discretisation matrix
E	elasticity matrix
E_{ab}	$(a,b)^{\text{th}}$ component of the elasticity matrix
$\boldsymbol{f}$	linear finite element nodal external load vector
$\boldsymbol{f}_{FE}^{j}$	linear finite element nodal external load vector
$\overline{\boldsymbol{f}}$	reduced linear finite element nodal external load vector
$\boldsymbol{f}_b$	boundary partition of the linear finite element nodal external load vector
$\boldsymbol{f}_i$	internal partition of the linear finite element nodal external load vector
$\boldsymbol{f}_{FF}^{j}$	traditional floating frame local external load vector of a single flexible body
$\boldsymbol{f}_{FF}$	traditional floating frame system external load vector
$\boldsymbol{f}_{FF,c}$	traditional floating frame system external load vector of constraint loads
$\boldsymbol{f}_{FF,e}$	traditional floating frame system external load vector of externally applied loads
$\boldsymbol{f}_{GS}^{j}$	generalised superelement local external load vector of a single flexible body
$\boldsymbol{f}_{GS}$	generalised superelement system external load vector
$\boldsymbol{f}_{GS,c}$	generalised superelement system external load vector of constraint loads
$\boldsymbol{f}_{GS,e}$	generalised superelement system external load vector of externally applied loads
$\widehat{\boldsymbol{F}}_i^j$	projected internal loads on node i
$\widehat{\mathrm{F}}^j$	projected internal load matrix

G	inertia-relief flexibility matrix
G_b	boundary columns of the inertia-relief flexibility matrix
G_{bb}	boundary partition of the boundary columns of the inertia-relief flexibility matrix
G_{ib}	internal partition of the boundary columns of the inertia-relief flexibility matrix
G^{r}	residual-flexibility matrix
$\mathrm{G}^{\mathrm{r}}_b$	boundary columns of the residual-flexibility matrix
$\mathrm{G}^{\mathrm{r}}_{bb}$	boundary partition of the boundary columns of the residual-flexibility matrix
$\mathrm{G}^{\mathrm{r}}_{ib}$	internal partition of the boundary columns of the residual-flexibility matrix
G_c	constrained flexibility matrix
H	generalised superelement constraint localisation matrix
H_i	internal partition of the inertia-relief modes
K	linear finite element stiffness matrix
K^j_{FE}	linear finite element stiffness matrix
$\overline{\mathrm{K}}$	reduced linear finite element stiffness matrix
K_{bb}	boundary-boundary partition of the linear finite element stiffness matrix
K_{bi}	boundary-internal partition of the linear finite element stiffness matrix
K_{ib}	internal-boundary partition of the linear finite element stiffness matrix
K_{ii}	internal-internal partition of the linear finite element stiffness matrix
K^j_{FF}	traditional floating frame local stiffness matrix of a single flexible body
K_{FF}	traditional floating frame system stiffness matrix
K^j_{GS}	generalised superelement local stiffness matrix of a single flexible body
K_{GS}	generalised superelement system stiffness matrix
K_t	tangent stiffness matrix
K^j_t	local tangent stiffness matrix
K^o_t	global tangent stiffness matrix
K_I	constant tangent stiffness matrix term
K_{II}	linear tangent stiffness matrix term
K_{III}	linear tangent stiffness matrix term
K_{IV}	quadratic tangent stiffness matrix term
K_V	linear and quadratic tangent stiffness matrix term
K^j_1	projected local tangent stiffness matrix term
K^j_2	projected local tangent stiffness matrix term
K^j_3	projected local tangent stiffness matrix term

$\mathbf{L}$	Green-Lagrange strain tensor
L_{pq}	$(p,q)^{\text{th}}$ component of the Green-Lagrange strain tensor
$\boldsymbol{L}$	Green-Lagrange strain vector
L_a	a^{th} component of the Green-Lagrange strain vector
M	linear finite element mass matrix
M_{FE}^{j}	linear finite element mass matrix
$\overline{\mathrm{M}}$	reduced linear finite element mass matrix
$\overline{\mathrm{M}}_{RR}$	modal mass matrix corresponding to the rigid-body modes
M_{bb}	boundary-boundary partition of the linear finite element mass matrix
M_{bi}	boundary-internal partition of the linear finite element mass matrix
M_{ib}	internal-boundary partition of the linear finite element mass matrix
M_{ii}	internal-internal partition of the linear finite element mass matrix
M_{FF}^{j}	traditional floating frame local mass matrix of a single flexible body
M_{FF}	traditional floating frame system mass matrix
M_{GS}^{j}	generalised superelement local mass matrix of a single flexible body
M_{GS}	generalised superelement system mass matrix
n	number of interface points
N	number of nodes
N_i	interpolation function corresponding to node i
N_i^{FF}	interpolation function corresponding to node i evaluated at the floating frame
N	interpolation matrix
$\mathbf{N}_{p,q}$	p^{th} row of the interpolation matrix differentiated with respect to the q^{th} material coordinate
$\boldsymbol{p}$	generalised superelement independent generalised coordinates
P	inertia-relief projection matrix
$\boldsymbol{q}$	nodal degrees of freedom
$\boldsymbol{q}_b$	boundary partition of the nodal degrees of freedom
$\boldsymbol{q}_r$	rigid-body boundary partition of the nodal degrees of freedom
$\boldsymbol{q}_e$	excess boundary partition of the nodal degrees of freedom
$\boldsymbol{q}_i$	internal partition of the nodal degrees of freedom

$\boldsymbol{q}_j^{o,o}$	global coordinates of the floating frame
$\boldsymbol{q}^{j,j}$	local nodal degrees of freedom
$\boldsymbol{q}_{IP}^{j,j}$	local nodal degrees of freedom of the interface points
$\boldsymbol{q}^{o,o}$	global nodal degrees of freedom
$\boldsymbol{q}_{IP}^{o,o}$	global nodal degrees of freedom of the interface points
$\boldsymbol{q}_{FF}$	traditional floating frame system generalised coordinate vector
$\boldsymbol{q}_{GS}^{j}$	generalised superelement local system generalised coordinate vector
$\boldsymbol{q}_{GS}^{o}$	generalised superelement global system generalised coordinate vector
$\boldsymbol{Q}$	internal load vector
$\boldsymbol{Q}^{j}$	local internal load vector
$\boldsymbol{Q}^{o}$	global internal load vector
$\boldsymbol{Q}_{I}$	linear internal load vector term
$\boldsymbol{Q}_{II}$	quadratic internal load vector term
$\boldsymbol{Q}_{III}$	quadratic internal load vector term
$\boldsymbol{Q}_{IV}$	cubic internal load vector term
$\widehat{\boldsymbol{Q}}^{j}$	projected local internal load vector
$\boldsymbol{Q}_{ext}^{o}$	global external load vector
$\boldsymbol{r}_j^{o,o}$	global position of the floating frame
$\boldsymbol{r}_i^{j,j}$	local position of node i
$\boldsymbol{r}_i^{o,o}$	global position of node i
R_j^{o}	global orientation of the floating frame
R_i^{j}	local orientation of node i
R_i^{o}	global orientation of node i
$[\mathrm{R}_j^{o}]$	assembly of rotation matrices
$[\tilde{\mathrm{R}}_j^{o}]$	assembly of rotation matrices
$[\hat{\mathrm{R}}_j^{o}]$	assembly of rotation matrices
$[\bar{\mathrm{R}}_j^{o}]$	assembly of rotation matrices
$\mathbf{S}$	second Piola-Kirchhoff stress tensor
S_{pq}	$(p,q)^{\text{th}}$ component of the second Piola-Kirchhoff stress tensor

$\boldsymbol{S}$	second Piola-Kirchhoff stress vector
S_a	a^{th} component of the second Piola-Kirchhoff stress vector
T	local transformation matrix in the generalised superelement formulation
T_{int}	local transformation matrix in the generalised superelement formulation
$\mathcal{T}$	local transformation matrix in the nonlinear floating frame formulation
u	horizontal deflection
$\boldsymbol{u}$	displacement field
$\boldsymbol{u}^{j,j}$	local displacement field
$\boldsymbol{u}_{FF}^{j,j}$	local displacement field evaluated at the location of the floating frame
$\boldsymbol{u}^{o,o}$	global displacement field
$u_{p,q}$	p^{th} displacement field component differentiated with respect to the q^{th} material coordinate
$\boldsymbol{u}_i^{j,j}$	local displacement of node i
$\boldsymbol{u}_i^{o,o}$	global displacement of node i
v	vertical deflection
V	undeformed volume
δW_{int}	internal virtual work
$\boldsymbol{x}$	material coordinates
$\boldsymbol{X}_i^{j,j}$	local undeformed position of node i
$\boldsymbol{X}_i^{o,o}$	global undeformed position of node i
Z	local transformation matrix in the generalised superelement formulation
Z_{int}	local transformation matrix in the generalised superelement formulation
$\mathcal{Z}$	local transformation matrix in the nonlinear floating frame formulation
γ	traditional floating frame constraint acceleration vector
$\boldsymbol{\zeta}$	preliminary boundary flexible coordinates
$\boldsymbol{\eta}$	internal flexible coordinates

$\boldsymbol{\eta}_R$ modal coordinates corresponding to the rigid-body modes
$\boldsymbol{\eta}_N$ modal coordinates corresponding to the kept normal modes
$\boldsymbol{\eta}_N^{rel}$ relative modal coordinates corresponding to the kept normal modes
$\boldsymbol{\eta}_d$ modal coordinates corresponding to the discarded normal modes
$\boldsymbol{\eta}_C$ constraint mode coordinates

$\boldsymbol{\theta}_i^{j,j}$ local rotation of node i
$\delta\boldsymbol{\theta}_j^{j,o}$ virtual rotations of the floating frame relative to the global frame expressed locally
$\delta\boldsymbol{\theta}_j^{o,o}$ virtual rotations of the floating frame relative to the global frame expressed globally

$\boldsymbol{\lambda}$ Lagrange multipliers

μ_N modal mass matrix corresponding to the kept normal modes
μ_d modal mass matrix corresponding to the discarded normal modes

$\boldsymbol{\xi}$ flexible coordinates

Ξ_{FF} floating frame constraint matrix

Υ internal reduction basis
Υ_{FF} internal reduction basis evaluated at the location of the floating frame
$\widehat{\Upsilon}$ preliminary internal reduction basis
$\widehat{\Upsilon}_{IP}$ preliminary internal reduction basis evaluated at the interface points

Φ reduction basis

Φ_R rigid-body modes
Φ_{Rb} boundary partition of the rigid-body modes
Φ_{Rr} rigid-body boundary partition of the rigid-body modes
Φ_{Re} excess boundary partition of the rigid-body modes
Φ_{Ri} internal partition of the rigid-body modes

Φ_r interface rigid-body modes

Φ_N kept normal modes
Φ_{Nb} boundary partition of the kept normal modes
Φ_{Ni} internal partition of the kept normal modes

Φ_d discarded normal modes

Φ_{Ci}	internal partition of the interface constraint modes
Φ_{Cie}	internal partition of the excess interface constraint modes
Φ_{Cir}	internal partition of the rigid-body interface constraint modes
Ψ	boundary reduction basis
Ψ_{FF}	boundary reduction basis evaluated at the location of the floating frame
$\widehat{\Psi}$	preliminary boundary reduction basis
$\widehat{\Psi}_{IP}$	preliminary boundary reduction basis evaluated at the interface points
ω	excitation frequency
Ω_N	modal frequency matrix corresponding to the kept normal modes
Ω_d	modal frequency matrix corresponding to the discarded normal modes
$\Delta(\cdot)$	increment
$\delta(\cdot)$	variation
$\dot{(\cdot)}$	first time-derivative
$\ddot{(\cdot)}$	second time-derivative
$\widetilde{(\cdot)}$	skew-symmetric matrix representation of vector

Contents

1 Introduction

In flexible multibody dynamics it is common to model the motion of a flexible body using the floating frame formulation. This formulation makes a distinction between the overall rigid-body motion of a body and its local deformations. The overall rigid-body motion can become arbitrarily large and is described by the global position and orientation of a floating frame of reference that moves along with the body. The local deformations are assumed to be small and the local flexible behaviour is therefore modelled using a linear finite element model that describes the local deformations by the local nodal degrees of freedom expressed relative to the floating frame. The linear finite element model may be reduced using a suitable reduction basis that relates the local nodal degrees of freedom to a set of local flexible coordinates through its modal expansion.

The most commonly used form of the floating frame formulation, referred to as the traditional floating frame formulation, expresses the equations of motion of a single flexible body in terms of the global coordinates of its floating frame and its set of local flexible coordinates [1]. This choice of generalised coordinates requires a dual coupling method to obtain the constrained equations of motion of a flexible multibody system [2]. The resulting differential-algebraic system of equations is then expressed in terms of all generalised coordinates and all constraint loads.

A more novel form of the floating frame formulation, referred to as the superelement formulation, expresses the equations of motion of a single flexible body in terms of the global nodal degrees of freedom of its interface points [1]. This choice of generalised coordinates allows for a primal coupling method to obtain the constrained equations of motion of a flexible multibody system [2]. The resulting differential system of equations is expressed only in terms of a set of independent generalised coordinates. Although the system matrices obtained with a primal coupling method are generally more dense than those obtained with a dual coupling method [3], the reduction in the number of generalised coordinates in terms of which the coupled equations of motion of a flexible multibody system are expressed could potentially make the superelement formulation more computationally efficient than the traditional floating frame formulation.

A limitation of the current state-of-the-art superelement formulation is that it requires the linear finite element model describing the local flexible behaviour to be reduced using a reduction basis that only contains boundary modes with the local nodal degrees of freedom of the interface points as the corresponding local flexible coordinates. This criterion is only fulfilled by the reduction basis obtained with Guyan's method [4]. The number of degrees of freedom in terms of which the equations of motion of a single flexible body are expressed is consequently limited by its number of interface points. The first objective of this text is therefore to generalise the superelement formulation to allow for the inclusion of internal modes. This generalisation is referred to as the generalised superelement formulation.

The generalised superelement formulation allows the linear finite element model describing the local flexible behaviour to be reduced using an arbitrary reduction basis that is able to (1) describe rigid-body motion and (2) describe the local nodal degrees of freedom of the interface points independently. These criteria are fulfilled by the reduction bases obtained with the most commonly used component mode synthesis methods: Guyan's method [4], Craig-Bampton's method [5], Hurty's method [6], Herting's method [7], Hintz's constraint mode method [8], Hintz's attachment mode method [8], Craig-Chang's method [9] and Rubin-Martinez's method [10], [11]. The generalised superelement formulation expresses the equations of motion of a single flexible body in terms of the global nodal degrees of freedom of its interface points as well as a set of internal flexible coordinates.

This choice of generalised coordinates does allow for a primal coupling method, while the inclusion of the internal flexible coordinates is expected to allow for a more accurate representation of the local flexible behaviour.

Another limitation of the current state-of-the-art superelement formulation is that its applicability is limited to problems in which the local deformations remain small. This limitation also applies to the co-rotational formulation of the nonlinear finite element method [12]–[18]. In this formulation, the motion of a flexible body is modelled by making a distinction between the overall rigid-body motion and local deformations of its individual elements. The equations of motion (or equilibrium) are expressed in terms of all global nodal degrees of freedom. Both the superelement formulation and the co-rotational formulation thus make a distinction between overall rigid-body motion and local deformations and express the governing equations in terms of global nodal degrees of freedom, while the applicability of both methods is limited to problems in which the local deformations remain small. The second objective of this text is therefore to present a unified framework for both methods and generalise this to allow for arbitrarily large local deformations. This nonlinear generalisation is referred to as the nonlinear floating frame formulation.

The nonlinear floating frame formulation makes a distinction between the overall rigid-body motion of a body or element and its local deformations and models the local flexible behaviour using a geometrically nonlinear model to allow for arbitrarily large local deformations. As a nonlinear model is used locally, classical reduction methods cannot be used and therefore no distinction is made between the interior nodes and the interface points. The governing equations are expressed in terms of all global nodal degrees of freedom. As the method allows for arbitrarily large local deformations, a distinction must be made between the deformed and undeformed volume and thus either a total or updated Lagrangian formulation must be adopted locally [19], [20]. The nonlinear floating frame formulation in this text adopts the total Lagrangian formulation in which the stress and strain measures are expressed in terms of the undeformed reference configuration and the integration is performed over the undeformed volume. The nonlinear floating frame formulation can be considered an alternative to the total and updated Lagrangian formulations of the nonlinear finite element method that also express the governing equations in terms of all global nodal degrees of freedom, but do not make a distinction between overall rigid-body motion and local deformations [19], [20].

The reduction bases obtained with the most commonly used component mode synthesis methods found in literature are presented in Chapter 2. Each of these reduction bases can be used in the generalised superelement formulation to reduce the linear finite element model describing the local flexible behaviour.

The generalised superelement formulation is formulated in Chapter 3. The focus is on the dynamic analysis of flexible multibody systems. The equations of motion of a single flexible body and the coupling method to obtain the constrained equations of motion of a flexible multibody system are formulated. Elements that have both translational and rotational degrees of freedom are considered.

The nonlinear floating frame formulation is formulated in Chapter 4. The focus is on obtaining the global internal load vector and tangent stiffness matrix that can be used in incremental solution procedures. As a further novelty, continuum elements that only have translational degrees of freedom are considered, as opposed to the superelement formulation and most forms of the co-rotational formulation in which elements with both translational and rotational degrees of freedom are considered [13], [14], [16].

Chapter 5 presents the numerical results of the implementation of both methods. The implementation of the generalised superelement formulation in a generic Python program is described and the validation of this implementation using a benchmark problem is presented. Also the implementation of the nonlinear floating frame formulation in an incremental solution procedure for static problems and its validation using a benchmark problem are described. The superelement formulation and corotational formulation are illustrated as simplified cases of the nonlinear floating frame formulation.

The conclusions are presented in Chapter 6. Recommendations for further research are provided in Chapter 7.

Appendix H presents a generic Python programme that was developed as a side project to pursue a personal interest in the development of (educational) simulations and to learn programming a Graphical User Interface in Python. It implements the traditional floating frame formulation to model the dynamic behaviour of an arbitrary user-defined two-dimensional rigid multibody system.

2 Component mode synthesis

The generalised superelement formulation generalises the original superelement formulation by allowing for the use of a wider range of reduction bases. These reduction bases are obtained from a dynamic substructuring technique referred to as component mode synthesis. This technique is generally applied for the dynamic analysis of large structural systems of which the motion can be described using a linear finite element model [2], [21]–[24]. It models the motion of such a structure by dividing it into distinct components, modelling the individual components separately, reducing the order of the individual component models and then coupling the reduced component models to obtain a reduced model of the full system. This Chapter presents the reduction bases with which the individual component models are reduced in the most commonly used component mode synthesis methods.

Consider a single flexible component or body that is subjected to small deformations and does not undergo rigid-body motion. The equations of motion governing its dynamic behaviour are then obtained from a linear finite element model as:

$$\mathrm{M}\ddot{\boldsymbol{q}} + \mathrm{K}\boldsymbol{q} = \boldsymbol{f}, \tag{1}$$

with M and K the linear finite element mass and stiffness matrix and $\boldsymbol{f}$ the nodal external load vector. These equations of motion are expressed in terms of all physical coordinates in the vector of nodal degrees of freedom $\boldsymbol{q}$. To reduce the order of the model, the generally large number of physical coordinates can be expressed in terms of a reduced set of flexible coordinates $\boldsymbol{\xi}$ as:

$$\boldsymbol{q} = \Phi\boldsymbol{\xi}, \tag{2}$$

in which the reduction basis Φ can contain any type of assumed mode shapes. With this modal expansion, the reduced equations of motion can be formulated as:

$$\overline{\mathrm{M}}\ddot{\boldsymbol{\xi}} + \overline{\mathrm{K}}\boldsymbol{\xi} = \overline{\boldsymbol{f}}, \tag{3}$$

with:

$$\begin{aligned} \overline{\mathrm{M}} &= \Phi^{\mathrm{T}}\mathrm{M}\Phi \\ \overline{\mathrm{K}} &= \Phi^{\mathrm{T}}\mathrm{K}\Phi \\ \overline{\boldsymbol{f}} &= \Phi^{\mathrm{T}}\boldsymbol{f} \end{aligned} \tag{4}$$

the reduced mass and stiffness matrix and modal external load vector.

One of the objectives of component mode synthesis is to formulate the smallest set of reduced equations of motion that still accurately describes the dynamic behaviour of the component. The different component mode synthesis methods are characterised by their definition of the reduction basis with which the equations of motion are reduced. They thus differ in the types of assumed modes included in the reduction basis and the corresponding flexible coordinates included in the reduced set of coordinates. Some methods retain the physical boundary by including the degrees of freedom of the boundary nodes in the reduced set of coordinates. This simplifies the coupling method by which the reduced model of the full system is obtained [11].

All component mode synthesis methods that are considered here are based on the truncation of a normal mode set and the static approximation of the response of the discarded normal modes [7], [25]. This is outlined in Section 2.1. An overview of the component mode synthesis methods is

presented in Section 2.2. The reduction bases obtained with each of these methods are presented in Sections 2.3, 2.4 and 2.5. Special emphasis is put on whether or not the physical boundary is retained, since this is convenient in the implementation of the generalised superelement formulation.

2.1 Modal truncation and static approximation

The equations of motion governing the dynamic behaviour of a single flexible component can be solved in the modal domain by using the transformation to modal coordinates given by:

$$\boldsymbol{q} = \begin{bmatrix} \Phi_R & \Phi_N & \Phi_d \end{bmatrix} \begin{Bmatrix} \boldsymbol{\eta}_R \\ \boldsymbol{\eta}_N \\ \boldsymbol{\eta}_d \end{Bmatrix}, \tag{5}$$

in which Φ_R are the rigid-body modes, $[\Phi_N \;\; \Phi_d]$ are the normal modes (eigenmodes) and $\boldsymbol{\eta}_R$, $\boldsymbol{\eta}_N$ and $\boldsymbol{\eta}_d$ are the corresponding modal coordinates. A distinction is made between the normal modes Φ_N with natural frequencies within the relevant frequency range that will be kept and the normal modes Φ_d with natural frequencies that exceed the relevant frequency range that will be discarded. The normal modes can be free-, fixed- or mixed-interface normal modes which are obtained from the generalised eigenvalue problem describing the unconstrained, fully constrained or partially constrained body respectively. If the set of included rigid-body modes is consistent with the constraints imposed to obtain the normal modes, the equations of motion uncouple in the modal domain as:

$$\begin{aligned} \overline{\mathrm{M}}_{RR}\ddot{\boldsymbol{\eta}}_R &= \Phi_R^{\mathrm{T}}\boldsymbol{f} \\ \mu_N\ddot{\boldsymbol{\eta}}_N + \mu_N\Omega_N^2\boldsymbol{\eta}_N &= \Phi_N^{\mathrm{T}}\boldsymbol{f} \\ \mu_d\ddot{\boldsymbol{\eta}}_d + \mu_d\Omega_d^2\boldsymbol{\eta}_d &= \Phi_d^{\mathrm{T}}\boldsymbol{f}, \end{aligned} \tag{6}$$

in which $\overline{\mathrm{M}}_{RR} = \Phi_R^{\mathrm{T}}\mathrm{M}\Phi_R$ represents the modal mass matrix corresponding to the rigid-body modes, $\mu_N = \Phi_N^{\mathrm{T}}\mathrm{M}\Phi_N$ and $\mu_d = \Phi_d^{\mathrm{T}}\mathrm{M}\Phi_d$ represent the diagonal modal mass matrices corresponding to the kept and discarded normal modes respectively and $\mu_N\Omega_N^2 = \Phi_N^{\mathrm{T}}\mathrm{K}\Phi_N$ and $\mu_d\Omega_d^2 = \Phi_d^{\mathrm{T}}\mathrm{K}\Phi_d$ represent their modal stiffness matrices with Ω_N and Ω_d the corresponding modal frequency matrices. When the external loads are prescribed, the uncoupled equations of motion in the modal domain can be solved for each of the modal coordinates, after which the solution in the physical domain is obtained by back substitution in the modal transformation. A schematic representation of the amplitude diagrams of the frequency response transfer functions for several modes is presented in Figure 1.

It can be seen that in the relevant frequency range the dynamic response of the modes in Φ_d can be approximated by the static response [7], [10], which is given by:

$$\boldsymbol{\eta}_d \approx \left[\mu_d\Omega_d^2\right]^{-1}\Phi_d^{\mathrm{T}}\boldsymbol{f}. \tag{7}$$

With this approximation, the solution in the physical domain reduces to:

$$\begin{aligned} \boldsymbol{q} &\approx \Phi_R\boldsymbol{\eta}_R + \Phi_N\boldsymbol{\eta}_N + \Phi_d\left[\mu_d\Omega_d^2\right]^{-1}\Phi_d^{\mathrm{T}}\boldsymbol{f} \\ &= \Phi_R\boldsymbol{\eta}_R + \Phi_N\left(\boldsymbol{\eta}_N - \left[\mu_N\Omega_N^2\right]^{-1}\Phi_N^{\mathrm{T}}\boldsymbol{f}\right) + \left(\Phi_N\left[\mu_N\Omega_N^2\right]^{-1}\Phi_N^{\mathrm{T}} + \Phi_d\left[\mu_d\Omega_d^2\right]^{-1}\Phi_d^{\mathrm{T}}\right)\boldsymbol{f}, \end{aligned} \tag{8}$$

which eliminates the need to compute the dynamic response of the discarded modes. All reduction methods discussed in this text are based on either of the two forms of this approximate solution, in which

$$\boldsymbol{\eta}_N^{\mathrm{rel}} = \boldsymbol{\eta}_N - \left[\mu_N\Omega_N^2\right]^{-1}\Phi_N^{\mathrm{T}}\boldsymbol{f} \tag{9}$$

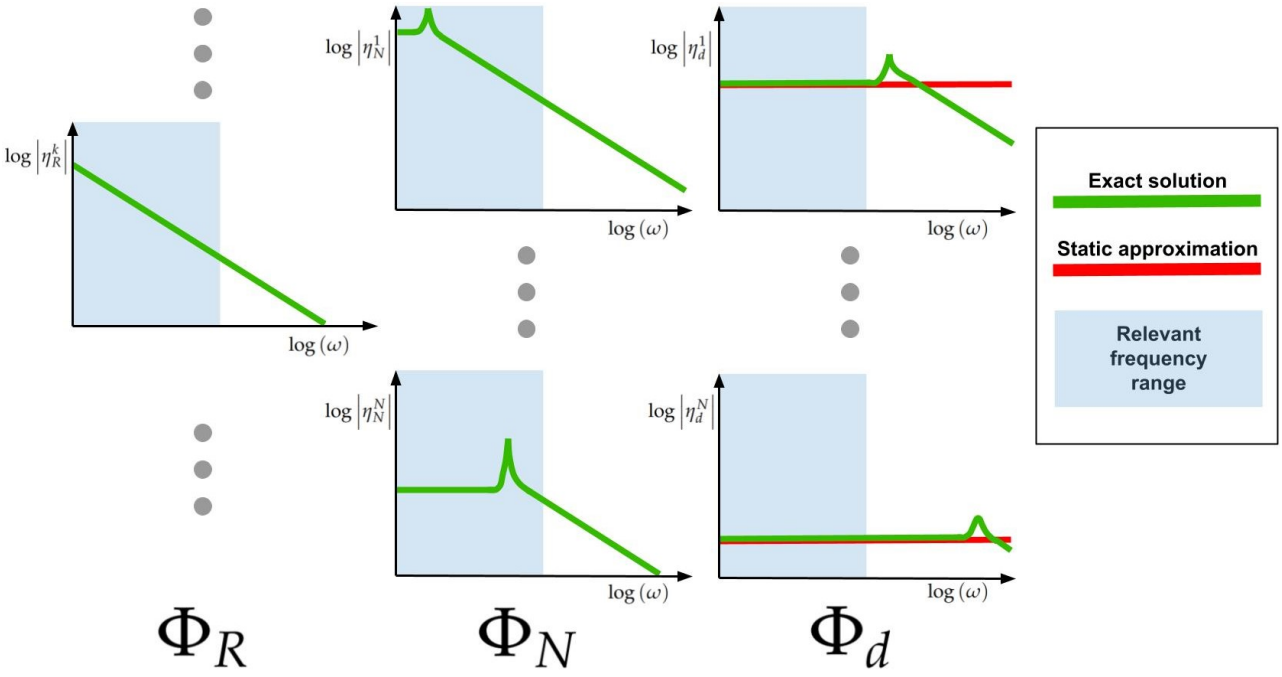

Figure 1: Amplitude diagrams of modal frequency response transfer functions – Schematic representation

are defined as the relative modal coordinates representing the dynamic response of the kept normal modes relative to their static response and

$$\begin{aligned} \mathrm{G} &= \Phi_N \left[\mu_N \Omega_N^2\right]^{-1} \Phi_N^{\mathrm{T}} + \Phi_d \left[\mu_d \Omega_d^2\right]^{-1} \Phi_d^{\mathrm{T}} \\ \mathrm{G}^{\mathrm{r}} &= \qquad\qquad\qquad\qquad \Phi_d \left[\mu_d \Omega_d^2\right]^{-1} \Phi_d^{\mathrm{T}} \end{aligned} \tag{10}$$

can be identified as the inertia-relief flexibility matrix and the residual-flexibility matrix respectively [21]. The inertia-relief flexibility matrix is a pseudo-inverse of the stiffness matrix obtained by eliminating the rigid-body freedom, hence the term *inertia-relief*. The residual-flexibility matrix additionally eliminates the contribution of the kept normal modes and only considers the contribution of the remaining discarded normal modes, hence the term *residual*.

Throughout this Chapter on component mode synthesis it will be assumed that the external loads are only applied to the boundary degrees of freedom, such that:

$$\boldsymbol{f} = \begin{Bmatrix} \boldsymbol{f}_b \\ \boldsymbol{f}_i \end{Bmatrix} = \begin{Bmatrix} \boldsymbol{f}_b \\ \boldsymbol{0} \end{Bmatrix}, \tag{11}$$

where, as throughout this Chapter, the subscripts b and i refer to the boundary and internal partitioning respectively. Then the approximate solution can be written in terms of the relative modal coordinates as:

$$\boxed{\boldsymbol{q} = \Phi_R \boldsymbol{\eta}_R + \Phi_N \boldsymbol{\eta}_N^{\mathrm{rel}} + \mathrm{G}_b \boldsymbol{f}_b} \tag{12}$$

or in terms of the absolute modal coordinates as:

$$\boxed{\boldsymbol{q} = \Phi_R \boldsymbol{\eta}_R + \Phi_N \boldsymbol{\eta}_N + \mathrm{G}_b^{\mathrm{r}} \boldsymbol{f}_b} \tag{13}$$

This solution is an approximation for the dynamic case, but it is exact for the static case (i.e. excitation by a time-invariant force), for which the equations of motion reduce to:

$$\mathrm{M}\Phi_R\ddot{\boldsymbol{\eta}}_R + \mathrm{KG}\boldsymbol{f} = \boldsymbol{f}, \tag{14}$$

which can be used to obtain an alternative expression for the inertia-relief flexibility matrix or to eliminate it from the formulation [7].

2.2 Overview of component mode synthesis methods

A schematic overview of the reduction methods considered in this text is presented in Figure 2.

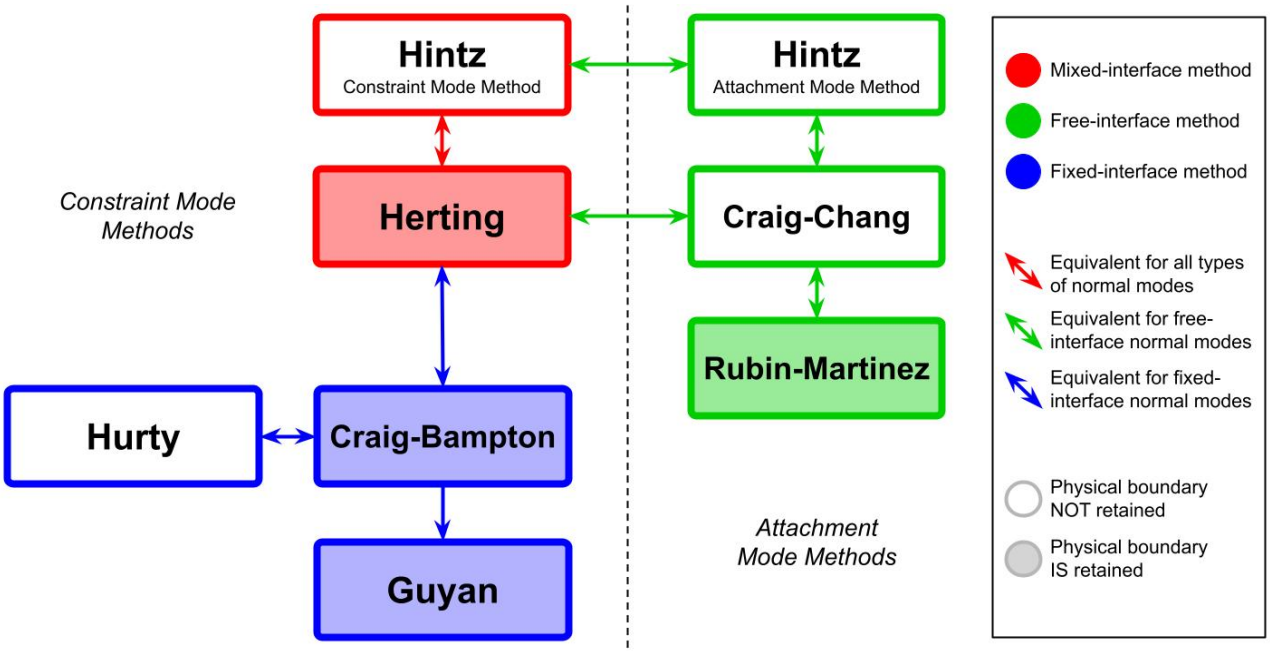

Figure 2: Component mode synthesis methods – Schematic overview

Hintz's attachment mode method, Craig-Chang's method and Rubin-Martinez's method are free-interface methods, meaning that they make use of the free-interface normal modes of the unconstrained body [22] and all rigid-body modes. Hintz's attachment mode method is formulated in terms of the relative modal coordinates and its reduction basis consists of rigid-body modes, free-interface normal modes and inertia-relief attachment modes represented by columns of the inertia-relief flexibility matrix [8]. Craig-Chang's method is formulated in terms of the absolute modal coordinates and its reduction basis consists of rigid-body modes, free-interface normal modes and residual-flexibility attachment modes represented by columns of the residual-flexibility matrix [9]. The physical boundary is not retained in either of these methods. Rubin-Martinez's method is a variation to Craig-Chang's method that does retain the physical boundary [10], [11]. The reduction bases of the three free-interface methods are all related through linear transformations and are thus equivalent. Due to the inclusion of the flexibility matrix in the formulations, the methods are classified as attachment mode methods [21], where the term *attachment mode* refers to a mode shape that occurs when a unit load is applied to one of the boundary degrees of freedom. As the discarded normal modes are generally not computed, the equations of motion for the static case are used to obtain an alternative expression for the inertia-relief flexibility matrix or the residual-flexibility matrix [7], [21],

[23].

Hintz's constraint mode method and Herting's method are mixed-interface methods, meaning that they make use of the mixed-interface normal modes of the partially constrained body and only the rigid-body modes that are not suppressed by the constraints are included. Free- and fixed-interface normal modes are special cases of mixed-interface normal modes and can thus also be used. Hintz's constraint mode method is formulated in terms of the relative modal coordinates and includes interface constraint modes, inertia-relief modes and free-, fixed- or mixed-interface normal modes in its reduction basis [8]. The physical boundary is not retained in this method. Herting's method is also formulated in terms of the relative modal coordinates and includes the same types of modes in its reduction basis, but due to the manipulation of the normal modes, the physical boundary is retained in this method [7], [26]. Both methods are equivalent and can be classified as constraint mode methods, where the term *constraint mode* refers to a mode shape that occurs when a unit displacement or rotation is applied to one of the boundary degrees of freedom. The flexibility matrix is eliminated from the formulations using the equations of motion for the static case, due to which the constraints imposed on the boundary degrees of freedom to obtain the normal modes are relaxed. This makes these methods suitable for free-, fixed- and mixed-interface normal modes [7], as opposed to the attachment mode methods that do not relax any imposed constraints and are thus only suitable for free-interface normal modes. When free-interface normal modes are used, the reduction bases of the mixed-interface methods are related to the reduction bases of the free-interface methods through linear transformations, which implies that for free-interface normal modes the methods are all equivalent [27].

Craig-Bampton's method, Hurty's method and Guyan's method are fixed-interface methods, meaning that they make use of the fixed-interface normal modes of the fully constrained body [22] and no rigid-body modes are included. Herting's method reduces to Craig-Bampton's method for fixed-interface normal modes and thus Craig-Bampton's method includes interface constraint modes and fixed-interface normal modes in its reduction basis [5]. Craig-Bampton's method again reduces to Guyan's method when all fixed-interface normal modes are discarded and thus the reduction basis for Guyan's method consists only of interface constraint modes [4]. The physical boundary is retained in both methods. Hurty's method is a variation to Craig-Bampton's method for which the physical boundary is not retained. It replaces a set of interface constraint modes by the rigid-body modes, such that its reduction basis consists of rigid-body modes, redundant-interface constraint modes and fixed-interface normal modes [6]. Hurty's method is equivalent to Craig-Bampton's method. As all three fixed-interface methods make use of interface constraint modes, the methods are classified as constraint mode methods [21].

In Section 2.3, the free-interface methods will be elaborated. Hintz's attachment mode method is discussed in Section 2.3.1. Section 2.3.2 presents Craig-Chang's method and its equivalence to Hintz's attachment mode method. Rubin-Martinez's method is discussed in Section 2.3.3, along with its equivalence to Craig-Chang's method.

In Section 2.4, the mixed-interface methods will be elaborated. Hintz's constraint mode method is discussed in Section 2.4.1, along with its equivalence to Hintz's attachment mode method for free-interface normal modes. Section 2.4.2 presents Herting's method, its equivalence to Hintz's constraint mode method, its equivalence to Craig-Chang's method for free-interface normal modes and its equivalence to Rubin-Martinez's method for free-interface normal modes.

In Section 2.5, the fixed-interface methods will be elaborated. Craig-Bampton's method is discussed

in Section 2.5.1, along with its equivalence to Herting's method for fixed-interface normal modes. Section 2.5.2 presents Guyan's method. Hurty's method is discussed in Section 2.5.3, along with its equivalence to Craig-Bampton's method.

2.3 Free-interface methods

2.3.1 Hintz's attachment mode method

Hintz's attachment mode method is a free-interface method based on the approximate dynamic solution in terms of the relative modal coordinates as formulated in Equation 12. For this method, the reduced set of coordinates consists of the rigid-body coordinates $\boldsymbol{\eta}_R$, the relative modal coordinates $\boldsymbol{\eta}_N^{\text{rel}}$ and the boundary loads $\boldsymbol{f}_b$. In partitioned form, the modal expansion for Hintz's attachment mode method [8] can thus directly be expressed as:

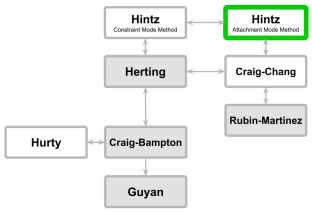

$$\begin{Bmatrix} \boldsymbol{q}_b \\ \boldsymbol{q}_i \end{Bmatrix} = \begin{bmatrix} \Phi_{Rb} & \Phi_{Nb} & \mathrm{G}_{bb} \\ \Phi_{Ri} & \Phi_{Ni} & \mathrm{G}_{ib} \end{bmatrix} \begin{Bmatrix} \boldsymbol{\eta}_R \\ \boldsymbol{\eta}_N^{\text{rel}} \\ \boldsymbol{f}_b \end{Bmatrix} \tag{15}$$

Due to the choice of coordinates, the physical boundary is not retained in this method. The reduction basis consists of rigid-body modes, free-interface normal modes and inertia-relief attachment modes [21]. The inertia-relief attachment modes are the boundary columns of the inertia-relief flexibility matrix and can be interpreted as the static shapes that occur due to unit loads applied at each of the boundary degrees of freedom. The modes are illustrated in Figure 3 for a two-dimensional beam of which the endpoints are boundary points.

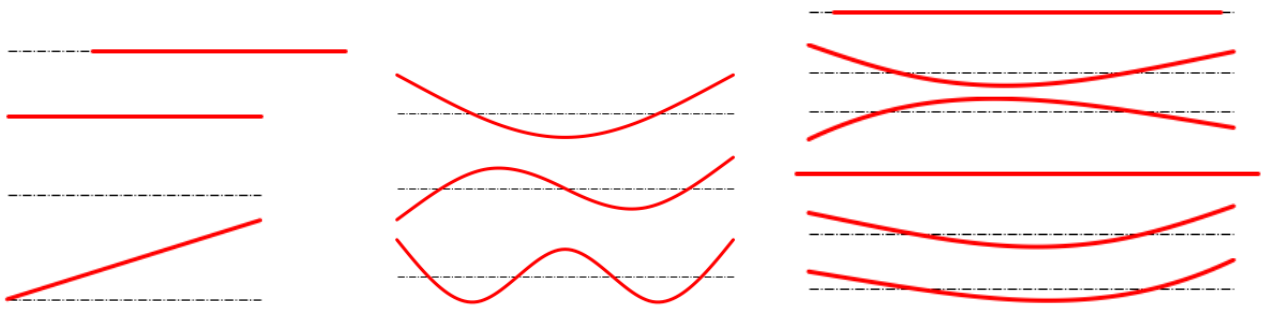

(a) Rigid-body modes (b) Free-interface normal modes (c) Inertia-relief attachment modes

Figure 3: Hintz's attachment mode method

Although an expression for the inertia-relief flexibility matrix G is given in Equation 10, the discarded free-interface normal modes are generally not computed. An alternative expression is obtained by considering the equations of motion for the static case given in Equation 14. Combining this with the first of Equation 6 yields:

$$\mathrm{KG}\boldsymbol{f} = \boldsymbol{f} - \mathrm{M}\Phi_R\overline{\mathrm{M}}_{RR}^{-1}\Phi_R^{\mathrm{T}}\boldsymbol{f} = \mathrm{P}\boldsymbol{f}, \tag{16}$$

in which $\mathrm{P} = \mathbf{1} - \mathrm{M}\Phi_R\overline{\mathrm{M}}_{RR}^{-1}\Phi_R^{\mathrm{T}}$ is the inertia-relief projection matrix [21], [23]. Due to rigid-body freedom the stiffness matrix cannot be inverted directly, but a general solution can be obtained as:

$$\mathrm{G}\boldsymbol{f} = \mathrm{G}_c\mathrm{P}\boldsymbol{f} + \Phi_R \boldsymbol{c}_R, \tag{17}$$

where G_c is the constrained flexibility matrix, a pseudo-inverse of the stiffness matrix obtained by inverting the constrained stiffness matrix and augmenting it with zeros. The arbitrary linear combination of rigid-body modes $\Phi_R \boldsymbol{c}_R$ is added to represent the full solution space. Since it follows from Equation 10 that the inertia-relief flexibility matrix is mass-orthogonal to the rigid-body modes, the specific solution is obtained by demanding that [23]:

$$\Phi_R^{\mathrm{T}}\mathrm{M}\mathrm{G}\boldsymbol{f} = \boldsymbol{0}. \tag{18}$$

Solving for the arbitrary constants $\boldsymbol{c}_R$ yields the alternative expression for the inertia-relief flexibility matrix:

$$\boxed{\mathrm{G} = \mathrm{P}^{\mathrm{T}}\mathrm{G}_c\mathrm{P}} \tag{19}$$

2.3.2 Craig-Chang's method

Craig-Chang's method is a free-interface method based on the approximate dynamic solution in terms of the absolute modal coordinates as formulated in Equation 13. For this method, the reduced set of coordinates consists of the rigid-body coordinates $\boldsymbol{\eta}_R$, the absolute modal coordinates $\boldsymbol{\eta}_N$ and the boundary loads $\boldsymbol{f}_b$. In partitioned form, the modal expansion for Craig-Chang's method [9] can thus directly be expressed as:

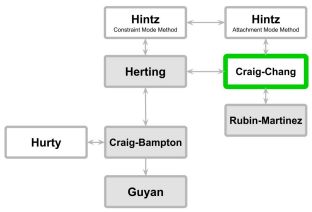

$$\boxed{\begin{Bmatrix} \boldsymbol{q}_b \\ \boldsymbol{q}_i \end{Bmatrix} = \begin{bmatrix} \Phi_{Rb} & \Phi_{Nb} & \mathrm{G}^{\mathrm{r}}_{bb} \\ \Phi_{Ri} & \Phi_{Ni} & \mathrm{G}^{\mathrm{r}}_{ib} \end{bmatrix} \begin{Bmatrix} \boldsymbol{\eta}_R \\ \boldsymbol{\eta}_N \\ \boldsymbol{f}_b \end{Bmatrix}} \tag{20}$$

Due to the choice of coordinates, the physical boundary is not retained in this method. The reduction basis consists of rigid-body modes, free-interface normal modes and residual-flexibility attachment modes and is thus considered an attachment mode method [21]. The residual-flexibility attachment modes are the boundary columns of the residual-flexibility matrix and can be interpreted as the static shapes that occur due to unit loads applied at each of the boundary degrees of freedom when the contribution of the kept free-interface normal modes is neglected. The modes are illustrated in Figure 4 for a two-dimensional beam of which the endpoints are boundary points.

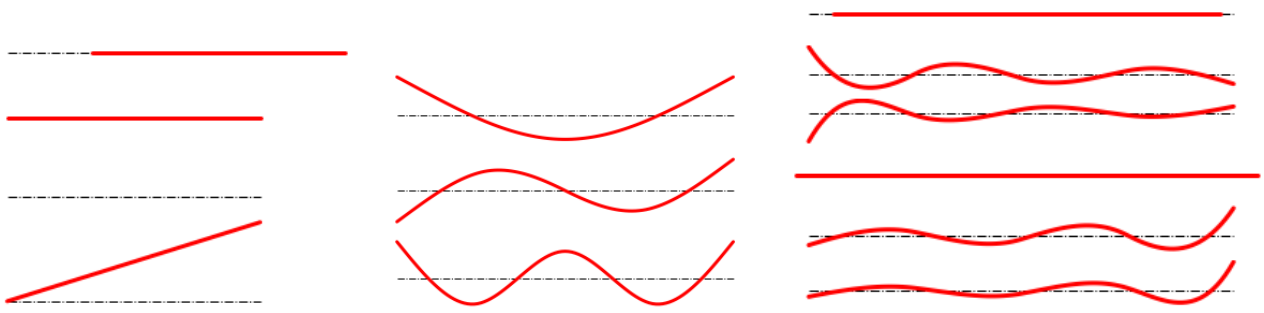

(a) Rigid-body modes (b) Free-interface normal modes (c) Residual-flexibility attachment modes

Figure 4: Craig-Chang's method

Although an expression for the residual-flexibility matrix G^r is given in Equation 10, the discarded free-interface normal modes are generally not computed. An alternative expression is obtained from the expression for the inertia-relief flexibility matrix given in Equation 19. Combining this with Equation 10 yields [21]:

$$\boxed{G^r = P^T G_c P - \Phi_N \left[\mu_N \Omega_N^2\right]^{-1} \Phi_N^T} \tag{21}$$

2.3.2.1 Equivalence to Hintz's attachment mode method

Craig-Chang's method is equivalent to Hintz's attachment mode method. From Equation 9 it follows that both coordinate sets are related as:

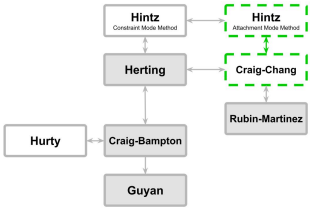

$$\boxed{\begin{Bmatrix} \eta_R \\ \eta_N^{\text{rel}} \\ f_b \end{Bmatrix} = \begin{bmatrix} \mathbf{1} & \mathbf{0} & \mathbf{0} \\ \mathbf{0} & \mathbf{1} & -\left[\mu_N \Omega_N^2\right]^{-1} \Phi_{Nb}^T \\ \mathbf{0} & \mathbf{0} & \mathbf{1} \end{bmatrix} \begin{Bmatrix} \eta_R \\ \eta_N \\ f_b \end{Bmatrix}} \tag{22}$$

Hintz Craig-Chang

Substitution of this coordinate transformation in the modal expansion for Hintz's attachment mode method (Equation 15) indeed yields the modal expansion for Craig-Chang's method (Equation 20):

$$\begin{aligned} \begin{Bmatrix} q_b \\ q_i \end{Bmatrix} &= \begin{bmatrix} \Phi_{Rb} & \Phi_{Nb} & G_{bb} \\ \Phi_{Ri} & \Phi_{Ni} & G_{ib} \end{bmatrix} \begin{Bmatrix} \eta_R \\ \eta_N^{\text{rel}} \\ f_b \end{Bmatrix} \\ &= \begin{bmatrix} \Phi_{Rb} & \Phi_{Nb} & G_{bb} \\ \Phi_{Ri} & \Phi_{Ni} & G_{ib} \end{bmatrix} \begin{bmatrix} \mathbf{1} & \mathbf{0} & \mathbf{0} \\ \mathbf{0} & \mathbf{1} & -\left[\mu_N \Omega_N^2\right]^{-1} \Phi_{Nb}^T \\ \mathbf{0} & \mathbf{0} & \mathbf{1} \end{bmatrix} \begin{Bmatrix} \eta_R \\ \eta_N \\ f_b \end{Bmatrix} \\ &= \begin{bmatrix} \Phi_{Rb} & \Phi_{Nb} & G_{bb} - \Phi_{Nb} \left[\mu_N \Omega_N^2\right]^{-1} \Phi_{Nb}^T \\ \Phi_{Ri} & \Phi_{Ni} & G_{ib} - \Phi_{Ni} \left[\mu_N \Omega_N^2\right]^{-1} \Phi_{Nb}^T \end{bmatrix} \begin{Bmatrix} \eta_R \\ \eta_N \\ f_b \end{Bmatrix} \\ &= \begin{bmatrix} \Phi_{Rb} & \Phi_{Nb} & G_{bb}^r \\ \Phi_{Ri} & \Phi_{Ni} & G_{ib}^r \end{bmatrix} \begin{Bmatrix} \eta_R \\ \eta_N \\ f_b \end{Bmatrix}. \end{aligned} \tag{23}$$

The difference between both methods is thus only the interpretation of the coordinates, or the part of the reduction basis in which the static contribution of the kept free-interface normal modes is included.

2.3.3 Rubin-Martinez's method

Rubin-Martinez's method is a free-interface method based on the approximate dynamic solution in terms of the absolute modal coordinates as formulated in Equation 13. For this method, the reduced set of coordinates consists of the boundary degrees of freedom q_b, the rigid-body coordinates η_R and the absolute modal coordinates η_N. The method is derived from Craig-Chang's method [11]. The boundary loads can be eliminated from the formulation using the boundary partition of Craig-Chang's modal expansion given in Equation 20:

$$f_b = G_{bb}^{r^{-1}} \left(q_b - \Phi_{Rb}\eta_R - \Phi_{Nb}\eta_N\right), \tag{24}$$

which can be substituted into the internal partition:

$$q_i = \mathrm{G}^{\mathrm{r}}_{ib}\mathrm{G}^{\mathrm{r}^{-1}}_{bb} q_b + \left(\Phi_{Ri} - \mathrm{G}^{\mathrm{r}}_{ib}\mathrm{G}^{\mathrm{r}^{-1}}_{bb}\Phi_{Rb}\right)\eta_R + \left(\Phi_{Ni} - \mathrm{G}^{\mathrm{r}}_{ib}\mathrm{G}^{\mathrm{r}^{-1}}_{bb}\Phi_{Nb}\right)\eta_N. \tag{25}$$

In partitioned form, the modal expansion for Rubin-Martinez's method [10], [11] is thus given by:

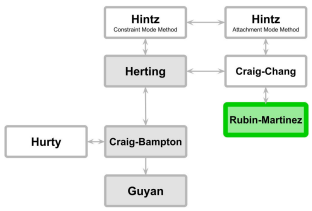

$$\begin{Bmatrix} q_b \\ q_i \end{Bmatrix} = \begin{bmatrix} \mathbf{1} & \mathbf{0} & \mathbf{0} \\ \mathrm{G}^{\mathrm{r}}_{ib}\mathrm{G}^{\mathrm{r}^{-1}}_{bb} & \Phi_{Ri} - \mathrm{G}^{\mathrm{r}}_{ib}\mathrm{G}^{\mathrm{r}^{-1}}_{bb}\Phi_{Rb} & \Phi_{Ni} - \mathrm{G}^{\mathrm{r}}_{ib}\mathrm{G}^{\mathrm{r}^{-1}}_{bb}\Phi_{Nb} \end{bmatrix} \begin{Bmatrix} q_b \\ \eta_R \\ \eta_N \end{Bmatrix} \tag{26}$$

Due to the choice of coordinates, the physical boundary is retained in this method. Since the reduction basis includes manipulated residual-flexibility attachment modes, the method is considered an attachment mode method [21]. The modes are illustrated in Figure 5 for a two-dimensional beam of which the endpoints are boundary points.

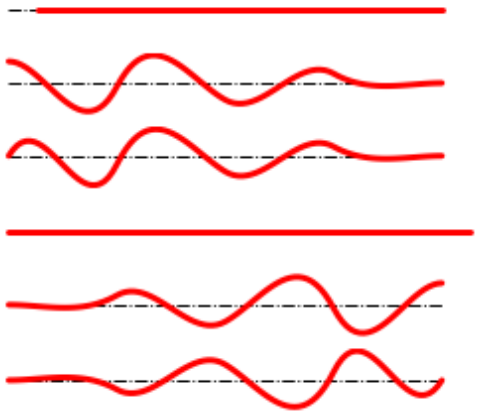

(a) Boundary modes

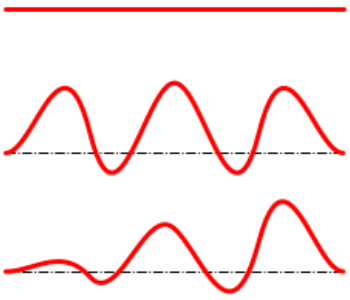

(b) Internal modes (contribution of rigid-body modes)

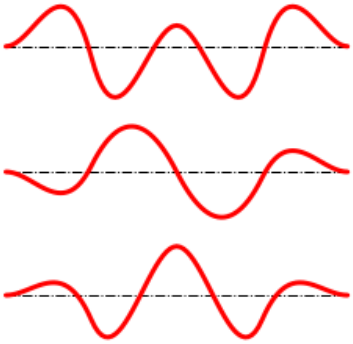

(c) Internal modes (contribution of normal modes)

Figure 5: Rubin-Martinez's method

2.3.3.1 Equivalence to Craig-Chang's method

Rubin-Martinez's method is equivalent to Craig-Chang's method [11]. From Equation 24 it follows that both coordinate sets are related as:

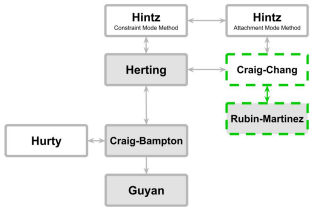

$$\begin{Bmatrix} \eta_R \\ \eta_N \\ f_b \end{Bmatrix} = \begin{bmatrix} \mathbf{0} & \mathbf{1} & \mathbf{0} \\ \mathbf{0} & \mathbf{0} & \mathbf{1} \\ \mathrm{G}^{\mathrm{r}^{-1}}_{bb} & -\mathrm{G}^{\mathrm{r}^{-1}}_{bb}\Phi_{Rb} & -\mathrm{G}^{\mathrm{r}^{-1}}_{bb}\Phi_{Nb} \end{bmatrix} \begin{Bmatrix} q_b \\ \eta_R \\ \eta_N \end{Bmatrix} \tag{27}$$

Craig-Chang Rubin-Martinez

Substitution of this coordinate transformation in the modal expansion for Craig-Chang's method (Equation 20) indeed yields the modal expansion for Rubin-Martinez's method (Equation 26):

$$\begin{aligned}
\begin{Bmatrix} \boldsymbol{q}_b \\ \boldsymbol{q}_i \end{Bmatrix} &= \begin{bmatrix} \Phi_{Rb} & \Phi_{Nb} & \mathrm{G}^{\mathrm{r}}_{bb} \\ \Phi_{Ri} & \Phi_{Ni} & \mathrm{G}^{\mathrm{r}}_{ib} \end{bmatrix} \begin{Bmatrix} \boldsymbol{\eta}_R \\ \boldsymbol{\eta}_N \\ \boldsymbol{f}_b \end{Bmatrix} \\
&= \begin{bmatrix} \Phi_{Rb} & \Phi_{Nb} & \mathrm{G}^{\mathrm{r}}_{bb} \\ \Phi_{Ri} & \Phi_{Ni} & \mathrm{G}^{\mathrm{r}}_{ib} \end{bmatrix} \begin{bmatrix} \mathbf{0} & \mathbf{1} & \mathbf{0} \\ \mathbf{0} & \mathbf{0} & \mathbf{1} \\ \mathrm{G}^{\mathrm{r}^{-1}}_{bb} & -\mathrm{G}^{\mathrm{r}^{-1}}_{bb}\Phi_{Rb} & -\mathrm{G}^{\mathrm{r}^{-1}}_{bb}\Phi_{Nb} \end{bmatrix} \begin{Bmatrix} \boldsymbol{q}_b \\ \boldsymbol{\eta}_R \\ \boldsymbol{\eta}_N \end{Bmatrix} \\
&= \begin{bmatrix} \mathbf{1} & \mathbf{0} & \mathbf{0} \\ \mathrm{G}^{\mathrm{r}}_{ib}\mathrm{G}^{\mathrm{r}^{-1}}_{bb} & \Phi_{Ri} - \mathrm{G}^{\mathrm{r}}_{ib}\mathrm{G}^{\mathrm{r}^{-1}}_{bb}\Phi_{Rb} & \Phi_{Ni} - \mathrm{G}^{\mathrm{r}}_{ib}\mathrm{G}^{\mathrm{r}^{-1}}_{bb}\Phi_{Nb} \end{bmatrix} \begin{Bmatrix} \boldsymbol{q}_b \\ \boldsymbol{\eta}_R \\ \boldsymbol{\eta}_N \end{Bmatrix}.
\end{aligned} \tag{28}$$

The difference between both methods is thus only the interpretation of the coordinates. In Rubin-Martinez's method the physical boundary is retained, whereas the full rigid-body modes, free-interface normal modes and residual-flexibility attachment modes appear in Craig-Chang's method.

2.4 Mixed-interface methods

2.4.1 Hintz's constraint mode method

Hintz's constraint mode method is based on the approximate dynamic solution in terms of the relative modal coordinates as formulated in Equation 12. As opposed to Hintz's attachment mode method, the inertia-relief flexibility matrix is eliminated from the formulation, which relaxes the constraints imposed on the boundary degrees of freedom to obtain the normal modes and thus allows free-, fixed- or mixed-interface normal modes to be used. For this method, the reduced set of coordinates consists of a set of constraint mode coordinates $\boldsymbol{\eta}_C$, the rigid-body accelerations $\ddot{\boldsymbol{\eta}}_R$ and the relative modal coordinates $\boldsymbol{\eta}_N^{\mathrm{rel}}$. To obtain the modal expansion, Equation 12 is premultiplied by the stiffness matrix:

$$\mathrm{K}\boldsymbol{q} = \mathrm{K}\Phi_N\boldsymbol{\eta}_N^{\mathrm{rel}} + \mathrm{K}\mathrm{G}_b\boldsymbol{f}_b \tag{29}$$

and the equations of motion for the static case given in Equation 14 are used to eliminate the inertia-relief flexibility matrix from the formulation:

$$\mathrm{K}\boldsymbol{q} = \mathrm{K}\Phi_N\boldsymbol{\eta}_N^{\mathrm{rel}} + \boldsymbol{f} - \mathrm{M}\Phi_R\ddot{\boldsymbol{\eta}}_R. \tag{30}$$

This can be partitioned as:

$$\begin{bmatrix} \mathrm{K}_{bb} & \mathrm{K}_{bi} \\ \mathrm{K}_{ib} & \mathrm{K}_{ii} \end{bmatrix} \begin{Bmatrix} \boldsymbol{q}_b \\ \boldsymbol{q}_i \end{Bmatrix} = \begin{bmatrix} \mathrm{K}_{bb} & \mathrm{K}_{bi} \\ \mathrm{K}_{ib} & \mathrm{K}_{ii} \end{bmatrix} \begin{bmatrix} \Phi_{Nb} \\ \Phi_{Ni} \end{bmatrix} \boldsymbol{\eta}_N^{\mathrm{rel}} + \begin{Bmatrix} \boldsymbol{f}_b \\ \mathbf{0} \end{Bmatrix} - \begin{bmatrix} \mathrm{M}_{bb} & \mathrm{M}_{bi} \\ \mathrm{M}_{ib} & \mathrm{M}_{ii} \end{bmatrix} \begin{bmatrix} \Phi_{Rb} \\ \Phi_{Ri} \end{bmatrix} \ddot{\boldsymbol{\eta}}_R, \tag{31}$$

from which it follows that:

$$\begin{aligned}
\boldsymbol{q}_i &= -\mathrm{K}_{ii}^{-1}\mathrm{K}_{ib}\boldsymbol{q}_b + \left(\Phi_{Ni} + \mathrm{K}_{ii}^{-1}\mathrm{K}_{ib}\Phi_{Nb}\right)\boldsymbol{\eta}_N^{\mathrm{rel}} - \mathrm{K}_{ii}^{-1}\left(\mathrm{M}_{ib}\Phi_{Rb} + \mathrm{M}_{ii}\Phi_{Ri}\right)\ddot{\boldsymbol{\eta}}_R \\
&= -\mathrm{K}_{ii}^{-1}\mathrm{K}_{ib}\left(\boldsymbol{q}_b - \Phi_{Nb}\boldsymbol{\eta}_N^{\mathrm{rel}}\right) + \Phi_{Ni}\boldsymbol{\eta}_N^{\mathrm{rel}} - \mathrm{K}_{ii}^{-1}\left(\mathrm{M}_{ib}\Phi_{Rb} + \mathrm{M}_{ii}\Phi_{Ri}\right)\ddot{\boldsymbol{\eta}}_R.
\end{aligned} \tag{32}$$

Introducing

$$\boldsymbol{\eta}_C = \boldsymbol{q}_b - \Phi_{Nb}\boldsymbol{\eta}_N^{\mathrm{rel}} \tag{33}$$

as the constraint mode coordinates and defining:

$$\begin{aligned}
\Phi_{Ci} &= -\mathrm{K}_{ii}^{-1}\mathrm{K}_{ib} \\
\mathrm{H}_i &= -\mathrm{K}_{ii}^{-1}\left(\mathrm{M}_{ib}\Phi_{Rb} + \mathrm{M}_{ii}\Phi_{Ri}\right),
\end{aligned} \tag{34}$$

the modal expansion for Hintz's constraint mode method [8] can be formulated as:

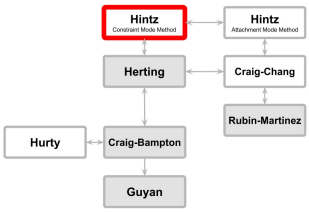

$$\begin{Bmatrix} q_b \\ q_i \end{Bmatrix} = \begin{bmatrix} \mathbf{1} & \mathbf{0} & \Phi_{Nb} \\ \Phi_{Ci} & \mathrm{H}_i & \Phi_{Ni} \end{bmatrix} \begin{Bmatrix} \eta_C \\ \ddot{\eta}_R \\ \eta_N^{\mathrm{rel}} \end{Bmatrix} \tag{35}$$

Due to the choice of coordinates, the physical boundary is not retained in this method. The reduction basis consists of interface constraint modes, inertia-relief modes and free-, fixed- or mixed-interface normal modes. The interface constraint modes can be interpreted as the static shapes that occur due to unit displacements or rotations of each of the boundary degrees of freedom, while the other boundary degrees of freedom remain fixed [21]. The inertia-relief modes ensure static completeness of the entire solution [8]. The complete normal modes appear in the formulation due to the introduction of the constraint mode coordinates. The modes are illustrated in Figure 6 for a two-dimensional beam of which the endpoints are boundary points and for which free-interface normal modes have been used.

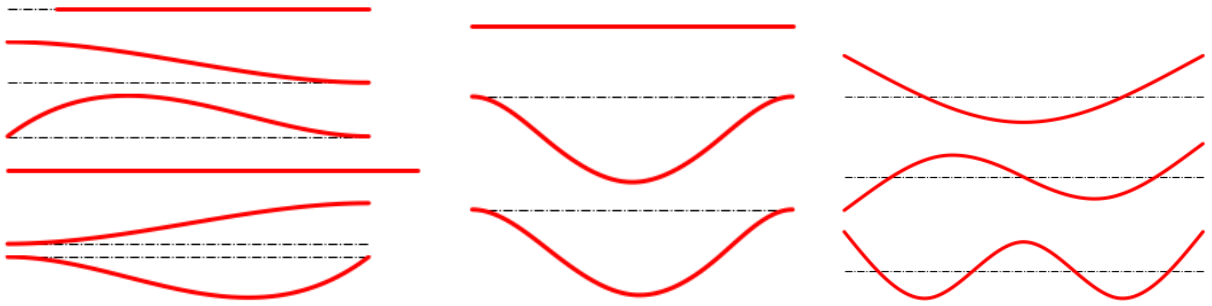

(a) Interface constraint modes (b) Inertia-relief modes (c) Free-interface normal modes

Figure 6: Hintz's constraint mode method – Free-interface

In Figure 7 the modes are illustrated for the same beam for which the translational degrees of freedom of the left endpoint have been suppressed to obtain the mixed-interface normal modes and where both translational rigid-body modes have been excluded in accordance with these constraints.

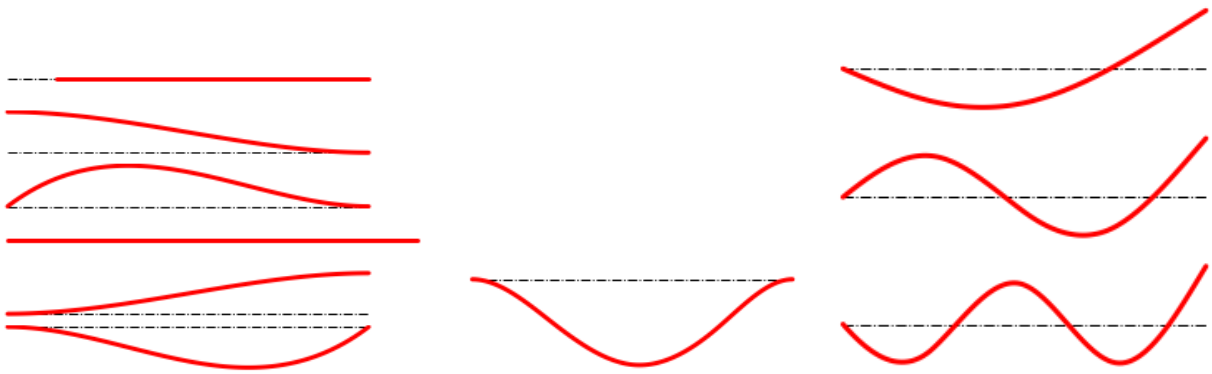

(a) Interface constraint modes (b) Inertia-relief modes (c) Mixed-interface normal modes

Figure 7: Hintz's constraint mode method – Mixed-interface

2.4.1.1 Equivalence to Hintz's attachment mode method [for free-interface normal modes]

When free-interface normal modes are used, Hintz's constraint mode method is equivalent to Hintz's attachment mode method. From Equations 12 and 33 and the first of Equation 6 it follows that both coordinate sets are related as:

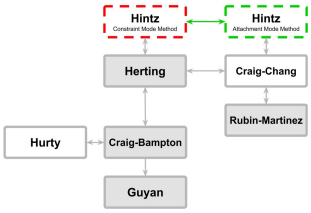

$$\begin{Bmatrix} \boldsymbol{\eta}_C \\ \ddot{\boldsymbol{\eta}}_R \\ \boldsymbol{\eta}_N^{\text{rel}} \end{Bmatrix} = \begin{bmatrix} \Phi_{Rb} & \mathbf{0} & \mathrm{G}_{bb} \\ \mathbf{0} & \mathbf{0} & \overline{\mathrm{M}}_{RR}^{-1}\Phi_{Rb}^{\mathrm{T}} \\ \mathbf{0} & \mathbf{1} & \mathbf{0} \end{bmatrix} \begin{Bmatrix} \boldsymbol{\eta}_R \\ \boldsymbol{\eta}_N^{\text{rel}} \\ \boldsymbol{f}_b \end{Bmatrix} \tag{36}$$

Constraint mode method Attachment mode method

Substitution of this coordinate transformation in the modal expansion for Hintz's constraint mode method (Equation 35) indeed yields the modal expansion for Hintz's attachment mode method (Equation 15):

$$\begin{aligned} \begin{Bmatrix} \boldsymbol{q}_b \\ \boldsymbol{q}_i \end{Bmatrix} &= \begin{bmatrix} \mathbf{1} & \mathbf{0} & \Phi_{Nb} \\ \Phi_{Ci} & \mathrm{H}_i & \Phi_{Ni} \end{bmatrix} \begin{Bmatrix} \boldsymbol{\eta}_C \\ \ddot{\boldsymbol{\eta}}_R \\ \boldsymbol{\eta}_N^{\text{rel}} \end{Bmatrix} \\ &= \begin{bmatrix} \mathbf{1} & \mathbf{0} & \Phi_{Nb} \\ \Phi_{Ci} & \mathrm{H}_i & \Phi_{Ni} \end{bmatrix} \begin{bmatrix} \Phi_{Rb} & \mathbf{0} & \mathrm{G}_{bb} \\ \mathbf{0} & \mathbf{0} & \overline{\mathrm{M}}_{RR}^{-1}\Phi_{Rb}^{\mathrm{T}} \\ \mathbf{0} & \mathbf{1} & \mathbf{0} \end{bmatrix} \begin{Bmatrix} \boldsymbol{\eta}_R \\ \boldsymbol{\eta}_N^{\text{rel}} \\ \boldsymbol{f}_b \end{Bmatrix} \\ &= \begin{bmatrix} \Phi_{Rb} & \Phi_{Nb} & \mathrm{G}_{bb} \\ \Phi_{Ci}\Phi_{Rb} & \Phi_{Ni} & \Phi_{Ci}\mathrm{G}_{bb} + \mathrm{H}_i\overline{\mathrm{M}}_{RR}^{-1}\Phi_{Rb}^{\mathrm{T}} \end{bmatrix} \begin{Bmatrix} \boldsymbol{\eta}_R \\ \boldsymbol{\eta}_N^{\text{rel}} \\ \boldsymbol{f}_b \end{Bmatrix} \\ &= \begin{bmatrix} \Phi_{Rb} & \Phi_{Nb} & \mathrm{G}_{bb} \\ \Phi_{Ri} & \Phi_{Ni} & \mathrm{G}_{ib} \end{bmatrix} \begin{Bmatrix} \boldsymbol{\eta}_R \\ \boldsymbol{\eta}_N^{\text{rel}} \\ \boldsymbol{f}_b \end{Bmatrix} \end{aligned} \tag{37}$$

where $\Phi_{Ri} = \Phi_{Ci}\Phi_{Rb}$ follows from the fact that $\mathrm{K}\Phi_R = \mathbf{0}$ and

$$\mathrm{G}_{ib}\boldsymbol{f}_b = \left(\Phi_{Ci}\mathrm{G}_{bb} + \mathrm{H}_i\overline{\mathrm{M}}_{RR}^{-1}\Phi_{Rb}^{\mathrm{T}}\right)\boldsymbol{f}_b \tag{38}$$

follows from Equations 14 and 34 and the first of Equation 6 in partitioned form.

Hintz's constraint mode method is only equivalent to Hintz's attachment mode method for free-interface normal modes. When fixed- or mixed-interface normal modes are used, the transformation matrix is singular due to rows of zeros and the inverse transformation does not exist.

2.4.2 Herting's method

Herting's method is based on the approximate dynamic solution in terms of the relative modal coordinates as formulated in Equation 12. As with Hintz's constraint mode method, the inertia-relief flexibility matrix is eliminated from the formulation and the method is suitable for the inclusion of free-, fixed- or mixed-interface normal modes. For this method, the reduced set of coordinates consists of the boundary degrees of freedom $\boldsymbol{q}_b$, the rigid-body accelerations $\ddot{\boldsymbol{\eta}}_R$ and the relative modal coordinates $\boldsymbol{\eta}_N^{\text{rel}}$. The modal expansion for Herting's method [7] is obtained directly from the first part of Equation 32 as:

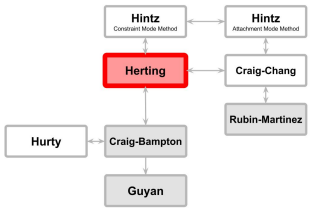

$$\begin{Bmatrix} q_b \\ q_i \end{Bmatrix} = \begin{bmatrix} \mathbf{1} & \mathbf{0} & \mathbf{0} \\ \Phi_{Ci} & \mathrm{H}_i & \Phi_{Ni} - \Phi_{Ci}\Phi_{Nb} \end{bmatrix} \begin{Bmatrix} q_b \\ \ddot{\eta}_R \\ \eta_N^{\mathrm{rel}} \end{Bmatrix} \tag{39}$$

Due to the choice of coordinates, the physical boundary is retained in this method. The reduction basis consists of interface constraint modes, inertia-relief modes and manipulated free-, fixed- or mixed-interface normal modes and is thus considered a constraint mode method. The modes are illustrated in Figure 8 for a two-dimensional beam of which the endpoints are boundary points and for which free-interface normal modes have been used.

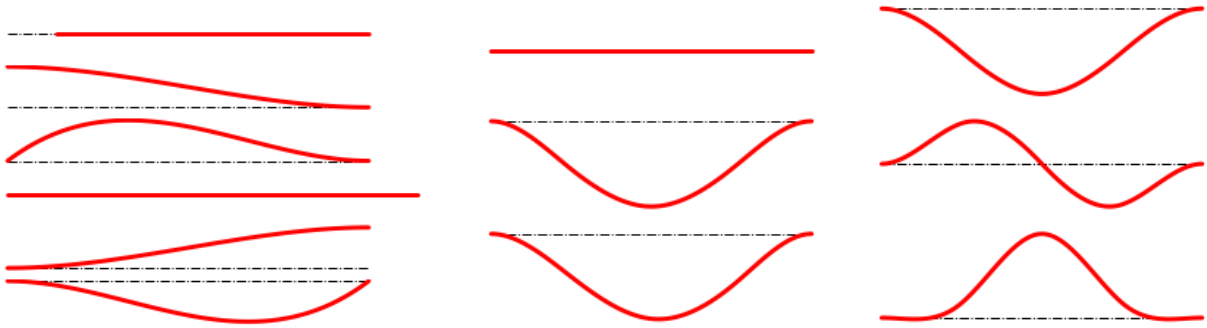

(a) Interface constraint modes (b) Inertia-relief modes (c) Manipulated free-interface normal modes

Figure 8: Herting's method – Free-interface

In Figure 9 the modes are illustrated for the same beam for which the translational degrees of freedom of the left endpoint have been suppressed to obtain the mixed-interface normal modes and where both translational rigid-body modes have been excluded in accordance with these constraints.

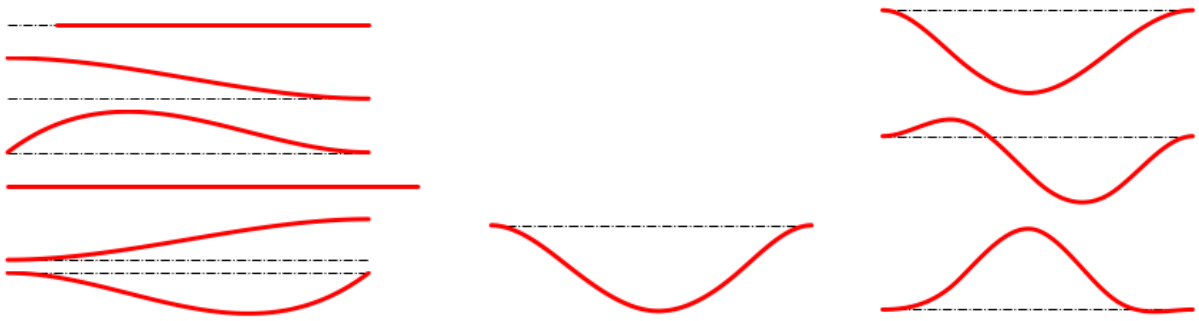

(a) Interface constraint modes (b) Inertia-relief modes (c) Manipulated mixed-interface normal modes

Figure 9: Herting's method – Mixed-interface

2.4.2.1 Equivalence to Hintz's constraint mode method

Herting's method is equivalent to Hintz's constraint mode method [7]. From the definition of Hintz's constraint mode coordinates in Equation 33 it follows that both coordinate sets are related as:

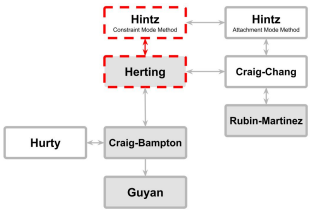

$$\begin{Bmatrix} \eta_C \\ \ddot{\eta}_R \\ \eta_N^{\text{rel}} \end{Bmatrix} = \begin{bmatrix} \mathbf{1} & \mathbf{0} & -\Phi_{Nb} \\ \mathbf{0} & \mathbf{1} & \mathbf{0} \\ \mathbf{0} & \mathbf{0} & \mathbf{1} \end{bmatrix} \begin{Bmatrix} q_b \\ \ddot{\eta}_R \\ \eta_N^{\text{rel}} \end{Bmatrix} \tag{40}$$

Hintz Herting

Substitution of this coordinate transformation in the modal expansion for Hintz's constraint mode method (Equation 35) indeed yields the modal expansion for Herting's method (Equation 39):

$$\begin{aligned} \begin{Bmatrix} q_b \\ q_i \end{Bmatrix} &= \begin{bmatrix} \mathbf{1} & \mathbf{0} & \Phi_{Nb} \\ \Phi_{Ci} & \mathrm{H}_i & \Phi_{Ni} \end{bmatrix} \begin{Bmatrix} \eta_C \\ \ddot{\eta}_R \\ \eta_N^{\text{rel}} \end{Bmatrix} \\ &= \begin{bmatrix} \mathbf{1} & \mathbf{0} & \Phi_{Nb} \\ \Phi_{Ci} & \mathrm{H}_i & \Phi_{Ni} \end{bmatrix} \begin{bmatrix} \mathbf{1} & \mathbf{0} & -\Phi_{Nb} \\ \mathbf{0} & \mathbf{1} & \mathbf{0} \\ \mathbf{0} & \mathbf{0} & \mathbf{1} \end{bmatrix} \begin{Bmatrix} q_b \\ \ddot{\eta}_R \\ \eta_N^{\text{rel}} \end{Bmatrix} \\ &= \begin{bmatrix} \mathbf{1} & \mathbf{0} & \mathbf{0} \\ \Phi_{Ci} & \mathrm{H}_i & \Phi_{Ni} - \Phi_{Ci}\Phi_{Nb} \end{bmatrix} \begin{Bmatrix} q_b \\ \ddot{\eta}_R \\ \eta_N^{\text{rel}} \end{Bmatrix}. \end{aligned} \tag{41}$$

The difference between both methods is thus only the interpretation of the coordinates. In Herting's method the physical boundary is retained, whereas in Hintz's constraint mode method the complete normal modes appear.

2.4.2.2 Equivalence to Craig-Chang's method [for free-interface normal modes]

When free-interface normal modes are used, Herting's method is equivalent to Craig-Chang's method [27]. From Equations 13 and 9 and the first of Equation 6 it follows that both coordinate sets are related as:

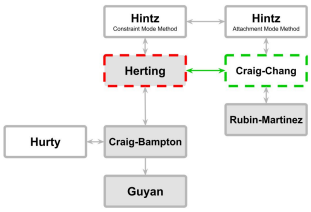

$$\begin{Bmatrix} q_b \\ \ddot{\eta}_R \\ \eta_N^{\text{rel}} \end{Bmatrix} = \begin{bmatrix} \Phi_{Rb} & \Phi_{Nb} & \mathrm{G}_{bb}^{\mathrm{r}} \\ \mathbf{0} & \mathbf{0} & \overline{\mathrm{M}}_{RR}^{-1}\Phi_{Rb}^{\mathrm{T}} \\ \mathbf{0} & \mathbf{1} & -\left[\mu_N\Omega_N^2\right]^{-1}\Phi_{Nb}^{\mathrm{T}} \end{bmatrix} \begin{Bmatrix} \eta_R \\ \eta_N \\ f_b \end{Bmatrix} \tag{42}$$

Herting Craig-Chang

Substitution of this coordinate transformation in the modal expansion for Herting's method (Equation 39) indeed yields the modal expansion for Craig-Chang's method (Equation 20):

$$\begin{Bmatrix} q_b \\ q_i \end{Bmatrix} = \begin{bmatrix} \mathbf{1} & \mathbf{0} & \mathbf{0} \\ \Phi_{Ci} & \mathrm{H}_i & \Phi_{Ni} - \Phi_{Ci}\Phi_{Nb} \end{bmatrix} \begin{Bmatrix} q_b \\ \ddot{\eta}_R \\ \eta_N^{\text{rel}} \end{Bmatrix}$$

$$
\begin{aligned}
&= \begin{bmatrix} \mathbf{1} & \mathbf{0} & \mathbf{0} \\ \Phi_{Ci} & \mathrm{H}_i & \Phi_{Ni} - \Phi_{Ci}\Phi_{Nb} \end{bmatrix} \begin{bmatrix} \Phi_{Rb} & \Phi_{Nb} & \mathrm{G}^{\mathrm{r}}_{bb} \\ \mathbf{0} & \mathbf{0} & \overline{\mathrm{M}}^{-1}_{RR}\Phi^{\mathrm{T}}_{Rb} \\ \mathbf{0} & \mathbf{1} & -\left[\mu_N\Omega^2_N\right]^{-1}\Phi^{\mathrm{T}}_{Nb} \end{bmatrix} \begin{Bmatrix} \eta_R \\ \eta_N \\ f_b \end{Bmatrix} \\
&= \begin{bmatrix} \Phi_{Rb} & \Phi_{Nb} & \mathrm{G}^{\mathrm{r}}_{bb} \\ \Phi_{Ci}\Phi_{Rb} & \Phi_{Ni} & \Phi_{Ci}\mathrm{G}^{\mathrm{r}}_{bb} + \mathrm{H}_i\overline{\mathrm{M}}^{-1}_{RR}\Phi^{\mathrm{T}}_{Rb} - \left(\Phi_{Ni} - \Phi_{Ci}\Phi_{Nb}\right)\left[\mu_N\Omega^2_N\right]^{-1}\Phi^{\mathrm{T}}_{Nb} \end{bmatrix} \begin{Bmatrix} \eta_R \\ \eta_N \\ f_b \end{Bmatrix} \\
&= \begin{bmatrix} \Phi_{Rb} & \Phi_{Nb} & \mathrm{G}^{\mathrm{r}}_{bb} \\ \Phi_{Ri} & \Phi_{Ni} & \mathrm{G}^{\mathrm{r}}_{ib} \end{bmatrix} \begin{Bmatrix} \eta_R \\ \eta_N \\ f_b \end{Bmatrix},
\end{aligned}
\tag{43}
$$

where

$$
\mathrm{G}^{\mathrm{r}}_{ib} f_b = \left(\Phi_{Ci}\mathrm{G}^{\mathrm{r}}_{bb} + \mathrm{H}_i\overline{\mathrm{M}}^{-1}_{RR}\Phi^{\mathrm{T}}_{Rb} - \left(\Phi_{Ni} - \Phi_{Ci}\Phi_{Nb}\right)\left[\mu_N\Omega^2_N\right]^{-1}\Phi^{\mathrm{T}}_{Nb}\right) f_b \tag{44}
$$

follows from Equations 10, 14 and 34 and the first of Equation 6 in partitioned form.

Herting's method is only equivalent to Craig-Chang's method for free-interface normal modes. When fixed- or mixed-interface normal modes are used, the transformation matrix is singular due to rows of zeros and the inverse transformation does not exist.

2.4.2.3 Equivalence to Rubin-Martinez's method [for free-interface normal modes]

When free-interface normal modes are used, Herting's method is equivalent to Rubin-Martinez's method. From Equations 27 and 42 it follows that both coordinate sets are related as:

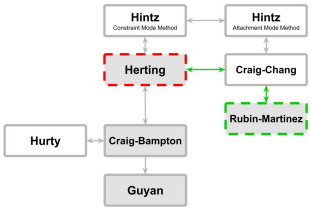

$$
\begin{Bmatrix} q_b \\ \ddot{\eta}_R \\ \eta^{\mathrm{rel}}_N \end{Bmatrix} = \begin{bmatrix} \Phi_{Rb} & \Phi_{Nb} & \mathrm{G}^{\mathrm{r}}_{bb} \\ \mathbf{0} & \mathbf{0} & \overline{\mathrm{M}}^{-1}_{RR}\Phi^{\mathrm{T}}_{Rb} \\ \mathbf{0} & \mathbf{1} & -\left[\mu_N\Omega^2_N\right]^{-1}\Phi^{\mathrm{T}}_{Nb} \end{bmatrix} \begin{bmatrix} \mathbf{0} & \mathbf{1} & \mathbf{0} \\ \mathbf{0} & \mathbf{0} & \mathbf{1} \\ \mathrm{G}^{\mathrm{r}^{-1}}_{bb} & -\mathrm{G}^{\mathrm{r}^{-1}}_{bb}\Phi_{Rb} & -\mathrm{G}^{\mathrm{r}^{-1}}_{bb}\Phi_{Nb} \end{bmatrix} \begin{Bmatrix} q_b \\ \eta_R \\ \eta_N \end{Bmatrix} \tag{45}
$$

Herting Rubin-Martinez

Substitution of this coordinate transformation in the modal expansion for Herting's method (Equation 39) indeed yields the modal expansion for Rubin-Martinez's method (Equation 26):

$$
\begin{aligned}
\begin{Bmatrix} q_b \\ q_i \end{Bmatrix} &= \begin{bmatrix} \mathbf{1} & \mathbf{0} & \mathbf{0} \\ \Phi_{Ci} & \mathrm{H}_i & \Phi_{Ni} - \Phi_{Ci}\Phi_{Nb} \end{bmatrix} \begin{Bmatrix} q_b \\ \ddot{\eta}_R \\ \eta^{\mathrm{rel}}_N \end{Bmatrix} \\
&= \begin{bmatrix} \mathbf{1} & \mathbf{0} & \mathbf{0} \\ \Phi_{Ci} & \mathrm{H}_i & \Phi_{Ni} - \Phi_{Ci}\Phi_{Nb} \end{bmatrix} \begin{bmatrix} \Phi_{Rb} & \Phi_{Nb} & \mathrm{G}^{\mathrm{r}}_{bb} \\ \mathbf{0} & \mathbf{0} & \overline{\mathrm{M}}^{-1}_{RR}\Phi^{\mathrm{T}}_{Rb} \\ \mathbf{0} & \mathbf{1} & -\left[\mu_N\Omega^2_N\right]^{-1}\Phi^{\mathrm{T}}_{Nb} \end{bmatrix} \begin{bmatrix} \mathbf{0} & \mathbf{1} & \mathbf{0} \\ \mathbf{0} & \mathbf{0} & \mathbf{1} \\ \mathrm{G}^{\mathrm{r}^{-1}}_{bb} & -\mathrm{G}^{\mathrm{r}^{-1}}_{bb}\Phi_{Rb} & -\mathrm{G}^{\mathrm{r}^{-1}}_{bb}\Phi_{Nb} \end{bmatrix} \begin{Bmatrix} q_b \\ \eta_R \\ \eta_N \end{Bmatrix}
\end{aligned}
$$

$$= \begin{bmatrix} \Phi_{Rb} & \Phi_{Nb} & \mathrm{G}^{\mathrm{r}}_{bb} \\ \Phi_{Ri} & \Phi_{Ni} & \mathrm{G}^{\mathrm{r}}_{ib} \end{bmatrix} \begin{bmatrix} \mathbf{0} & \mathbf{1} & \mathbf{0} \\ \mathbf{0} & \mathbf{0} & \mathbf{1} \\ \mathrm{G}^{\mathrm{r}\,-1}_{bb} & -\mathrm{G}^{\mathrm{r}\,-1}_{bb}\Phi_{Rb} & -\mathrm{G}^{\mathrm{r}\,-1}_{bb}\Phi_{Nb} \end{bmatrix} \begin{Bmatrix} \boldsymbol{q}_b \\ \boldsymbol{\eta}_R \\ \boldsymbol{\eta}_N \end{Bmatrix} \tag{46}$$

$$= \begin{bmatrix} \mathbf{1} & \mathbf{0} & \mathbf{0} \\ \mathrm{G}^{\mathrm{r}}_{ib}\mathrm{G}^{\mathrm{r}\,-1}_{bb} & \Phi_{Ri} - \mathrm{G}^{\mathrm{r}}_{ib}\mathrm{G}^{\mathrm{r}\,-1}_{bb}\Phi_{Rb} & \Phi_{Ni} - \mathrm{G}^{\mathrm{r}}_{ib}\mathrm{G}^{\mathrm{r}\,-1}_{bb}\Phi_{Nb} \end{bmatrix} \begin{Bmatrix} \boldsymbol{q}_b \\ \boldsymbol{\eta}_R \\ \boldsymbol{\eta}_N \end{Bmatrix},$$

where the third equality follows from Equations 43 and 27.

Herting's method is only equivalent to Rubin-Martinez's method for free-interface normal modes. When fixed- or mixed-interface normal modes are used, the transformation matrix is singular due to rows of zeros and the inverse transformation does not exist.

2.5 Fixed-interface methods

2.5.1 Craig-Bampton's method

Craig-Bampton's method is a fixed-interface method based on the approximate dynamic solution in terms of the absolute modal coordinates as formulated in Equation 13. Due to the fixation of the boundary degrees of freedom, there are no rigid-body modes, the boundary partition of the normal modes is zero and the boundary columns of the residual-flexibility matrix vanish, such that the approximate solution in terms of absolute modal coordinates reduces to:

$$\boldsymbol{q} = \Phi_N \boldsymbol{\eta}_N. \tag{47}$$

For this method, the reduced set of coordinates consists of the boundary degrees of freedom $\boldsymbol{q}_b$ and the absolute modal coordinates $\boldsymbol{\eta}_N$. To obtain the modal expansion, Equation 47 is partitioned and premultiplied by the stiffness matrix:

$$\begin{bmatrix} \mathrm{K}_{bb} & \mathrm{K}_{bi} \\ \mathrm{K}_{ib} & \mathrm{K}_{ii} \end{bmatrix} \begin{Bmatrix} \boldsymbol{q}_b \\ \boldsymbol{q}_i \end{Bmatrix} = \begin{bmatrix} \mathrm{K}_{bb} & \mathrm{K}_{bi} \\ \mathrm{K}_{ib} & \mathrm{K}_{ii} \end{bmatrix} \begin{bmatrix} \mathbf{0} \\ \Phi_{Ni} \end{bmatrix} \boldsymbol{\eta}_N, \tag{48}$$

from which it follows that:

$$\boldsymbol{q}_i = -\mathrm{K}^{-1}_{ii}\mathrm{K}_{ib}\boldsymbol{q}_b + \Phi_{Ni}\boldsymbol{\eta}_N. \tag{49}$$

The modal expansion for Craig-Bampton's method [5] can thus be formulated as:

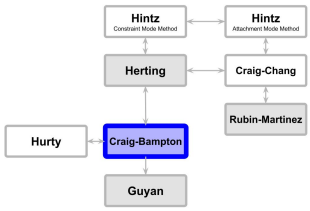

$$\boxed{\begin{Bmatrix} \boldsymbol{q}_b \\ \boldsymbol{q}_i \end{Bmatrix} = \begin{bmatrix} \mathbf{1} & \mathbf{0} \\ \Phi_{Ci} & \Phi_{Ni} \end{bmatrix} \begin{Bmatrix} \boldsymbol{q}_b \\ \boldsymbol{\eta}_N \end{Bmatrix}} \tag{50}$$

Due to the choice of coordinates, the physical boundary is retained in this method. The reduction basis consists of interface constraint modes and fixed-interface normal modes and is thus considered a constraint mode method. The modes are illustrated in Figure 10 for a two-dimensional beam of which the endpoints are boundary points.

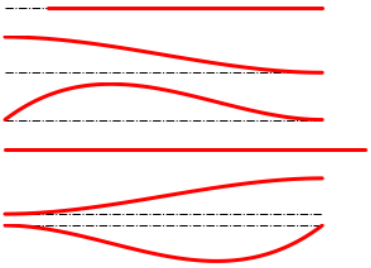

(a) Interface constraint modes

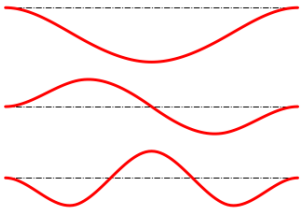

(b) Fixed-interface normal modes

Figure 10: Craig-Bampton's method

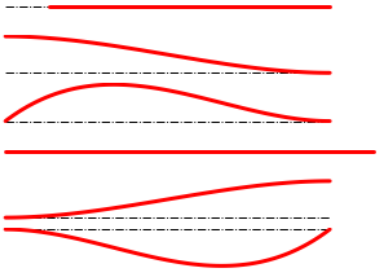

(a) Interface constraint modes

Figure 11: Guyan's method

2.5.1.1 Equivalence to Herting's method [for fixed-interface normal modes]

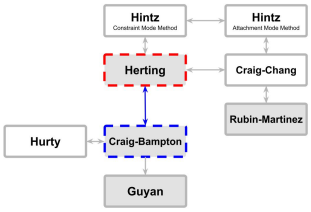

Herting's method reduces to Craig-Bampton's method when fixed-interface normal modes are used [7]. Craig-Bampton's method is thus equivalent to Herting's method for fixed-interface normal modes.

2.5.2 Guyan's method

Craig-Bampton's method reduces to Guyan's method when all fixed-interface normal modes are discarded. For Guyan's method, the set of coordinates thus only consists of the boundary degrees of freedom $\boldsymbol{q}_b$ and the method is also referred to as a static condensation method. The modal expansion for Guyan's method [4] can be formulated as:

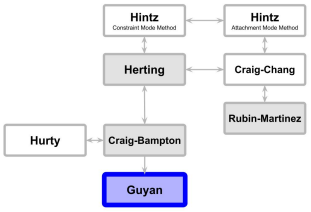

$$\boxed{\begin{Bmatrix} \boldsymbol{q}_b \\ \boldsymbol{q}_i \end{Bmatrix} = \begin{bmatrix} \mathbf{1} \\ \Phi_{Ci} \end{bmatrix} \boldsymbol{q}_b} \tag{51}$$

Due to the choice of coordinates, the physical boundary is retained in this method. The reduction basis consists only of interface constraint modes and thus Guyan's method is considered a constraint mode method. The modes are illustrated in Figure 11 for a two-dimensional beam of which the endpoints are boundary points.

2.5.3 Hurty's method

Hurty's method is a variation to Craig-Bampton's method. It replaces the interface constraint modes by the rigid-body modes and a set of redundant-interface constraint modes. To this end, the boundary degrees of freedom are partitioned into a set of rigid-body boundary degrees of freedom $\boldsymbol{q}_r$ that is just sufficient to describe rigid-body motion and a set of excess boundary degrees of freedom $\boldsymbol{q}_e$. The interface constraint modes corresponding to unit displacements or rotations of the rigid-body boundary degrees of freedom are replaced by rigid-body modes. The remaining interface constraint

modes with corresponding constraint mode coordinates η_C are referred to as redundant-interface constraint modes. The modal expansion for Hurty's method [6] can be expressed as:

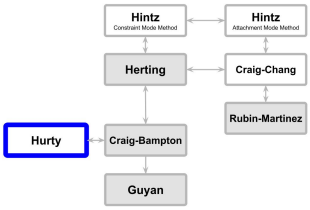

$$\begin{Bmatrix} q_r \\ q_e \\ q_i \end{Bmatrix} = \begin{bmatrix} \Phi_{Rr} & \mathbf{0} & \mathbf{0} \\ \Phi_{Re} & \mathbf{1} & \mathbf{0} \\ \Phi_{Ri} & \Phi_{Cie} & \Phi_{Ni} \end{bmatrix} \begin{Bmatrix} \eta_R \\ \eta_C \\ \eta_N \end{Bmatrix} \tag{52}$$

with

$$\Phi_{Cie} = -\mathrm{K}_{ii}^{-1}\mathrm{K}_{ie}. \tag{53}$$

As opposed to Craig-Bampton's method, the physical boundary is not retained in this method. The reduction basis consists of rigid-body modes, redundant-interface constraint modes and fixed-interface normal modes and is thus considered a constraint mode method. The modes are illustrated in Figure 12 for a two-dimensional beam of which the endpoints are boundary points.

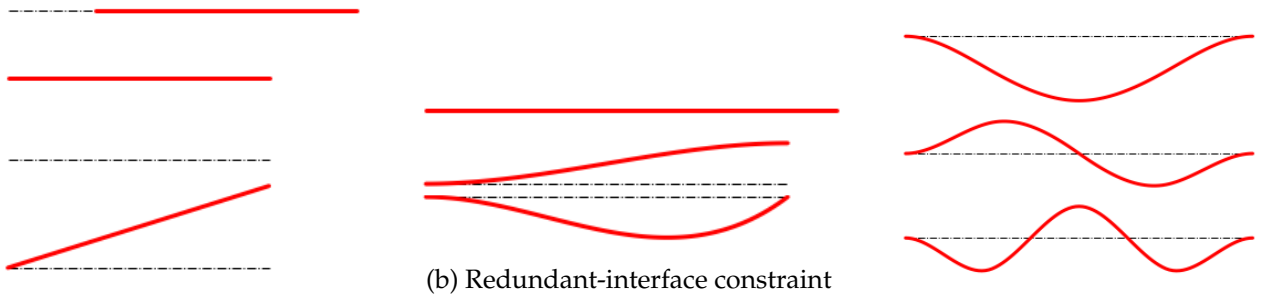

(a) Rigid-body modes

(b) Redundant-interface constraint modes

(c) Fixed-interface normal modes

Figure 12: Hurty's method

2.5.3.1 Equivalence to Craig-Bampton's method

Hurty's method is equivalent to Craig-Bampton's method. From the modal expansion for Hurty's method it follows that both coordinate sets are related as:

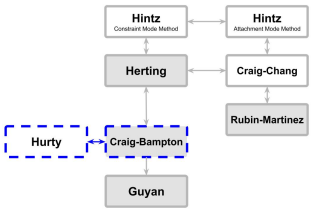

$$\begin{Bmatrix} q_r \\ q_e \\ \eta_N \end{Bmatrix} = \begin{bmatrix} \Phi_{Rr} & \mathbf{0} & \mathbf{0} \\ \Phi_{Re} & \mathbf{1} & \mathbf{0} \\ \mathbf{0} & \mathbf{0} & \mathbf{1} \end{bmatrix} \begin{Bmatrix} \eta_R \\ \eta_C \\ \eta_N \end{Bmatrix} \tag{54}$$

Craig-Bampton Hurty

Substitution of this coordinate transformation in the partitioned form of the modal expansion for Craig-Bampton's method (Equation 50) indeed yields the modal expansion for Hurty's method (Equation 52):

$$\begin{Bmatrix} q_r \\ q_e \\ q_i \end{Bmatrix} = \begin{bmatrix} \mathbf{1} & \mathbf{0} & \mathbf{0} \\ \mathbf{0} & \mathbf{1} & \mathbf{0} \\ \Phi_{Cir} & \Phi_{Cie} & \Phi_{Ni} \end{bmatrix} \begin{Bmatrix} q_r \\ q_e \\ \eta_N \end{Bmatrix}$$

$$
\begin{aligned}
&= \begin{bmatrix} \mathbf{1} & \mathbf{0} & \mathbf{0} \\ \mathbf{0} & \mathbf{1} & \mathbf{0} \\ \Phi_{Cir} & \Phi_{Cie} & \Phi_{Ni} \end{bmatrix} \begin{bmatrix} \Phi_{Rr} & \mathbf{0} & \mathbf{0} \\ \Phi_{Re} & \mathbf{1} & \mathbf{0} \\ \mathbf{0} & \mathbf{0} & \mathbf{1} \end{bmatrix} \begin{Bmatrix} \eta_R \\ \eta_C \\ \eta_N \end{Bmatrix} \\
&= \begin{bmatrix} \Phi_{Rr} & \mathbf{0} & \mathbf{0} \\ \Phi_{Re} & \mathbf{1} & \mathbf{0} \\ \Phi_{Cir}\Phi_{Rr} + \Phi_{Cie}\Phi_{Re} & \Phi_{Cie} & \Phi_{Ni} \end{bmatrix} \begin{Bmatrix} \eta_R \\ \eta_C \\ \eta_N \end{Bmatrix} \\
&= \begin{bmatrix} \Phi_{Rr} & \mathbf{0} & \mathbf{0} \\ \Phi_{Re} & \mathbf{1} & \mathbf{0} \\ \Phi_{Ri} & \Phi_{Cie} & \Phi_{Ni} \end{bmatrix} \begin{Bmatrix} \eta_R \\ \eta_C \\ \eta_N \end{Bmatrix}
\end{aligned}
\tag{55}
$$

where $\Phi_{Cir} = -\mathrm{K}_{ii}^{-1}\mathrm{K}_{ir}$ by definition and $\Phi_{Ri} = \Phi_{Cir}\Phi_{Rr} + \Phi_{Cie}\Phi_{Re}$ follows from the fact that $\mathrm{K}\Phi_R = \mathbf{0}$.

3 The generalised superelement formulation

The first limitation of the superelement formulation that is addressed is that it requires the use of a reduction basis that only contains boundary modes and can thus only be implemented using Guyan's reduction basis. The proposed generalised superelement formulation that allows for the use of a wider range of reduction bases is presented in this Chapter. It can be implemented using any of the reduction bases obtained with the component mode synthesis methods presented in Chapter 2.

The generalised superelement formulation is presented as an alternative to the traditional floating frame formulation. Both are a form of the floating frame formulation that models the motion of a flexible body by making a distinction between its overall rigid-body motion and its local deformations. The corresponding kinematic description is schematically represented in Figure 13.

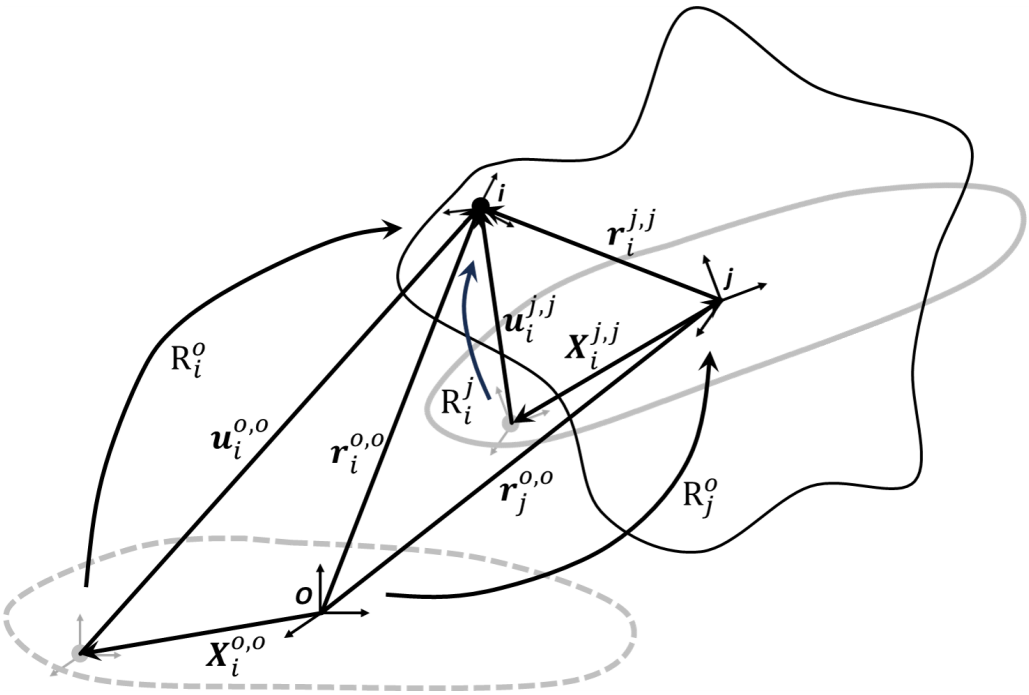

Figure 13: Schematic illustration of kinematic description

The black line represents the current deformed configuration of a body. The original undeformed configuration is represented by the dashed grey line and is described by inertial frame of reference O. The undeformed reference configuration that captures the overall rigid-body motion is represented by the solid grey line and is described by floating frame of reference j.

The global position of the floating frame is represented by position vector $\boldsymbol{r}_j^{o,o}$, where the subscript j refers to the coordinates of the floating frame, the second superscript o indicates that the coordinates are measured relative to the inertial frame and the first superscript o indicates that this vector is expressed in the inertial frame. The global orientation of the floating frame is represented by rotation matrix R_j^o. The variation of the rotation matrix is given by [1]:

$$\delta \mathrm{R}_j^o = \mathrm{R}_j^o \delta \widetilde{\boldsymbol{\theta}}_j^{j,o}, \tag{56}$$

in which $\delta \boldsymbol{\theta}_j^{j,o}$ can be interpreted as the local vector of virtual rotations and the tilde operator is defined by:

$$\boldsymbol{a} = \begin{Bmatrix} a_1 \\ a_2 \\ a_3 \end{Bmatrix} \quad \longrightarrow \quad \widetilde{\boldsymbol{a}} \equiv \begin{bmatrix} 0 & -a_3 & a_2 \\ a_3 & 0 & -a_1 \\ -a_2 & a_1 & 0 \end{bmatrix}. \tag{57}$$

In variational form, the generalised coordinate vector describing the motion of the floating frame is given by:

$$\delta \boldsymbol{q}_j^{o,o} \equiv \begin{Bmatrix} \delta \boldsymbol{r}_j^{o,o} \\ \delta \boldsymbol{\theta}_j^{o,o} \end{Bmatrix}, \tag{58}$$

while the generalised coordinate vector itself has no physical meaning. The generalised coordinates in this vector will be referred to as the global coordinates of the floating frame.

The local deformations in Figure 13 are exaggerated for illustration purposes, but are assumed to be small and are modelled using a linear finite element model. The local position and orientation of node i are represented by:

$$\boldsymbol{r}_i^{j,j} = \boldsymbol{X}_i^{j,j} + \boldsymbol{u}_i^{j,j} \qquad \text{and} \qquad \mathrm{R}_i^j \tag{59}$$

respectively, with $\boldsymbol{X}_i^{j,j}$ its local position in the undeformed configuration and $\boldsymbol{u}_i^{j,j}$ its local displacement. As the local deformations are small, the orientation of node i can alternatively be represented by local rotation vector $\boldsymbol{\theta}_i^{j,j}$. The rotation matrix R_i^j is then a function of this local rotation vector. The local vectors of nodal degrees of freedom are defined as:

$$\boldsymbol{q}^{j,j} \equiv \begin{Bmatrix} \boldsymbol{u}_1^{j,j} \\ \boldsymbol{\theta}_1^{j,j} \\ \vdots \\ \boldsymbol{u}_N^{j,j} \\ \boldsymbol{\theta}_N^{j,j} \end{Bmatrix}; \qquad \boldsymbol{q}_{IP}^{j,j} \equiv \begin{Bmatrix} \boldsymbol{u}_1^{j,j} \\ \boldsymbol{\theta}_1^{j,j} \\ \vdots \\ \boldsymbol{u}_n^{j,j} \\ \boldsymbol{\theta}_n^{j,j} \end{Bmatrix}, \tag{60}$$

where $\boldsymbol{q}^{j,j}$ contains the local displacements and rotations of all N nodes and $\boldsymbol{q}_{IP}^{j,j}$ only contains the local displacements and rotations of the n boundary nodes that are referred to as interface points in the context of the floating frame formulation. All generalised coordinates in these vectors will be referred to as local nodal degrees of freedom.

The linear finite element model is reduced by expressing the local nodal degrees of freedom in terms of a set of local flexible coordinates that correspond to the mode shapes in a selected reduction basis. For the generalised superelement formulation it is required that this reduction basis is able to ...:

- ... describe rigid-body motion;
- ... describe the local nodal degrees of freedom of the interface points independently.

These imposed restrictions are satisfied by all of the reduction bases presented in Chapter 2. It allows the reduction basis to be transformed to a boundary reduction basis Ψ and internal reduction basis Υ, such that the modal expansion can be expressed as:

$$\boldsymbol{q}^{j,j} = \Psi \boldsymbol{q}_{IP}^{j,j} + \Upsilon \boldsymbol{\eta}, \tag{61}$$

in which the local nodal degrees of freedom of the interface points are the local flexible coordinates corresponding to the boundary modes and the internal flexible coordinates $\boldsymbol{\eta}$ are the local flexible

coordinates corresponding to the internal modes.

The global position and orientation of node i are represented by:

$$\boldsymbol{r}_i^{o,o} = \boldsymbol{X}_i^{o,o} + \boldsymbol{u}_i^{o,o} \qquad \text{and} \qquad \mathrm{R}_i^o \tag{62}$$

respectively, with $\boldsymbol{X}_i^{o,o} = \boldsymbol{X}_i^{j,j}$ its position in the undeformed configuration and $\boldsymbol{u}_i^{o,o}$ its global displacement. In variational form, the global vectors of nodal degrees of freedom are defined as:

$$\delta\boldsymbol{q}^{o,o} \equiv \begin{Bmatrix} \delta\boldsymbol{u}_1^{o,o} \\ \delta\boldsymbol{\theta}_1^{o,o} \\ \vdots \\ \delta\boldsymbol{u}_N^{o,o} \\ \delta\boldsymbol{\theta}_N^{o,o} \end{Bmatrix}; \qquad \delta\boldsymbol{q}_{IP}^{o,o} \equiv \begin{Bmatrix} \delta\boldsymbol{u}_1^{o,o} \\ \delta\boldsymbol{\theta}_1^{o,o} \\ \vdots \\ \delta\boldsymbol{u}_n^{o,o} \\ \delta\boldsymbol{\theta}_n^{o,o} \end{Bmatrix}, \tag{63}$$

while the global vectors of nodal degrees of freedom themselves have no physical meaning due to the arbitrarily large global rotations. All generalised coordinates in these vectors will be referred to as global nodal degrees of freedom.

The global position and orientation of node i are related to its local position and orientation and the position and orientation of the floating frame as:

$$\boldsymbol{r}_i^{o,o} = \boldsymbol{r}_j^{o,o} + \mathrm{R}_j^o \boldsymbol{r}_i^{j,j} \qquad \mathrm{R}_i^o = \mathrm{R}_j^o \mathrm{R}_i^j. \tag{64}$$

In the traditional floating frame formulation, the equations of motion are expressed in terms of the global coordinates of the floating frame and the local flexible coordinates that are here assumed to consist of the local nodal degrees of freedom of the interface points and the internal flexible coordinates. In the generalised superelement formulation, the equations of motion are expressed in terms of the global nodal degrees of freedom of the interface points and the internal flexible coordinates.

The equations of motion of a single flexible body in the generalised superelement formulation can be derived from the equations of motion of a single flexible body in the traditional floating frame formulation using a coordinate transformation. This derivation is similar to the derivation of the equations of motion of a single flexible body in the original superelement formulation, as outlined in [1].

In Section 3.1, the equations of motion of a single flexible body and the coupling method to obtain the constrained equations of motion of a flexible multibody system in the traditional floating frame formulation are presented. In Section 3.2, the coordinate transformation is derived with which the equations of motion of a single flexible body in the traditional floating frame formulation can be transformed to the equations of motion of a single flexible body in the generalised superelement formulation. These equations of motion are formulated in Section 3.3, in which also the coupling method for the generalised superelement formulation is outlined and compared to the coupling method in the traditional floating frame formulation. Section 3.4 explains how an arbitrary reduction basis that satisfies the imposed restrictions can be transformed to the boundary and internal reduction basis.

3.1 Traditional floating frame formulation

In the traditional floating frame formulation, the equations of motion are expressed in terms of the global coordinates of the floating frame, the local nodal degrees of freedom of the interface points

and the internal flexible coordinates. In Section 3.1.1 the equations of motion of a single flexible body are presented and in Section 3.1.2 the coupling method is outlined.

3.1.1 Equations of motion of a single flexible body

The equations of motion of a single flexible body in the traditional floating frame formulation can be derived using the principle of virtual work as outlined in [1]. They are given by:

$$\boxed{[\tilde{\mathrm{R}}_j^o]\,\mathrm{M}_{FF}^j\,[\tilde{\mathrm{R}}_o^j]\begin{Bmatrix}\ddot{\boldsymbol{q}}_j^{o,o}\\ \ddot{\boldsymbol{q}}_{IP}^{j,j}\\ \ddot{\boldsymbol{\eta}}\end{Bmatrix}+[\tilde{\mathrm{R}}_j^o]\,\mathrm{C}_{FF}^j\,[\tilde{\mathrm{R}}_o^j]\begin{Bmatrix}\dot{\boldsymbol{q}}_j^{o,o}\\ \dot{\boldsymbol{q}}_{IP}^{j,j}\\ \dot{\boldsymbol{\eta}}\end{Bmatrix}+\mathrm{K}_{FF}^j\begin{Bmatrix}\boldsymbol{q}_j^{o,o}\\ \boldsymbol{q}_{IP}^{j,j}\\ \boldsymbol{\eta}\end{Bmatrix}=[\tilde{\mathrm{R}}_j^o]\,\boldsymbol{f}_{FF}^j} \tag{65}$$

with M_{FF}^j the local mass matrix, C_{FF}^j the local matrix of fictitious forces, K_{FF}^j the local stiffness matrix and $\boldsymbol{f}_{FF}^j$ the local external load vector. The local mass and stiffness matrix can be obtained from the linear finite element model as:

$$\begin{aligned}\mathrm{M}_{FF}^j &= \begin{bmatrix}\Phi_R^{\mathrm{T}}\\ \Psi^{\mathrm{T}}\\ \Upsilon^{\mathrm{T}}\end{bmatrix}\mathrm{M}_{FE}^j\begin{bmatrix}\Phi_R & \Psi & \Upsilon\end{bmatrix}\\ \mathrm{K}_{FF}^j &= \begin{bmatrix}\mathbf{0} & \mathbf{0} & \mathbf{0}\\ \mathbf{0} & \Psi^{\mathrm{T}}\mathrm{K}_{FE}^j\Psi & \Psi^{\mathrm{T}}\mathrm{K}_{FE}^j\Upsilon\\ \mathbf{0} & \Upsilon^{\mathrm{T}}\mathrm{K}_{FE}^j\Psi & \Upsilon^{\mathrm{T}}\mathrm{K}_{FE}^j\Upsilon\end{bmatrix}\end{aligned} \tag{66}$$

with M_{FE}^j and K_{FE}^j the linear finite element mass and stiffness matrix, in which the subscripts FE are now included to distinguish the mass and stiffness matrix in the linear finite element method from those in the floating frame formulation and the superscripts j are now included to indicate that the linear finite element model describes the local flexible behaviour. The rigid-body modes of the deformed body Φ_R are given by:

$$\Phi_R \equiv \begin{bmatrix}\mathbf{1} & -\tilde{\boldsymbol{r}}_1^{j,j}\\ \mathbf{0} & \mathbf{1}\\ & \vdots\\ \mathbf{1} & -\tilde{\boldsymbol{r}}_N^{j,j}\\ \mathbf{0} & \mathbf{1}\end{bmatrix}. \tag{67}$$

The local matrix of fictitious forces C_{FF}^j depends on the angular velocity of the floating frame and the corresponding part of the equations of motion contains quadratic velocity terms. If the body is not rotating at high velocities or, in the case of a slender member, rotating around its own axis, this term can generally be neglected [1]. The local matrix of fictitious forces is therefore not further elaborated on.

The local external load vector can be obtained from the linear finite element model as:

$$\boldsymbol{f}_{FF}^j = \begin{bmatrix}\Phi_R^{\mathrm{T}}\\ \Psi^{\mathrm{T}}\\ \Upsilon^{\mathrm{T}}\end{bmatrix}\boldsymbol{f}_{FE}^j \tag{68}$$

with $\boldsymbol{f}_{FE}^j$ the linear finite element nodal external load vector. The local external load vector contains both loads that are external to the system and constraint loads that are internal to the system, but

external to the body itself.

The local matrices and vectors are transformed to the global matrices and vectors using the assembled rotation matrices given by:

$$\left[\tilde{\mathrm{R}}_j^o\right] \equiv \begin{bmatrix} \mathrm{R}_j^o & \mathbf{0} & \mathbf{0} & \mathbf{0} \\ \mathbf{0} & \mathrm{R}_j^o & \mathbf{0} & \mathbf{0} \\ \mathbf{0} & \mathbf{0} & \mathbf{1} & \mathbf{0} \\ \mathbf{0} & \mathbf{0} & \mathbf{0} & \mathbf{1} \end{bmatrix} \equiv \begin{bmatrix} \left[\mathrm{R}_j^o\right] & \mathbf{0} & \mathbf{0} \\ \mathbf{0} & \mathbf{1} & \mathbf{0} \\ \mathbf{0} & \mathbf{0} & \mathbf{1} \end{bmatrix} = \left[\tilde{\mathrm{R}}_o^j\right]^{\mathrm{T}}. \tag{69}$$

3.1.2 Coupled equations of motion of a flexible multibody system

The motion of the flexible bodies in a flexible multibody system is constrained by the way in which the bodies are connected to each other at the interface points. These constraints can be expressed as a set of constraint equations $C\left(\boldsymbol{q}_{FF}\right) = \mathbf{0}$ in terms of the generalised coordinates of all flexible bodies. Due to the choice of generalised coordinates in terms of which the equations of motion of a single flexible body are expressed in the traditional floating frame formulation, it is in general not possible to solve the constraint equations analytically and express the dependent generalised coordinates in terms of the independent generalised coordinates. This means that a dual coupling method is required to obtain the coupled equations of motion of a flexible multibody system. The coupling method described below is comparable to the dual coupling methods used in dynamic substructuring, such as outlined in [2] or [3].

Let the assembled equations of motion of a flexible multibody system be given by:

$$\mathrm{M}_{FF}\ddot{\boldsymbol{q}}_{FF} + \mathrm{C}_{FF}\dot{\boldsymbol{q}}_{FF} + \mathrm{K}_{FF}\boldsymbol{q}_{FF} = \boldsymbol{f}_{FF,e} + \boldsymbol{f}_{FF,c}, \tag{70}$$

with M_{FF} the assembled block-diagonal system mass matrix containing all global mass matrices, C_{FF} the assembled block-diagonal system matrix of fictitious forces containing all global matrices of fictitious forces, K_{FF} the assembled block-diagonal system stiffness matrix containing all local stiffness matrices and $\boldsymbol{q}_{FF}$ the assembled generalised coordinate vector containing the generalised coordinates of all flexible bodies. The assembled vector of external loads $\boldsymbol{f}_{FF}$ containing the global external load vectors of all bodies is split into a vector $\boldsymbol{f}_{FF,e}$ with the loads external to the system and a vector $\boldsymbol{f}_{FF,c}$ with internal constraint loads.

In the dual coupling method, the assembled equations of motion must be solved for all generalised coordinates and all constraint loads simultaneously. To this end, the constraint loads are expressed in terms of a set of Lagrange multipliers and the system of equations is augmented with an additional set of equations originating from the constraint equations. The full derivation is omitted here, but the resulting equations of motion of the coupled flexible multibody system are given by:

$$\boxed{\begin{bmatrix} \mathrm{M}_{FF} & C_q^{\mathrm{T}} \\ C_q & \mathbf{0} \end{bmatrix} \begin{Bmatrix} \ddot{\boldsymbol{q}}_{FF} \\ \boldsymbol{\lambda} \end{Bmatrix} = \begin{Bmatrix} \boldsymbol{f}_{FF,e} - \mathrm{K}_{FF}\boldsymbol{q}_{FF} - \mathrm{C}_{FF}\dot{\boldsymbol{q}}_{FF} \\ \boldsymbol{\gamma} \end{Bmatrix}} \tag{71}$$

with $\boldsymbol{\lambda}$ the vector of Lagrange multipliers. The matrix C_q is the Jacobian of the constraint equations given by:

$$C_q = \frac{\partial C}{\partial \boldsymbol{q}_{FF}} \tag{72}$$

and the vector $\boldsymbol{\gamma}$ is given by:

$$\gamma = -\left(\left[C_q \dot{\boldsymbol{q}}_{FF}\right]_q \dot{\boldsymbol{q}}_{FF} + 2C_{qt}\dot{\boldsymbol{q}}_{FF} + C_{tt}\right) \tag{73}$$

where the subscript $\boldsymbol{q}$ denotes differentiation with respect to $\boldsymbol{q}_{FF}$ and the subscript t denotes differentiation with respect to time.

3.2 Coordinate transformation

The generalised superelement formulation requires a coordinate transformation that relates the global nodal degrees of freedom of the interface points and the internal flexible coordinates to the global coordinates of the floating frame, the local nodal degrees of freedom of the interface points and the internal flexible coordinates. This coordinate transformation allows the overall rigid-body motion to be separated from the local deformations and enables the transformation of the equations of motion of a single flexible body in the traditional floating frame formulation to the equations of motion of a single flexible body in the generalised superelement formulation.

The geometric nonlinearities in the rotation matrix require the coordinate transformation to be expressed in variational form. It is derived from (1) a set of kinematic relations that express the variations of the global nodal degrees of freedom of the interface points in terms of the variations of the local nodal degrees of freedom of the interface points and the variations of the global coordinates of the floating frame and (2) a set of relations referred to as the floating frame constraints that define how the floating frame moves along with the body.

The required kinematic relations are derived in [1] and are given by:

$$\delta \boldsymbol{q}_{IP}^{o,o} = \left[\bar{\mathrm{R}}_j^o\right] \delta \boldsymbol{q}_{IP}^{j,j} + \left[\bar{\mathrm{R}}_j^o\right] \Phi_r \left[\mathrm{R}_o^j\right] \delta \boldsymbol{q}_j^{o,o} \tag{74}$$

with

$$\left[\bar{\mathrm{R}}_j^o\right] \equiv \begin{bmatrix} \left[\mathrm{R}_j^o\right] & & \\ & \ddots & \\ & & \left[\mathrm{R}_j^o\right] \end{bmatrix} \tag{75}$$

and

$$\Phi_r \equiv \begin{bmatrix} \mathbf{1} & -\tilde{\boldsymbol{r}}_1^{j,j} \\ \mathbf{0} & \mathbf{1} \\ & \vdots \\ \mathbf{1} & -\tilde{\boldsymbol{r}}_n^{j,j} \\ \mathbf{0} & \mathbf{1} \end{bmatrix} \tag{76}$$

the interface rigid-body modes.

Uniquely defining the reverse kinematic relations requires the formulation of the floating frame constraints. In the generalised superelement formulation these are defined by requiring the floating frame to remain rigidly attached to a single material point and thus the local elastic deformations at the location of the floating frame must vanish. Using the modal expansion in Equation 61, this can mathematically be expressed in variational form as:

$$\Psi_{FF} \delta \boldsymbol{q}_{IP}^{j,j} + \Upsilon_{FF} \delta \boldsymbol{\eta} = \mathbf{0}, \tag{77}$$

in which Ψ_{FF} and Υ_{FF} represent the boundary and internal reduction bases evaluated at the location of the floating frame. This requirement can in general only be satisfied if the reduction basis is able to describe rigid-body motion and hence this restriction is imposed on the reduction basis.

Using the floating frame constraints in Equation 77, the kinematic relations in Equation 74 can be inverted to obtain the required coordinate transformation. As this only requires standard algebraic manipulations, the details are omitted here. For the sake of completeness, the full derivation can be found in Appendix A. The resulting coordinate transformation is given by:

$$\boxed{\begin{Bmatrix} \delta \boldsymbol{q}_j^{o,o} \\ \delta \boldsymbol{q}_{IP}^{j,j} \\ \delta \boldsymbol{\eta} \end{Bmatrix} = \begin{bmatrix} \left[\mathrm{R}_j^o\right] & \mathbf{0} & \mathbf{0} \\ \mathbf{0} & \mathbf{1} & \mathbf{0} \\ \mathbf{0} & \mathbf{0} & \mathbf{1} \end{bmatrix} \begin{bmatrix} \mathrm{Z} & \mathrm{Z}_{int} \\ \mathrm{T} & \mathrm{T}_{int} \\ \mathbf{0} & \mathbf{1} \end{bmatrix} \begin{bmatrix} \left[\bar{\mathrm{R}}_o^j\right] & \mathbf{0} \\ \mathbf{0} & \mathbf{1} \end{bmatrix} \begin{Bmatrix} \delta \boldsymbol{q}_{IP}^{o,o} \\ \delta \boldsymbol{\eta} \end{Bmatrix} = \mathrm{A} \begin{Bmatrix} \delta \boldsymbol{q}_{IP}^{o,o} \\ \delta \boldsymbol{\eta} \end{Bmatrix}} \tag{78}$$

with

$$\begin{aligned} \mathrm{Z} &\equiv \left(\Psi_{FF}\Phi_r\right)^{-1}\Psi_{FF} \\ \mathrm{Z}_{int} &\equiv \left(\Psi_{FF}\Phi_r\right)^{-1}\Upsilon_{FF} \end{aligned} \tag{79}$$

and

$$\begin{aligned} \mathrm{T} &\equiv \mathbf{1} - \Phi_r \mathrm{Z} \\ \mathrm{T}_{int} &\equiv -\Phi_r \mathrm{Z}_{int} \end{aligned} \tag{80}$$

the local transformation matrices and A the total transformation matrix.

3.3 Generalised superelement formulation

In the generalised superelement formulation, the equations of motion are expressed in terms of the global nodal degrees of freedom of the interface points and the internal flexible coordinates. In Section 3.3.1 the equations of motion of a single flexible body in the generalised superelement formulation are derived from the equations of motion of a single flexible body in the traditional floating frame formulation and the coordinate transformation. In Section 3.3.2 the coupling method that is suitable for the generalised superelement formulation is described.

3.3.1 Equations of motion of a single flexible body

The equations of motion of a single flexible body in the traditional floating frame formulation (Equation 65) can be transformed to the equations of motion of a single flexible body in the generalised superelement formulation using the coordinate transformation (Equation 78). Although the coordinate transformation is expressed in variational form, a similar approach can be followed to obtain expressions for the generalised velocities and accelerations:

$$\begin{aligned} \begin{Bmatrix} \dot{\boldsymbol{q}}_j^{o,o} \\ \dot{\boldsymbol{q}}_{IP}^{j,j} \\ \dot{\boldsymbol{\eta}} \end{Bmatrix} &= \mathrm{A} \begin{Bmatrix} \dot{\boldsymbol{q}}_{IP}^{o,o} \\ \dot{\boldsymbol{\eta}} \end{Bmatrix} \\ \begin{Bmatrix} \ddot{\boldsymbol{q}}_j^{o,o} \\ \ddot{\boldsymbol{q}}_{IP}^{j,j} \\ \ddot{\boldsymbol{\eta}} \end{Bmatrix} &= \mathrm{A} \begin{Bmatrix} \ddot{\boldsymbol{q}}_{IP}^{o,o} \\ \ddot{\boldsymbol{\eta}} \end{Bmatrix} + \dot{\mathrm{A}} \begin{Bmatrix} \dot{\boldsymbol{q}}_{IP}^{o,o} \\ \dot{\boldsymbol{\eta}} \end{Bmatrix}. \end{aligned} \tag{81}$$

Substitution into Equation 65 and premultiplication by A^{T} yields the equations of motion of a single flexible body in the generalised superelement formulation:

$$\boxed{\left[\hat{\mathrm{R}}_j^o\right]\mathrm{M}_{GS}^j\left[\hat{\mathrm{R}}_o^j\right]\begin{Bmatrix}\ddot{\boldsymbol{q}}_{IP}^{o,o}\\ \ddot{\boldsymbol{\eta}}\end{Bmatrix}+\mathrm{C}_{GS}^o\begin{Bmatrix}\dot{\boldsymbol{q}}_{IP}^{o,o}\\ \dot{\boldsymbol{\eta}}\end{Bmatrix}+\left[\hat{\mathrm{R}}_j^o\right]\mathrm{K}_{GS}^j\begin{Bmatrix}\boldsymbol{q}_{IP}^{j,j}\\ \boldsymbol{\eta}\end{Bmatrix}=\left[\hat{\mathrm{R}}_j^o\right]\boldsymbol{f}_{GS}^j} \tag{82}$$

with M_{GS}^j the local mass matrix, C_{GS}^o the global matrix of fictitious forces, K_{GS}^j the local stiffness matrix and $\boldsymbol{f}_{GS}^j$ the local external load vector. It must be noted that the transformation has only been applied to the generalised velocities and accelerations, while the stiffness term is still expressed in terms of the local nodal degrees of freedom of the interface points. The local mass and stiffness matrix are given by:

$$\begin{aligned}\mathrm{M}_{GS}^j&=\begin{bmatrix}\mathrm{Z}^{\mathrm{T}} & \mathrm{T}^{\mathrm{T}} & \mathbf{0}\\ \mathrm{Z}_{int}^{\mathrm{T}} & \mathrm{T}_{int}^{\mathrm{T}} & \mathbf{1}\end{bmatrix}\begin{bmatrix}\Phi_R^{\mathrm{T}}\\ \Psi^{\mathrm{T}}\\ \Upsilon^{\mathrm{T}}\end{bmatrix}\mathrm{M}_{FE}^j\begin{bmatrix}\Phi_R & \Psi & \Upsilon\end{bmatrix}\begin{bmatrix}\mathrm{Z} & \mathrm{Z}_{int}\\ \mathrm{T} & \mathrm{T}_{int}\\ \mathbf{0} & \mathbf{1}\end{bmatrix}\\ \mathrm{K}_{GS}^j&=\begin{bmatrix}\mathrm{T}^{\mathrm{T}} & \mathbf{0}\\ \mathrm{T}_{int}^{\mathrm{T}} & \mathbf{1}\end{bmatrix}\begin{bmatrix}\Psi^{\mathrm{T}}\mathrm{K}_{FE}^j\Psi & \Psi^{\mathrm{T}}\mathrm{K}_{FE}^j\Upsilon\\ \Upsilon^{\mathrm{T}}\mathrm{K}_{FE}^j\Psi & \Upsilon^{\mathrm{T}}\mathrm{K}_{FE}^j\Upsilon\end{bmatrix}.\end{aligned} \tag{83}$$

The global matrix of fictitious forces is given by:

$$\mathrm{C}_{GS}^o=\mathrm{A}^{\mathrm{T}}\left(\left[\tilde{\mathrm{R}}_j^o\right]\mathrm{M}_{FF}^j\left[\tilde{\mathrm{R}}_o^j\right]\dot{\mathrm{A}}+\left[\tilde{\mathrm{R}}_j^o\right]\mathrm{C}_{FF}^j\left[\tilde{\mathrm{R}}_o^j\right]\mathrm{A}\right). \tag{84}$$

The quadratic velocity term containing this matrix can often be neglected for the same reason as in the traditional floating frame formulation and thus the global matrix of fictitious forces will not be further elaborated on.

The local external load vector is given by:

$$\boldsymbol{f}_{GS}^j=\begin{bmatrix}\mathrm{Z}^{\mathrm{T}} & \mathrm{T}^{\mathrm{T}} & \mathbf{0}\\ \mathrm{Z}_{int}^{\mathrm{T}} & \mathrm{T}_{int}^{\mathrm{T}} & \mathbf{1}\end{bmatrix}\begin{bmatrix}\Phi_R^{\mathrm{T}}\\ \Psi^{\mathrm{T}}\\ \Upsilon^{\mathrm{T}}\end{bmatrix}\boldsymbol{f}_{FE}^j. \tag{85}$$

This local external load vector again contains both loads that are external to the system and constraint loads that are internal to the system, but external to the body itself.

The local matrices and vectors are transformed to the global matrices and vectors using the assembled rotation matrix:

$$\left[\hat{\mathrm{R}}_j^o\right]\equiv\begin{bmatrix}\left[\bar{\mathrm{R}}_j^o\right] & \mathbf{0}\\ \mathbf{0} & \mathbf{1}\end{bmatrix}=\left[\hat{\mathrm{R}}_o^j\right]^{\mathrm{T}}. \tag{86}$$

3.3.2 Coupled equations of motion of a flexible multibody system

Whereas the coupling of a flexible multibody system in the traditional floating frame formulation requires a dual coupling method with Lagrange multipliers, the coupling of a flexible multibody system in the generalised superelement formulation can be achieved by a primal coupling method due to the convenient selection of the generalised coordinates in terms of which the equations of motion of a single flexible body are expressed. The coupling method described below is comparable to the

primal coupling methods used in dynamic substructuring, such as outlined in [2] or [3].

Let the assembled equations of motion of a flexible multibody system be given by:

$$\mathrm{M}_{GS}\ddot{\boldsymbol{q}}^{o}_{GS} + \mathrm{C}_{GS}\dot{\boldsymbol{q}}^{o}_{GS} + \mathrm{K}_{GS}\boldsymbol{q}^{j}_{GS} = \boldsymbol{f}_{GS,e} + \boldsymbol{f}_{GS,c}, \tag{87}$$

with M_{GS} the assembled block-diagonal system mass matrix containing all global mass matrices, C_{GS} the assembled block-diagonal system matrix of fictitious forces containing all global matrices of fictitious forces, K_{GS} the assembled block-diagonal system stiffness matrix containing all stiffness matrices, $\boldsymbol{q}^{o}_{GS}$ the assembled global generalised coordinate vector containing the global nodal degrees of freedom of the interface points and internal flexible coordinates of each body and $\boldsymbol{q}^{j}_{GS}$ the assembled local generalised coordinate vector containing the local nodal degrees of freedom of the interface points and internal flexible coordinates of each body. The assembled vector of external loads $\boldsymbol{f}_{GS}$ containing the global external load vectors of all bodies is split into a vector $\boldsymbol{f}_{GS,e}$ with the loads external to the system and a vector $\boldsymbol{f}_{GS,c}$ with internal constraint loads.

Due to the convenient selection of generalised coordinates, the constraints can be formulated as:

$$\delta\boldsymbol{q}^{o}_{GS} = \mathrm{H}\delta\boldsymbol{p}, \tag{88}$$

with H the constraint localisation matrix that depends on the specific way in which the flexible multibody system is constrained and $\boldsymbol{p}$ a vector of independent generalised coordinates that can contain both elements of $\boldsymbol{q}^{o}_{GS}$ and newly introduced (relative) coordinates. A similar relation can be found for the velocities and accelerations:

$$\begin{aligned} \dot{\boldsymbol{q}}^{o}_{GS} &= \mathrm{H}\dot{\boldsymbol{p}} \\ \ddot{\boldsymbol{q}}^{o}_{GS} &= \mathrm{H}\ddot{\boldsymbol{p}} + \dot{\mathrm{H}}\dot{\boldsymbol{p}}. \end{aligned} \tag{89}$$

Since the virtual work done by the constraint loads must be zero for any virtual displacement vector $\delta\boldsymbol{p}$, it also follows that:

$$\mathrm{H}^{\mathrm{T}}\boldsymbol{f}_{GS,c} = \boldsymbol{0}. \tag{90}$$

Substitution of Equations 89 and 90 into Equation 87 yields the coupled equations of motion of the flexible multibody system:

$$\boxed{\mathrm{H}^{\mathrm{T}}\mathrm{M}_{GS}\mathrm{H}\ddot{\boldsymbol{p}} = \mathrm{H}^{\mathrm{T}}\left(\boldsymbol{f}_{GS,e} - \left(\mathrm{M}_{GS}\dot{\mathrm{H}} + \mathrm{C}_{GS}\mathrm{H}\right)\dot{\boldsymbol{p}} - \mathrm{K}_{GS}\boldsymbol{q}^{j}_{GS}\right)} \tag{91}$$

3.4 Boundary and internal reduction basis

The generalised superelement formulation requires the reduction basis to be transformed to a boundary and internal reduction basis with the corresponding modal expansion as given in Equation 61. To obtain the boundary and internal reduction bases, the original reduction basis is separated into a preliminary boundary reduction basis $\widehat{\Psi}$ containing $6n$ modes with which the local nodal degrees of freedom of the interface points can be described independently and a preliminary internal reduction basis $\widehat{\Upsilon}$ containing the remaining modes. This separation is only possible if the reduction basis is able to describe the local nodal degrees of freedom of the interface points independently and hence this restriction is imposed on the reduction basis. The local nodal degrees of freedom can then be expressed in terms of the preliminary boundary flexible coordinates $\boldsymbol{\zeta}$ and internal flexible coordinates $\boldsymbol{\eta}$ as:

$$\boldsymbol{q}^{j,j} = \widehat{\Psi}\boldsymbol{\zeta} + \widehat{\Upsilon}\boldsymbol{\eta}. \tag{92}$$

Evaluating this at the interface points yields:

$$\boldsymbol{q}_{IP}^{j,j} = \widehat{\Psi}_{IP}\boldsymbol{\zeta} + \widehat{\Upsilon}_{IP}\boldsymbol{\eta}, \tag{93}$$

with $\widehat{\Psi}_{IP}$ and $\widehat{\Upsilon}_{IP}$ the preliminary boundary and internal reduction bases evaluated at the interface points. Since the preliminary boundary reduction basis is able to describe the local nodal degrees of freedom of the interface points independently, the matrix $\widehat{\Psi}_{IP}$ is full rank and can thus be inverted to give:

$$\boldsymbol{\zeta} = \widehat{\Psi}_{IP}^{-1}\left(\boldsymbol{q}_{IP}^{j,j} - \widehat{\Upsilon}_{IP}\boldsymbol{\eta}\right). \tag{94}$$

Back substitution into Equation 92 yields:

$$\begin{aligned}\boldsymbol{q}^{j,j} &= \widehat{\Psi}\widehat{\Psi}_{IP}^{-1}\boldsymbol{q}_{IP}^{j,j} + \left(\widehat{\Upsilon} - \widehat{\Psi}\widehat{\Psi}_{IP}^{-1}\widehat{\Upsilon}_{IP}\right)\boldsymbol{\eta} \\ &= \Psi\boldsymbol{q}_{IP}^{j,j} + \Upsilon\boldsymbol{\eta}.\end{aligned} \tag{95}$$

The boundary and internal reduction bases are thus defined as:

$$\boxed{\begin{aligned}\Psi &= \widehat{\Psi}\widehat{\Psi}_{IP}^{-1} \\ \Upsilon &= \widehat{\Upsilon} - \widehat{\Psi}\widehat{\Psi}_{IP}^{-1}\widehat{\Upsilon}_{IP}\end{aligned}} \tag{96}$$

For component mode synthesis methods that retain the physical boundary it holds that the reduction basis can directly be separated into a boundary and internal reduction basis and no transformation is required.

4 The nonlinear floating frame formulation

The second limitation of the superelement formulation that is addressed is that its applicability is limited to problems in which the local deformations remain small. The proposed nonlinear floating frame formulation that allows for arbitrarily large local deformations is presented in this Chapter. It can be considered a nonlinear extension of both the superelement floating frame formulation and the co-rotational nonlinear finite element formulation. The nonlinear floating frame formulation as proposed here is a contribution to a paper in preparation [28].

The nonlinear floating frame formulation is based on the same principles as the generalised superelement formulation as presented in Chapter 3. Both model the motion of a flexible body or element by making a distinction between its overall rigid-body motion and its local deformations and both express the governing equations in the global frame of reference. However, also some differences can be identified. First of all, the nonlinear floating frame formulation models the local flexible behaviour using a nonlinear model that is not reduced and therefore no distinction is made between the nodal degrees of freedom of the interface points and those of the interior nodes. Secondly, the nonlinear floating frame formulation is formulated for the use of continuum elements that only have translational and no rotational degrees of freedom. Lastly, the focus of the nonlinear floating frame formulation as presented here is on obtaining the internal load vector and tangent stiffness matrix of a single flexible body rather than its full equations of motion.

The nonlinear floating frame formulation is presented as an alternative to the total and updated Lagrangian nonlinear finite element formulations, henceforth simply referred to as the nonlinear finite element method. Both model the motion of a flexible body by discretising it using a finite element mesh. In the nonlinear floating frame formulation a distinction is made between the overall rigid-body motion of a body or element and its local deformations. In the nonlinear finite element method no such distinction is made. The kinematic description corresponding to both formulations is schematically represented in Figure 14.

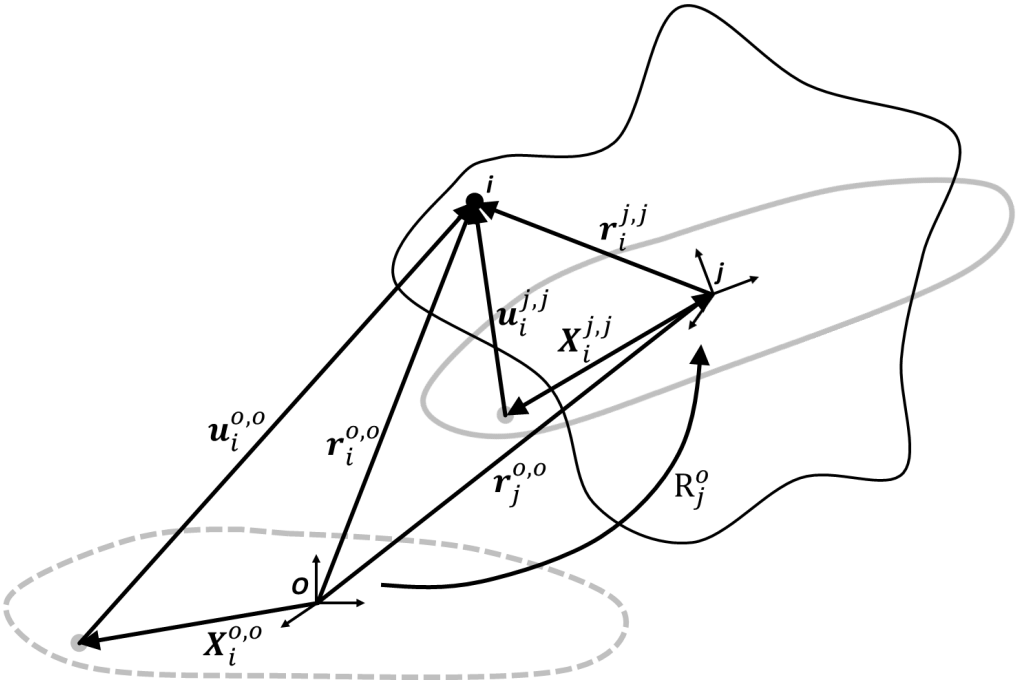

Figure 14: Schematic illustration of kinematic description

The black line represents the current deformed configuration, which can be either that of an entire body or that of an individual element. The original undeformed configuration is represented by the dashed grey line and is described by global frame of reference O. The undeformed reference configuration that captures the overall rigid-body motion is represented by the solid grey line and is described by floating frame of reference j.

As in the generalised superelement formulation, the global position and orientation of the floating frame are represented by position vector $\boldsymbol{r}_j^{o,o}$ and rotation matrix R_j^o respectively. In variational form, the generalised coordinate vector describing the motion of the floating frame is again given by:

$$\{\delta \boldsymbol{q}_j^{o,o}\} \equiv \begin{Bmatrix} \delta \boldsymbol{r}_j^{o,o} \\ \delta \boldsymbol{\theta}_j^{o,o} \end{Bmatrix}, \tag{97}$$

while the generalised coordinate vector itself has no physical meaning. The generalised coordinates in this vector will be referred to as the global coordinates of the floating frame.

The local position of node i is described by its local position vector:

$$\boldsymbol{r}_i^{j,j} = \boldsymbol{X}_i^{j,j} + \boldsymbol{u}_i^{j,j}, \tag{98}$$

with $\boldsymbol{X}_i^{j,j}$ its local position in the undeformed configuration and $\boldsymbol{u}_i^{j,j}$ its arbitrarily large local displacement. As the nonlinear floating frame formulation is formulated for continuum elements that only have translational degrees of freedom, the rotations of node i are not considered. The continuous local displacement field $\boldsymbol{u}^{j,j} = \boldsymbol{u}^{j,j}(\boldsymbol{x})$ is a function of the material coordinates $\boldsymbol{x}$. It is assumed that the local displacement field can be obtained by interpolating the local nodal displacements as:

$$\boldsymbol{u}^{j,j} = N_i \boldsymbol{u}_i^{j,j}, \tag{99}$$

in which, as throughout this Chapter on the nonlinear floating frame formulation, the Einstein summation convention is applied and N_i is the continuous finite element interpolation function corresponding to node i. The local vector of nodal degrees of freedom is defined as:

$$\{\boldsymbol{q}^{j,j}\} = \begin{Bmatrix} \boldsymbol{u}_1^{j,j} \\ \vdots \\ \boldsymbol{u}_N^{j,j} \end{Bmatrix}, \tag{100}$$

with N the total number of nodes in the body or element. All generalised coordinates in this vector will be referred to as local nodal degrees of freedom. Using this definition, the discretisation of the local displacement field can also be expressed in matrix-vector form as:

$$\boldsymbol{u}^{j,j} = [\mathrm{N}]\{\boldsymbol{q}^{j,j}\} \tag{101}$$

with

$$[\mathrm{N}] = \begin{bmatrix} N_1 & 0 & 0 & & N_N & 0 & 0 \\ 0 & N_1 & 0 & \dots & 0 & N_N & 0 \\ 0 & 0 & N_1 & & 0 & 0 & N_N \end{bmatrix}. \tag{102}$$

The global position of node i is described by its global position vector:

$$\boldsymbol{r}_i^{o,o} = \boldsymbol{X}_i^{o,o} + \boldsymbol{u}_i^{o,o}, \tag{103}$$

with $\boldsymbol{X}_i^{o,o} = \boldsymbol{X}_i^{j,j}$ its position in the undeformed configuration and $\boldsymbol{u}_i^{o,o}$ its global displacement. The global vector of nodal degrees of freedom is defined as:

$$\{\boldsymbol{q}^{o,o}\} = \begin{Bmatrix} \boldsymbol{u}_1^{o,o} \\ \vdots \\ \boldsymbol{u}_N^{o,o} \end{Bmatrix}. \tag{104}$$

All generalised coordinates in this vector will be referred to as global nodal degrees of freedom. It is assumed that also the global displacement field $\boldsymbol{u}^{o,o} = \boldsymbol{u}^{o,o}(\boldsymbol{x})$ can be obtained by interpolating the global nodal degrees of freedom and thus the discretisation of the global displacement field is given by:

$$\boldsymbol{u}^{o,o} = N_i \boldsymbol{u}_i^{o,o} = [\mathrm{N}]\{\boldsymbol{q}^{o,o}\}. \tag{105}$$

The global position of node i is again related to its local position and the global position and orientation of the floating frame as:

$$\boldsymbol{r}_i^{o,o} = \boldsymbol{r}_j^{o,o} + \mathrm{R}_j^o \boldsymbol{r}_i^{j,j}. \tag{106}$$

In the nonlinear finite element method, the motion of a flexible body is described in terms of its global nodal degrees of freedom. In the nonlinear floating frame formulation, the motion of a flexible body or element is described in terms of the global position and orientation of its floating frame and its local nodal degrees of freedom.

The nonlinear floating frame formulation as presented here is concerned with obtaining the internal load vector and tangent stiffness matrix that can be used in incremental solution procedures to model the static or dynamic behaviour of a single flexible body. The global internal load vector $\{\boldsymbol{Q}^o\}$ is dual to the global vector of nodal degrees of freedom. The local internal load vector $\{\boldsymbol{Q}^j\}$ is dual to the local vector of nodal degrees of freedom. They are defined by:

$$\delta W_{int} = \{\delta \boldsymbol{q}^{o,o}\}^{\mathrm{T}} \{\boldsymbol{Q}^o\} \tag{107}$$

$$\delta W_{int} = \{\delta \boldsymbol{q}^{j,j}\}^{\mathrm{T}} \{\boldsymbol{Q}^j\} \tag{108}$$

with δW_{int} the internal virtual work that is invariant under rigid-body motion and is thus equal in the global and the local frame. The global tangent stiffness matrix $[\mathrm{K}_t^o]$ and the local tangent stiffness matrix $[\mathrm{K}_t^j]$ are defined by:

$$\{\delta \boldsymbol{Q}^o\} = [\mathrm{K}_t^o]\{\delta \boldsymbol{q}^{o,o}\} \tag{109}$$

$$\{\delta \boldsymbol{Q}^j\} = [\mathrm{K}_t^j]\{\delta \boldsymbol{q}^{j,j}\}. \tag{110}$$

In the nonlinear finite element method, the global internal load vector and tangent stiffness matrix are computed from the global nodal degrees of freedom. In the nonlinear floating frame formulation, the local internal load vector and tangent stiffness matrix are computed from the local nodal degrees of freedom.

Both the nonlinear finite element method and the nonlinear floating frame formulation express the governing equations in the global frame. In the nonlinear finite element method, the global internal load vector and tangent stiffness matrix are computed directly from the global nodal degrees of freedom. In the nonlinear floating frame formulation, (1) the local nodal degrees of freedom are extracted

from the global nodal degrees of freedom, (2) the local internal load vector and tangent stiffness matrix are computed from the local nodal degrees of freedom and (3) the local internal load vector and tangent stiffness matrix are transformed back to the global frame.

In Section 4.1, the coordinate transformation is derived with which the global position and orientation of the floating frame and the local nodal degrees of freedom can be obtained from the global nodal degrees of freedom in the nonlinear floating frame formulation. In Section 4.2, expressions are derived that can be used to compute the global internal load vector and tangent stiffness matrix from the global nodal degrees of freedom in the nonlinear finite element method and to compute the local internal load vector and tangent stiffness matrix from the local nodal degrees of freedom in the nonlinear floating frame formulation. In Section 4.3, the transformation is derived by which the internal load vector and tangent stiffness matrix can be transformed from the local to the global frame in the nonlinear floating frame formulation.

The derivations in this Chapter apply to three-dimensional problems. The derivations for one- and two-dimensional problems are similar. An overview is presented in Appendix B, C and D.

4.1 Coordinate transformation

The nonlinear floating frame formulation requires a coordinate transformation that relates the global nodal degrees of freedom to the global coordinates of the floating frame and the local nodal degrees of freedom. This coordinate transformation can be performed both at the body and at the element level and allows the overall rigid-body motion to be separated from the local deformations.

The geometric nonlinearities in the rotation matrix require the coordinate transformation to be expressed in variational form. It is derived from (1) a set of kinematic relations that express the variations of the global nodal degrees of freedom in terms of the variations of the local nodal degrees of freedom and the variations of the global coordinates of the floating frame and (2) a set of relations referred to as the floating frame constraints that define how the floating frame moves along with the body or element. The combined set of equations can then be inverted to obtain expressions for (1) the variations of the global coordinates of the floating frame and (2) the variations of the local nodal degrees of freedom, both in terms of the global nodal degrees of freedom.

The kinematic relations are obtained by first considering the kinematics of a single node i. Using Equations 56, 98, 103 and 106, the variation in its global displacement can be expressed as:

$$\begin{aligned}
\delta \boldsymbol{u}_i^{o,o} = \delta \boldsymbol{r}_i^{o,o} &= \delta \boldsymbol{r}_j^{o,o} + \mathrm{R}_j^o \delta \boldsymbol{r}_i^{j,j} + \mathrm{R}_j^o \delta \widetilde{\boldsymbol{\theta}}_j^{j,o} \boldsymbol{r}_i^{j,j} \\
&= \delta \boldsymbol{r}_j^{o,o} + \mathrm{R}_j^o \delta \boldsymbol{u}_i^{j,j} - \mathrm{R}_j^o \widetilde{\boldsymbol{r}}_i^{j,j} \delta \boldsymbol{\theta}_j^{j,o} \\
&= \delta \boldsymbol{r}_j^{o,o} + \mathrm{R}_j^o \delta \boldsymbol{u}_i^{j,j} - \mathrm{R}_j^o \widetilde{\boldsymbol{r}}_i^{j,j} \mathrm{R}_o^j \delta \boldsymbol{\theta}_j^{o,o} = \mathrm{R}_j^o \delta \boldsymbol{u}_i^{j,j} + \mathrm{R}_j^o \begin{bmatrix} \mathbf{1} & -\widetilde{\boldsymbol{r}}_i^{j,j} \end{bmatrix} \begin{bmatrix} \mathrm{R}_o^j & \mathbf{0} \\ \mathbf{0} & \mathrm{R}_o^j \end{bmatrix} \begin{Bmatrix} \delta \boldsymbol{r}_j^{o,o} \\ \delta \boldsymbol{\theta}_j^{o,o} \end{Bmatrix}.
\end{aligned} \tag{111}$$

Application of the definitions in Equations 97, 100 and 104 then results in the required kinematic relations:

$$\boxed{\{\delta\boldsymbol{q}^{o,o}\} = [\overline{\mathrm{R}}_j^o]\{\delta\boldsymbol{q}^{j,j}\} + [\overline{\mathrm{R}}_j^o][\Phi_R][\mathrm{R}_o^j]\{\delta\boldsymbol{q}_j^{o,o}\}}$$

$$[\mathrm{R}_j^o] \equiv \begin{bmatrix} \mathrm{R}_j^o & \mathbf{0} \\ \mathbf{0} & \mathrm{R}_j^o \end{bmatrix} = [\mathrm{R}_o^j]^{\mathrm{T}}; \quad [\overline{\mathrm{R}}_j^o] \equiv \begin{bmatrix} \mathrm{R}_j^o & & \\ & \ddots & \\ & & \mathrm{R}_j^o \end{bmatrix} = [\overline{\mathrm{R}}_o^j]^{\mathrm{T}}; \quad [\Phi_R] \equiv \begin{bmatrix} \mathbf{1} & -\tilde{\boldsymbol{r}}_1^{j,j} \\ & \vdots \\ \mathbf{1} & -\tilde{\boldsymbol{r}}_N^{j,j} \end{bmatrix} \tag{112}$$

Uniquely defining the reverse kinematic relations requires the formulation of the floating frame constraints. In the nonlinear floating frame formulation these are defined by requiring the floating frame to remain rigidly attached to a single material point on the body or element and thus the local elastic displacements and rotations at the location of the floating frame must vanish. Since the local variational rotation field is related to the curl of the local variational displacement field, these requirements can mathematically be expressed in variational form as:

$$\begin{aligned} \delta\boldsymbol{u}_{FF}^{j,j} &= \mathbf{0} \\ \frac{1}{2}\left(\nabla \times \delta\boldsymbol{u}^{j,j}\right)_{FF} &= \mathbf{0}, \end{aligned} \tag{113}$$

where the subscript FF indicates evaluation at the location of the floating frame. Substitution of Equation 99 yields:

$$\begin{aligned} N_i^{FF}\delta\boldsymbol{u}_i^{j,j} &= \mathbf{0} \\ \frac{1}{2}\left(\nabla \times N_i\delta\boldsymbol{u}_i^{j,j}\right)_{FF} = \frac{1}{2}\left(\nabla N_i\right)_{FF} \times \delta\boldsymbol{u}_i^{j,j} &= \frac{1}{2}\widetilde{\nabla \mathrm{N}}_i^{FF}\delta\boldsymbol{u}_i^{j,j} = \mathbf{0}, \end{aligned} \tag{114}$$

where the superscript FF again denotes evaluation at the location of the floating frame. Conversion to matrix-vector notation then results in the required floating frame constraints:

$$\boxed{[\Xi_{FF}]\{\delta\boldsymbol{q}^{j,j}\} = \{\mathbf{0}\}} \qquad [\Xi_{FF}] \equiv \begin{bmatrix} \mathbf{1}N_1^{FF} & \cdots & \mathbf{1}N_N^{FF} \\ \frac{1}{2}\widetilde{\nabla N}_1^{FF} & \cdots & \frac{1}{2}\widetilde{\nabla N}_N^{FF} \end{bmatrix} \tag{115}$$

The kinematic relations given in Equation 112 and the floating frame constraints given in Equation 115 can be inverted to obtain the required coordinate transformation. To this end, Equation 112 is first rewritten to:

$$\{\delta\boldsymbol{q}^{j,j}\} = [\overline{\mathrm{R}}_o^j]\{\delta\boldsymbol{q}^{o,o}\} - [\Phi_R][\mathrm{R}_o^j]\{\delta\boldsymbol{q}_j^{o,o}\}. \tag{116}$$

Substitution into Equation 115 then yields:

$$[\Xi_{FF}][\overline{\mathrm{R}}_o^j]\{\delta\boldsymbol{q}^{o,o}\} - [\Xi_{FF}][\Phi_R][\mathrm{R}_o^j]\{\delta\boldsymbol{q}_j^{o,o}\} = \{\mathbf{0}\}. \tag{117}$$

From this it follows that the variations in the global coordinates of the floating frame are related to the variations in the global nodal degrees of freedom as:

$$\boxed{\{\delta \boldsymbol{q}_j^{o,o}\} = [\mathrm{R}_j^o][\mathcal{Z}][\overline{\mathrm{R}}_o^j]\{\delta \boldsymbol{q}^{o,o}\}} \qquad [\mathcal{Z}] \equiv \left([\Xi_{FF}][\Phi_R]\right)^{-1}[\Xi_{FF}] \tag{118}$$

Back substitution into Equation 116 then yields the expression for the variations of the local nodal degrees of freedom in terms of the variations of the global nodal degrees of freedom:

$$\boxed{\{\delta \boldsymbol{q}^{j,j}\} = \quad [\mathcal{T}][\overline{\mathrm{R}}_o^j]\{\delta \boldsymbol{q}^{o,o}\}} \qquad [\mathcal{T}] \equiv \mathbf{1} - [\Phi_R][\mathcal{Z}] \tag{119}$$

The coordinate transformations in Equations 118 and 119 allow the global position and orientation of the floating frame and the local nodal degrees of freedom to be extracted from the global nodal degrees of freedom in the nonlinear floating frame formulation.

4.2 Computation of internal load vector and tangent stiffness matrix

Expressions for the internal load vector and tangent stiffness matrix are obtained by discretising the expression for the internal virtual work given by:

$$\delta W_{int} = \int_V \delta \mathbf{L} : \mathbf{S} \mathrm{d}V, \tag{120}$$

with $\delta \mathbf{L} = \delta \mathbf{L}(\boldsymbol{x})$ the variation of the Green-Lagrange strain tensor and $\mathbf{S} = \mathbf{S}(\boldsymbol{x})$ the second Piola-Kirchhoff stress tensor and where the integration is performed over the undeformed volume [19], [20]. The invariance under rigid-body motion of the internal virtual work, Green-Lagrange strain tensor and second Piola-Kirchhoff stress tensor implies invariance to the frame of reference in which they are expressed and thus superscripts referring to the global or local frame are omitted [29].

The symmetry properties of the Green-Lagrange strain tensor and second Piola-Kirchhoff stress tensor can be exploited to express the internal virtual work in Voigt notation [20] as:

$$\delta W_{int} = \int_V \{\delta \boldsymbol{L}\}^{\mathrm{T}} \{\boldsymbol{S}\} \mathrm{d}V, \tag{121}$$

in which the Green-Lagrange strain vector and second Piola-Kirchhoff stress vector are given by:

$$\{\boldsymbol{L}\} \equiv \begin{Bmatrix} L_1 \\ L_2 \\ L_3 \\ L_4 \\ L_5 \\ L_6 \end{Bmatrix} \equiv \begin{Bmatrix} L_{11} \\ L_{22} \\ L_{33} \\ L_{23} + L_{32} \\ L_{31} + L_{13} \\ L_{12} + L_{21} \end{Bmatrix}; \qquad \{\boldsymbol{S}\} \equiv \begin{Bmatrix} S_1 \\ S_2 \\ S_3 \\ S_4 \\ S_5 \\ S_6 \end{Bmatrix} \equiv \begin{Bmatrix} S_{11} \\ S_{22} \\ S_{33} \\ S_{23} \\ S_{31} \\ S_{12} \end{Bmatrix}, \tag{122}$$

where single indices refer to vector elements and double indices indicate tensor elements. By definition of the Green-Lagrange strain tensor, the strains are related to the displacement field as:

$$L_{pq} = \frac{1}{2}\left(u_{q,p} + u_{p,q} + u_{m,p}u_{m,q}\right), \qquad p, q = 1, 2, 3 \tag{123}$$

in which $u_{p,q}$ indicates the p^{th} component of the displacement field differentiated with respect to the q^{th} material coordinate and the displacement field can be expressed either in the global or local frame. Linear elastic material behaviour is considered that can be described by the Saint Venant-Kirchhoff model. Its constitutive law is given by:

$$\{\boldsymbol{S}\} = [\mathrm{E}]\,\{\boldsymbol{L}\}, \tag{124}$$

with $[\mathrm{E}]$ the elasticity matrix.

The continuous expression for the internal virtual work is discretised by applying the assumption that the displacement field can be obtained by interpolating the nodal degrees of freedom. In the nonlinear finite element method, the interpolation of the global nodal degrees of freedom as given in Equation 105 is used and this results in the discretisation as given in Equations 107 and 109. In the nonlinear floating frame formulation, the interpolation of the local nodal degrees of freedom as given in Equation 101 is used and this results in the discretisation as given in Equations 108 and 110. The derivation of both discretisations is identical. Superscripts are thus omitted and the interpolation of the displacement field is generally written as:

$$\boldsymbol{u} = [\mathrm{N}]\{\boldsymbol{q}\}. \tag{125}$$

Substitution into Equation 123 results in a discretised expression for the Green-Lagrange strain tensor components given by:

$$\begin{aligned} L_{pq} &= \frac{1}{2}\left(\left[\mathbf{N}_{q,p}\right]\{\boldsymbol{q}\} + \left[\mathbf{N}_{p,q}\right]\{\boldsymbol{q}\} + \left[\mathbf{N}_{m,p}\right]\{\boldsymbol{q}\}\left[\mathbf{N}_{m,q}\right]\{\boldsymbol{q}\}\right) \\ &= \left(\frac{1}{2}\left(\left[\mathbf{N}_{p,q}\right] + \left[\mathbf{N}_{q,p}\right]\right) + \frac{1}{2}\{\boldsymbol{q}\}^{\mathrm{T}}\left(\left[\mathbf{N}_{m,p}\right]^{\mathrm{T}}\left[\mathbf{N}_{m,q}\right]\right)\right)\{\boldsymbol{q}\}, \end{aligned} \qquad p,q = 1,2,3 \tag{126}$$

where $\left[\mathbf{N}_{p,q}\right]$ represents the p^{th} row of the interpolation matrix differentiated with respect to the q^{th} material coordinate. Combining this with Equation 122 results in discretised expressions for the Green-Lagrange strain vector components as:

$$\boxed{\begin{aligned} &\boxed{L_a = \left([\mathbf{B}_a] + \frac{1}{2}\{\boldsymbol{q}\}^{\mathrm{T}}[\mathrm{D}_a]\right)\{\boldsymbol{q}\} \qquad a = 1,2,...,6} \\ &[\mathbf{B}_1] \equiv [\mathbf{N}_{1,1}]\,; \qquad [\mathrm{D}_1] \equiv [\mathbf{N}_{m,1}]^{\mathrm{T}}[\mathbf{N}_{m,1}] = [\mathrm{D}_1]^{\mathrm{T}} \\ &[\mathbf{B}_2] \equiv [\mathbf{N}_{2,2}]\,; \qquad [\mathrm{D}_2] \equiv [\mathbf{N}_{m,2}]^{\mathrm{T}}[\mathbf{N}_{m,2}] = [\mathrm{D}_2]^{\mathrm{T}} \\ &[\mathbf{B}_3] \equiv [\mathbf{N}_{3,3}]\,; \qquad [\mathrm{D}_3] \equiv [\mathbf{N}_{m,3}]^{\mathrm{T}}[\mathbf{N}_{m,3}] = [\mathrm{D}_3]^{\mathrm{T}} \\ &[\mathbf{B}_4] \equiv [\mathbf{N}_{2,3}] + [\mathbf{N}_{3,2}]\,; \qquad [\mathrm{D}_4] \equiv [\mathbf{N}_{m,2}]^{\mathrm{T}}[\mathbf{N}_{m,3}] + [\mathbf{N}_{m,3}]^{\mathrm{T}}[\mathbf{N}_{m,2}] = [\mathrm{D}_4]^{\mathrm{T}} \\ &[\mathbf{B}_5] \equiv [\mathbf{N}_{3,1}] + [\mathbf{N}_{1,3}]\,; \qquad [\mathrm{D}_5] \equiv [\mathbf{N}_{m,3}]^{\mathrm{T}}[\mathbf{N}_{m,1}] + [\mathbf{N}_{m,1}]^{\mathrm{T}}[\mathbf{N}_{m,3}] = [\mathrm{D}_5]^{\mathrm{T}} \\ &[\mathbf{B}_6] \equiv [\mathbf{N}_{1,2}] + [\mathbf{N}_{2,1}]\,; \qquad [\mathrm{D}_6] \equiv [\mathbf{N}_{m,1}]^{\mathrm{T}}[\mathbf{N}_{m,2}] + [\mathbf{N}_{m,2}]^{\mathrm{T}}[\mathbf{N}_{m,1}] = [\mathrm{D}_6]^{\mathrm{T}} \end{aligned}} \tag{127}$$

Consequently, the variations of the Green-Lagrange strain vector components are given by:

$$\delta L_a = \left([\mathbf{B}_a] + \{\boldsymbol{q}\}^{\mathrm{T}}[\mathrm{D}_a]\right)\{\delta\boldsymbol{q}\} \qquad a = 1,2,...,6. \tag{128}$$

The expression for the internal virtual work (Equation 121) can be discretised by substitution of the constitutive law (Equation 124) and the discretised expressions for the Green-Lagrange strain vector components (Equation 127) and its variations (Equation 128). In index notation this results in:

$$\begin{aligned}\delta W_{int} = \int_V \delta L_a S_a \mathrm{d}V = \int_V \delta L_a E_{ab} L_b \mathrm{d}V = \{\delta \boldsymbol{q}\}^{\mathrm{T}} \int_V \Big([\mathbf{B}_a]^{\mathrm{T}} + [\mathrm{D}_a]\{\boldsymbol{q}\} \Big) E_{ab} \left([\mathbf{B}_b] + \frac{1}{2}\{\boldsymbol{q}\}^{\mathrm{T}} [\mathrm{D}_b] \right) \mathrm{d}V \{\boldsymbol{q}\} \\ = \{\delta \boldsymbol{q}\}^{\mathrm{T}} \{\boldsymbol{Q}\},\end{aligned} \tag{129}$$

where the last equality follows from the definition of the internal load vector as given in Equation 107 or 108. The expression for the internal load vector thus obtained is given by:

$$\boxed{\{\boldsymbol{Q}\} = \{\boldsymbol{Q}_I\} + \{\boldsymbol{Q}_{II}\} + \{\boldsymbol{Q}_{III}\} + \{\boldsymbol{Q}_{IV}\}}$$

$$\begin{aligned}
\{\boldsymbol{Q}_I\} &\equiv [\mathrm{K}_I]\{\boldsymbol{q}\}; & [\mathrm{K}_I] &\equiv E_{ab} \int_V [\mathbf{B}_a]^{\mathrm{T}} [\mathbf{B}_b] \,\mathrm{d}V & &= [\mathrm{K}_I]^{\mathrm{T}} \\
\{\boldsymbol{Q}_{II}\} &\equiv \frac{1}{2}[\mathrm{K}_{II}]\{\boldsymbol{q}\}; & [\mathrm{K}_{II}] &\equiv E_{ab} \int_V [\mathbf{B}_a]^{\mathrm{T}} \{\boldsymbol{q}\}^{\mathrm{T}} [\mathrm{D}_b] \,\mathrm{d}V & &= [\mathrm{K}_{III}]^{\mathrm{T}} \\
\{\boldsymbol{Q}_{III}\} &\equiv [\mathrm{K}_{III}]\{\boldsymbol{q}\}; & [\mathrm{K}_{III}] &\equiv E_{ab} \int_V [\mathrm{D}_a]\{\boldsymbol{q}\} [\mathbf{B}_b] \,\mathrm{d}V & &= [\mathrm{K}_{II}]^{\mathrm{T}} \\
\{\boldsymbol{Q}_{IV}\} &\equiv \frac{1}{2}[\mathrm{K}_{IV}]\{\boldsymbol{q}\}; & [\mathrm{K}_{IV}] &\equiv E_{ab} \int_V [\mathrm{D}_a]\{\boldsymbol{q}\}\{\boldsymbol{q}\}^{\mathrm{T}} [\mathrm{D}_b] \,\mathrm{d}V & &= [\mathrm{K}_{IV}]^{\mathrm{T}}
\end{aligned} \tag{130}$$

It can be seen that stiffness matrix $[\mathrm{K}_I]$ is constant, $[\mathrm{K}_{II}]$ and $[\mathrm{K}_{III}]$ depend linearly on the nodal degrees of freedom and $[\mathrm{K}_{IV}]$ has a quadratic dependence. Similarly, it can be seen that internal load vector term $\{\boldsymbol{Q}_I\}$ is linear, $\{\boldsymbol{Q}_{II}\}$ and $\{\boldsymbol{Q}_{III}\}$ are quadratic and $\{\boldsymbol{Q}_{IV}\}$ is cubic. The symmetry properties of the stiffness matrices follow from the symmetry properties of the elasticity matrix.

An expression for the tangent stiffness matrix is obtained by taking the variation of the internal load vector as:

$$\begin{aligned}\{\delta \boldsymbol{Q}\} = [\mathrm{K}_I]\{\delta \boldsymbol{q}\} + \frac{1}{2}[\mathrm{K}_{II}]\{\delta \boldsymbol{q}\} + [\mathrm{K}_{III}]\{\delta \boldsymbol{q}\} + \frac{1}{2}[\mathrm{K}_{IV}]\{\delta \boldsymbol{q}\} \\ + [\delta \mathrm{K}_I]\{\boldsymbol{q}\} + \frac{1}{2}[\delta \mathrm{K}_{II}]\{\boldsymbol{q}\} + [\delta \mathrm{K}_{III}]\{\boldsymbol{q}\} + \frac{1}{2}[\delta \mathrm{K}_{IV}]\{\boldsymbol{q}\} = [\mathrm{K}_t]\{\delta \boldsymbol{q}\},\end{aligned} \tag{131}$$

where the last equality follows from the definition of the tangent stiffness matrix as given in Equation 109 or 110. The terms containing variations of the stiffness matrices can be further elaborated as:

$$\begin{aligned}[\delta \mathrm{K}_I]\{\boldsymbol{q}\} &= [\,\mathbf{0}\,]\{\boldsymbol{q}\} = \{\mathbf{0}\} \\ \frac{1}{2}[\delta \mathrm{K}_{II}]\{\boldsymbol{q}\} &= \frac{1}{2} E_{ab} \int_V [\mathbf{B}_a]^{\mathrm{T}} \{\delta \boldsymbol{q}\}^{\mathrm{T}} [\mathrm{D}_b] \,\mathrm{d}V \{\boldsymbol{q}\} \\ &= \frac{1}{2} E_{ab} \int_V [\mathbf{B}_a]^{\mathrm{T}} \{\boldsymbol{q}\}^{\mathrm{T}} [\mathrm{D}_b] \,\mathrm{d}V \{\delta \boldsymbol{q}\} = \frac{1}{2}[\mathrm{K}_{II}]\{\delta \boldsymbol{q}\}\end{aligned}$$

$$
\begin{aligned}
[\delta \mathrm{K}_{III}]\{\boldsymbol{q}\} + \frac{1}{2}[\delta \mathrm{K}_{IV}]\{\boldsymbol{q}\} &= E_{ab}\int_V [\mathrm{D}_a]\{\delta\boldsymbol{q}\}[\mathbf{B}_b]\,\mathrm{d}V\{\boldsymbol{q}\} \\
&\quad + \frac{1}{2}E_{ab}\int_V [\mathrm{D}_a]\{\delta\boldsymbol{q}\}\{\boldsymbol{q}\}^{\mathrm{T}}[\mathrm{D}_b]\,\mathrm{d}V\{\boldsymbol{q}\} \\
&\quad + \frac{1}{2}E_{ab}\int_V [\mathrm{D}_a]\{\boldsymbol{q}\}\{\delta\boldsymbol{q}\}^{\mathrm{T}}[\mathrm{D}_b]\,\mathrm{d}V\{\boldsymbol{q}\} \\
&= E_{ab}\int_V [\mathrm{D}_a]\left(\left([\mathbf{B}_b] + \frac{1}{2}\{\boldsymbol{q}\}^{\mathrm{T}}[\mathrm{D}_b]\right)\{\boldsymbol{q}\}\right)\mathrm{d}V\{\delta\boldsymbol{q}\} \\
&\quad + \frac{1}{2}E_{ab}\int_V [\mathrm{D}_a]\{\boldsymbol{q}\}\{\boldsymbol{q}\}^{\mathrm{T}}[\mathrm{D}_b]\,\mathrm{d}V\{\delta\boldsymbol{q}\} \\
&= E_{ab}\int_V [\mathrm{D}_a]\,L_b\mathrm{d}V + \frac{1}{2}[\mathrm{K}_{IV}]\{\delta\boldsymbol{q}\}
\end{aligned}
\tag{132}
$$

Substitution of these terms into the expression for the variation of the internal load vector in Equation 131 results in the expression for the tangent stiffness matrix given by:

$$
\boxed{
\begin{aligned}
&\boxed{[\mathrm{K}_t] = [\mathrm{K}_I] + [\mathrm{K}_{II}] + [\mathrm{K}_{III}] + [\mathrm{K}_{IV}] + [\mathrm{K}_V]} \\
&[\mathrm{K}_V] \equiv E_{ab}\int_V [\mathrm{D}_a]\,L_b\mathrm{d}V \qquad\qquad = [\mathrm{K}_V]^{\mathrm{T}}
\end{aligned}
}
\tag{133}
$$

From the discretisation of the Green-Lagrange strain vector components in Equation 127 it follows that stiffness matrix $[\mathrm{K}_V]$ consists of both a linear and a quadratic term.

The expressions for the internal load vector and tangent stiffness matrix in Equations 130 and 133 can be used to compute the global internal load vector and tangent stiffness matrix from the global nodal degrees of freedom in the nonlinear finite element method and to compute the local internal load vector and tangent stiffness matrix from the local nodal degrees of freedom in the nonlinear floating frame formulation.

4.3 Internal load vector and tangent stiffness matrix transformation

The nonlinear floating frame formulation requires a transformation that transforms the local internal load vector and tangent stiffness matrix to the global frame. This transformation can be performed both at the body and at the element level and allows the governing equations to be expressed in the global frame.

From the definition of the global and local internal load vectors in Equations 107 and 108 it follows that:

$$
\begin{aligned}
\{\delta\boldsymbol{q}^{o,o}\}^{\mathrm{T}}\{\boldsymbol{Q}^o\} = \delta W_{int} &= \{\delta\boldsymbol{q}^{j,j}\}^{\mathrm{T}}\{\boldsymbol{Q}^j\} \\
&= \{\delta\boldsymbol{q}^{o,o}\}^{\mathrm{T}}[\overline{\mathrm{R}}_j^o][\mathcal{T}]^{\mathrm{T}}\{\boldsymbol{Q}^j\},
\end{aligned}
\tag{134}
$$

in which the coordinate transformation given in Equation 119 has been substituted. The internal load vector can thus be transformed as:

$$\boxed{\{\boldsymbol{Q}^o\} = [\overline{\mathrm{R}}_j^o][\mathcal{T}]^{\mathrm{T}}\{\boldsymbol{Q}^j\}} \tag{135}$$

An expression for the transformation of the tangent stiffness matrix is obtained by taking the variation of this expression for the global internal load vector as:

$$\{\delta\boldsymbol{Q}^o\} = \boxed{[\overline{\mathrm{R}}_j^o][\mathcal{T}]^{\mathrm{T}}\{\delta\boldsymbol{Q}^j\}} + \boxed{[\overline{\mathrm{R}}_j^o]\delta[\mathcal{T}]^{\mathrm{T}}\{\boldsymbol{Q}^j\}} + \boxed{\delta[\overline{\mathrm{R}}_j^o][\mathcal{T}]^{\mathrm{T}}\{\boldsymbol{Q}^j\}} = [\mathrm{K}_t^o]\{\delta\boldsymbol{q}^{o,o}\}, \tag{136}$$

where the last equality follows by definition of the global tangent stiffness matrix in Equation 109. Each of the three terms is elaborated to obtain expressions in the form of a stiffness matrix multiplied by the variation of the global vector of nodal degrees of freedom.

The first term is rewritten as:

$$\begin{aligned}\boxed{\begin{aligned}[\overline{\mathrm{R}}_j^o][\mathcal{T}]^{\mathrm{T}}\{\delta\boldsymbol{Q}^j\} &= [\overline{\mathrm{R}}_j^o][\mathcal{T}]^{\mathrm{T}}[\mathrm{K}_t^j]\{\delta\boldsymbol{q}^{j,j}\} \\ &= [\overline{\mathrm{R}}_j^o][\mathcal{T}]^{\mathrm{T}}[\mathrm{K}_t^j][\mathcal{T}][\overline{\mathrm{R}}_o^j]\{\delta\boldsymbol{q}^{o,o}\},\end{aligned}}\end{aligned} \tag{137}$$

where the first equality follows from the definition of the local tangent stiffness matrix in Equation 110 and the second equality follows from the coordinate transformation given in Equation 119.

Elaboration of the second term requires an expression for the variation of transformation matrix $[\mathcal{Z}]$ and this is obtained from Equation 118 as:

$$\begin{aligned}\delta[\mathcal{Z}] &= \delta\left([\Xi_{FF}][\Phi_R]\right)^{-1}[\Xi_{FF}] \\ &= -\left([\Xi_{FF}][\Phi_R]\right)^{-1}[\Xi_{FF}]\delta[\Phi_R]\left([\Xi_{FF}][\Phi_R]\right)^{-1}[\Xi_{FF}] = -[\mathcal{Z}]\delta[\Phi_R][\mathcal{Z}],\end{aligned} \tag{138}$$

where it has been used that for an invertible matrix [A] it holds that $\delta[\mathrm{A}]^{-1} = -[\mathrm{A}]^{-1}\delta[\mathrm{A}][\mathrm{A}]^{-1}$. The required expression for the variation of transformation matrix $[\mathcal{T}]$ is then obtained from Equation 119 as:

$$\begin{aligned}\delta[\mathcal{T}] &= -\delta[\Phi_R][\mathcal{Z}] - [\Phi_R]\delta[\mathcal{Z}] \\ &= -\delta[\Phi_R][\mathcal{Z}] + [\Phi_R][\mathcal{Z}]\delta[\Phi_R][\mathcal{Z}] = -[\mathcal{T}]\delta[\Phi_R][\mathcal{Z}].\end{aligned} \tag{139}$$

For convenience the following notation is introduced:

$$\boxed{\{\widehat{\boldsymbol{Q}}^j\} \equiv [\mathcal{T}]^{\mathrm{T}}\{\boldsymbol{Q}^j\} \equiv \begin{Bmatrix}\widehat{\boldsymbol{F}}_1^j \\ \vdots \\ \widehat{\boldsymbol{F}}_N^j\end{Bmatrix} \qquad [\widehat{\mathrm{F}}^j] \equiv \begin{bmatrix}\mathbf{0} & \widetilde{\widehat{\boldsymbol{F}}}_1^j \\ & \vdots \\ \mathbf{0} & \widetilde{\widehat{\boldsymbol{F}}}_N^j\end{bmatrix}} \tag{140}$$

and it is noted that:

$$\delta[\Phi_R]^{\mathrm{T}}[\mathcal{T}]^{\mathrm{T}}\{\boldsymbol{Q}^j\} = \delta[\Phi_R]^{\mathrm{T}}\{\widehat{\boldsymbol{Q}}^j\} = \begin{bmatrix}\mathbf{0} & \cdots & \mathbf{0} \\ \delta\widetilde{\boldsymbol{r}}_1^{j,j} & \cdots & \delta\widetilde{\boldsymbol{r}}_N^{j,j}\end{bmatrix}\begin{Bmatrix}\widehat{\boldsymbol{F}}_1^j \\ \vdots \\ \widehat{\boldsymbol{F}}_N^j\end{Bmatrix}$$

$$= \begin{bmatrix} \mathbf{0} & \cdots & \mathbf{0} \\ -\widetilde{\widehat{\boldsymbol{F}}}_1^j & \cdots & -\widetilde{\widehat{\boldsymbol{F}}}_N^j \end{bmatrix} \begin{Bmatrix} \delta \boldsymbol{r}_1^{j,j} \\ \vdots \\ \delta \boldsymbol{r}_N^{j,j} \end{Bmatrix} \tag{141}$$

$$= \begin{bmatrix} \mathbf{0} & \cdots & \mathbf{0} \\ -\widetilde{\widehat{\boldsymbol{F}}}_1^j & \cdots & -\widetilde{\widehat{\boldsymbol{F}}}_N^j \end{bmatrix} \begin{Bmatrix} \delta \boldsymbol{u}_1^{j,j} \\ \vdots \\ \delta \boldsymbol{u}_N^{j,j} \end{Bmatrix} = [\widehat{\mathrm{F}}^j]^{\mathrm{T}} \{\delta \boldsymbol{q}^{j,j}\},$$

such that the second expression can finally be rewritten as:

$$\begin{aligned} [\overline{\mathrm{R}}_j^o]\delta[\mathcal{T}]^{\mathrm{T}}\{\boldsymbol{Q}^j\} &= -[\overline{\mathrm{R}}_j^o][\mathcal{Z}]^{\mathrm{T}}\delta[\Phi_R]^{\mathrm{T}}[\mathcal{T}]^{\mathrm{T}}\{\boldsymbol{Q}^j\} \\ &= -[\overline{\mathrm{R}}_j^o][\mathcal{Z}]^{\mathrm{T}}[\widehat{\mathrm{F}}^j]^{\mathrm{T}}\{\delta \boldsymbol{q}^{j,j}\} \\ &= -[\overline{\mathrm{R}}_j^o][\mathcal{Z}]^{\mathrm{T}}[\widehat{\mathrm{F}}^j]^{\mathrm{T}}[\mathcal{T}][\overline{\mathrm{R}}_o^j]\{\delta \boldsymbol{q}^{o,o}\}, \end{aligned} \tag{142}$$

where the first equality follows from Equation 139, the second equality follows from Equation 141 and the last equality follows from the coordinate transformation given in Equation 119.

For rewriting the third term it is considered that:

$$\begin{aligned} \delta[\overline{\mathrm{R}}_j^o]\{\widehat{\boldsymbol{Q}}^j\} &= \begin{bmatrix} \mathrm{R}_j^o\delta\widetilde{\boldsymbol{\theta}}_j^{j,o} & & \\ & \ddots & \\ & & \mathrm{R}_j^o\delta\widetilde{\boldsymbol{\theta}}_j^{j,o} \end{bmatrix} \begin{Bmatrix} \widehat{\boldsymbol{F}}_1^j \\ \vdots \\ \widehat{\boldsymbol{F}}_N^j \end{Bmatrix} = \begin{bmatrix} \mathrm{R}_j^o & & \\ & \ddots & \\ & & \mathrm{R}_j^o \end{bmatrix} \begin{Bmatrix} \delta\widetilde{\boldsymbol{\theta}}_j^{j,o}\widehat{\boldsymbol{F}}_1^j \\ \vdots \\ \delta\widetilde{\boldsymbol{\theta}}_j^{j,o}\widehat{\boldsymbol{F}}_N^j \end{Bmatrix} \\ &= \begin{bmatrix} \mathrm{R}_j^o & & \\ & \ddots & \\ & & \mathrm{R}_j^o \end{bmatrix} \begin{Bmatrix} -\widetilde{\widehat{\boldsymbol{F}}}_1^j\delta\boldsymbol{\theta}_j^{j,o} \\ \vdots \\ -\widetilde{\widehat{\boldsymbol{F}}}_N^j\delta\boldsymbol{\theta}_j^{j,o} \end{Bmatrix} = \begin{bmatrix} \mathrm{R}_j^o & & \\ & \ddots & \\ & & \mathrm{R}_j^o \end{bmatrix} \begin{bmatrix} \mathbf{0} & -\widetilde{\widehat{\boldsymbol{F}}}_1^j \\ & \vdots \\ \mathbf{0} & -\widetilde{\widehat{\boldsymbol{F}}}_N^j \end{bmatrix} \begin{Bmatrix} \delta\boldsymbol{r}_j^{j,o} \\ \delta\boldsymbol{\theta}_j^{j,o} \end{Bmatrix} \\ &= \begin{bmatrix} \mathrm{R}_j^o & & \\ & \ddots & \\ & & \mathrm{R}_j^o \end{bmatrix} \begin{bmatrix} \mathbf{0} & -\widetilde{\widehat{\boldsymbol{F}}}_1^j \\ & \vdots \\ \mathbf{0} & -\widetilde{\widehat{\boldsymbol{F}}}_N^j \end{bmatrix} \begin{bmatrix} \mathrm{R}_o^j & \mathbf{0} \\ \mathbf{0} & \mathrm{R}_o^j \end{bmatrix} \begin{Bmatrix} \delta\boldsymbol{r}_j^{o,o} \\ \delta\boldsymbol{\theta}_j^{o,o} \end{Bmatrix}, \end{aligned} \tag{143}$$

from which it follows that the third term can be rewritten as:

$$\begin{aligned} \delta[\overline{\mathrm{R}}_j^o][\mathcal{T}]^{\mathrm{T}}\{\boldsymbol{Q}^j\} = \delta[\overline{\mathrm{R}}_j^o]\{\widehat{\boldsymbol{Q}}^j\} &= -[\overline{\mathrm{R}}_j^o][\widehat{\mathrm{F}}^j][\mathrm{R}_o^j]\{\delta\boldsymbol{q}_j^{o,o}\} \\ &= -[\overline{\mathrm{R}}_j^o][\widehat{\mathrm{F}}^j][\mathcal{Z}][\overline{\mathrm{R}}_o^j]\{\delta\boldsymbol{q}^{o,o}\}, \end{aligned} \tag{144}$$

where the last equality follows from the coordinate transformation given in Equation 118.

Substitution of the rewritten terms (Equations 137, 142 and 144) into the expression for the variation of the global internal load vector (Equation 136) yields the required expression for the global tangent stiffness matrix:

$$\boxed{\boxed{[\mathrm{K}_t^o] = [\overline{\mathrm{R}}_j^o]\left([\mathrm{K}_1^j] + [\mathrm{K}_2^j] + [\mathrm{K}_3^j]\right)[\overline{\mathrm{R}}_o^j]}}$$

$$[\mathrm{K}_1^j] \equiv [\mathcal{T}]^{\mathrm{T}}[\mathrm{K}_t^j][\mathcal{T}]; \qquad [\mathrm{K}_2^j] \equiv -[\mathcal{Z}]^{\mathrm{T}}[\widehat{\mathrm{F}}^j]^{\mathrm{T}}[\mathcal{T}]; \qquad [\mathrm{K}_3^j] \equiv -[\widehat{\mathrm{F}}^j][\mathcal{Z}] \tag{145}$$

The transformations in Equations 135 and 145 allow the local internal load vector and tangent stiffness matrix to be transformed to the global frame in the nonlinear floating frame formulation.

5 Numerical results

Both the generalised superelement formulation and the nonlinear floating frame formulation have been implemented and their implementation has been validated using simulations of benchmark problems. The implementation of the generalised superelement formulation is presented in Section 5.1. Its validation is presented in Section 5.2. The implementation and validation of the nonlinear floating frame formulation is presented in Section 5.3. Section 5.4 presents the superelement formulation and co-rotational formulation as simplified cases of the nonlinear floating frame formulation using several illustrative problems.

5.1 Implementation of the generalised superelement formulation

The generalised superelement formulation as presented in Chapter 3 has been implemented in a generic Python program that can simulate the dynamic behaviour of an arbitrary flexible multibody system. It allows for the use of an arbitrary reduction basis that satisfies the imposed restrictions. A schematic overview is presented in Figure 15.

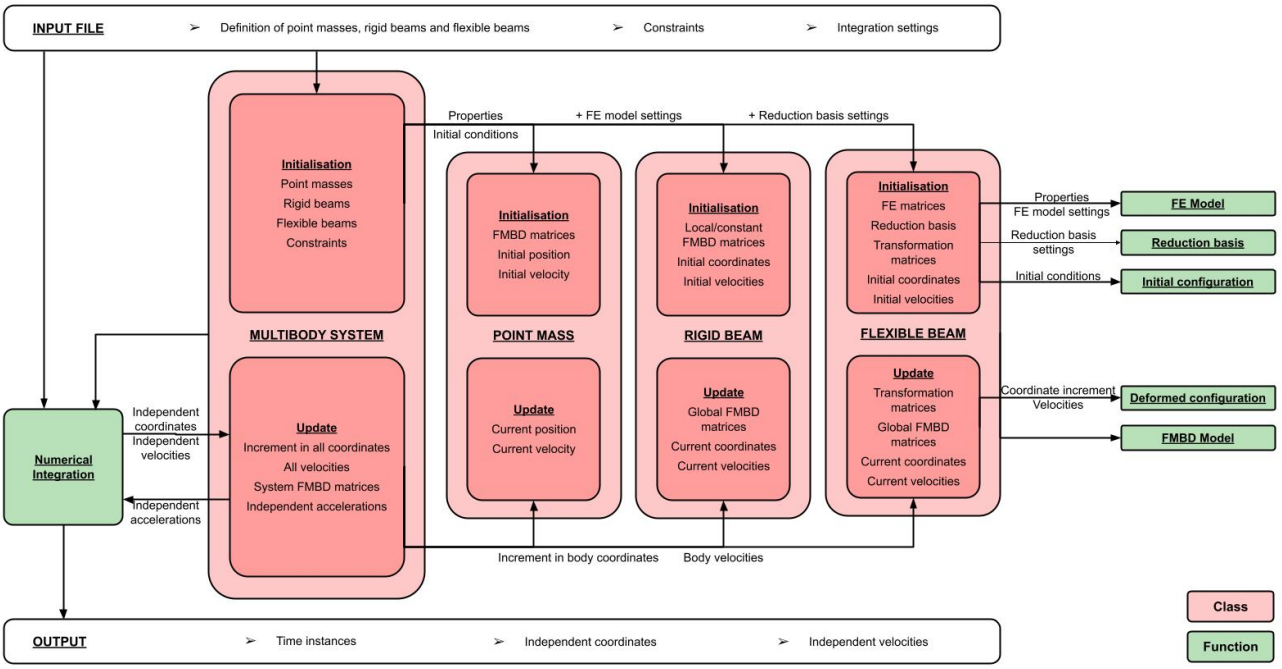

Figure 15: Implementation of the generalised superelement formulation in a generic Python program – Schematic overview

The flexible multibody system is completely defined in the input file. First of all, the components of the system are defined: properties and initial conditions are specified for point masses; properties, finite element model settings and initial conditions are specified for rigid beams; and properties, finite element model settings, reduction basis settings and initial conditions are specified for flexible beams. Secondly, the constraints are defined that specify how the individual components are connected in the multibody system and how the system is driven. Additionally, integration settings, such as the initial time step and final simulation time, are defined.

The generic program initialises and object of the class "Multibody System" with the properties as defined in the input file. This in turn initialises all objects of the classes "Point Mass", "Rigid beam"

and "Flexible beam" that are components of the multibody system. For a point mass, the mass matrix and gravity vector as well as the initial position and velocity are assigned. For a rigid beam, the constant parts of the local flexible multibody dynamics (FMBD) matrices are computed and the initial conditions are assigned. For a flexible beam, the finite element (FE) matrices are assembled using the function "FE Model", the required boundary and internal reduction bases are computed by the function "Reduction basis" and the initial transformation matrices and initial conditions are computed and assigned using the function "Initial configuration". The initialised point masses, rigid beams and flexible beams as well as the constraints are stored in the object multibody system.

The multibody system and the integration settings are provided as input to the function "Numerical Integration", which executes the simulation using the Runge-Kutta integration scheme from the Assimulo package [30]. In this function, the multibody system is updated using the computed independent generalised coordinates and velocities at every time instant. In the multibody system, the defined constraints are used to extract the increments in both the dependent and independent generalised coordinates and to extract the dependent and independent velocities. The increments in the body coordinates and the body velocities are then used to update each of the components in the multibody system.

A point mass only requires its coordinates and velocities to be updated. A rigid body also requires its global FMBD matrices to be computed, as these depend on the current configuration. A flexible body requires several properties to be updated. First of all, the rotation matrix corresponding to the global orientation of the floating frame, the transformation matrices and the local nodal degrees of freedom of the interface points are computed from the increments in the global nodal degrees of freedom of the interface points and the internal flexible coordinates in the function "Deformed configuration". Several iterations are required for this, as the transformation matrices used to compute the deformed configuration are dependent on this deformed configuration. Also the global velocities of the floating frame and the local velocities of the interface points are computed in the function "Deformed configuration". The global FMBD matrices, which depend on the current deformed configuration, are then computed using the function "FMBD Model".

Using the global FMBD matrices of all updated components, the FMBD matrices of the total multibody system are assembled. The constraints are then implemented to compute the independent accelerations, which are integrated in the function "Numerical Integration" to obtain the independent generalised coordinates and velocities at the next time instant, at which the process is repeated. The outputs of the numerical integration are the independent generalised coordinates and velocities at specific time instants. In an additional post-processing step, the relevant coordinates and velocities of all components are extracted.

In the current version of the program, the function "FE Model" assembles the finite element matrices for three-dimensional beam elements, but it is also possible to import the required matrices from finite element software, such that the simulation can be extended to include arbitrarily shaped rigid and flexible bodies. Moreover, the current version of the program implements the constraints for two-dimensional flexible multibody systems, but extension of the simulation to three-dimensional problems only requires adjustments to the implementation of the constraints in the class "Multibody System".

5.2 Validation of the generalised superelement formulation

The implementation of the generalised superelement formulation has been validated using a benchmark problem that consists of a two-dimensional slider-crank mechanism of which the motion has

been simulated using eight different types of reduction bases.

A schematic drawing of the two-dimensional slider-crank mechanism is presented in Figure 16. The rigid crank has a length of 0.15 m and rotates at a constant angular velocity of 150 rad/s. The flexible connector has a length of 0.30 m and a circular cross-section with a radius of 3 mm. It is made of steel with a mass density of 7870 kg/m^3, a Young's modulus of 200 GPa and a shear modulus of 80 GPa. A point mass with half the mass of the flexible connector is attached to the end of the flexible connector. The flexible connector is initially undeformed and oriented horizontally.

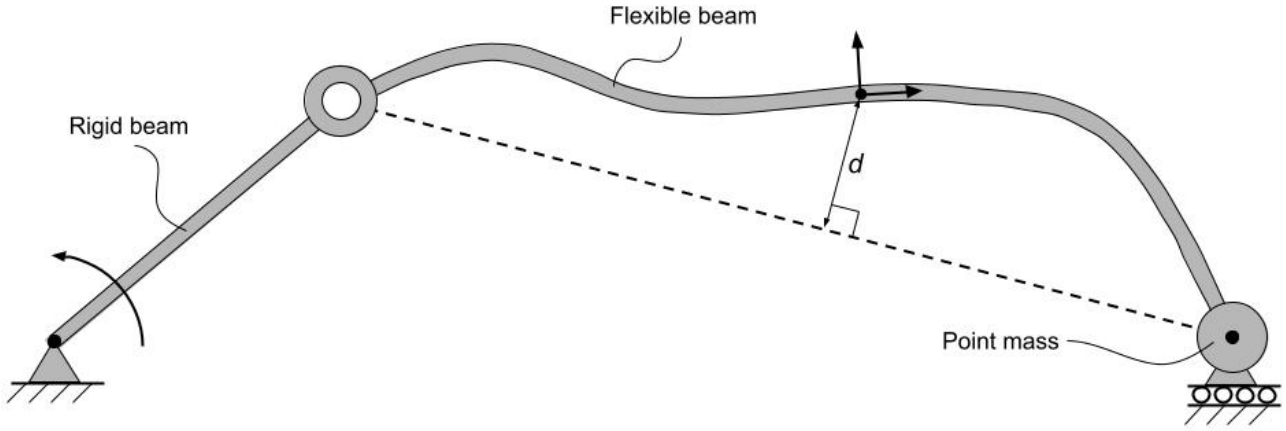

Figure 16: Benchmark problem – Two-dimensional slider-crank mechanism

The flexible connector has been modelled both as a single flexible body and as two connected flexible bodies. In the first model the flexible body was modelled as a three-dimensional flexible beam consisting of eight beam elements and in the second model both flexible bodies were modelled as a three-dimensional flexible beam consisting of four beam elements, resulting in the same mesh density for both models. The interface points were constrained in out-of-plane direction. It has been verified that increasing the number of beam elements has no significant influence on the results.

Both models have been simulated using each of the reduction bases presented in Chapter 2: Guyan's [4], Craig-Bampton's [5], Hurty's [6], Rubin-Martinez's [10], [11], Craig-Chang's [9], Hintz's attachment mode method's (AMM) [8], Herting's [7] and Hintz's constraint mode method's (CMM) [8]. Each of these reduction bases satisfies the imposed restrictions.

Guyan's reduction basis consists only of boundary modes and no internal modes. It is the reduction basis with which the original superelement formulation was implemented and it is included here for comparison purposes. In all the other simulations, the internal reduction basis obtained after the transformation consists of six internal modes. For each method it has been ensured that the three-dimensional modes in a pair of transverse modes were either both included or both excluded.

Craig-Bampton's reduction basis consists of interface constraint modes and six fixed-interface normal modes. As the physical boundary is retained in this reduction method, the reduction basis can directly be separated into a boundary and internal reduction basis. Hurty's reduction basis consists of rigid-body modes, redundant-interface constraint modes and six fixed-interface normal modes. As the physical boundary is not retained in this method, a transformation is required to obtain the boundary and internal reduction basis. After this transformation, both the boundary and internal reduction basis are always the same as those obtained with Craig-Bampton's method.

Rubin-Martinez's reduction basis consists of manipulated residual-flexibility attachment modes, rigid-body modes and zero free-interface normal modes. As the physical boundary is retained in this method, the reduction basis can directly be separated into a boundary and internal reduction basis. Craig-Chang's reduction basis consists of residual-flexibility attachment modes, rigid-body modes and zero free-interface normal modes. As the physical boundary is not retained in this method, a transformation is required to obtain the boundary and internal reduction basis. After this transformation, both the boundary and internal reduction basis are the same as those obtained with Rubin-Martinez's method if the preliminary boundary reduction basis is composed of the residual-flexibility attachment modes. Hintz AMM's reduction basis consists of inertia-relief attachment modes, rigid-body modes and zero free-interface normal modes. Since no normal modes are included in order to obtain six internal modes after the transformation, the inertia-relief attachment modes are the same as the residual-flexibility attachment modes, such that Hintz AMM's reduction basis is the same as Craig-Chang's reduction basis.

Herting's and Hintz CMM's reduction methods have been implemented as free-interface methods. Herting's reduction basis then consists of interface constraint modes, inertia-relief modes and zero manipulated free-interface normal modes. As the physical boundary is retained in this method, the reduction basis can directly be separated into a boundary and internal reduction basis. The boundary reduction basis obtained with Herting's method is the same as that obtained with Craig-Bampton's method, but the internal reduction bases differ. Moreover, Herting's method is equivalent to Rubin-Martinez's method, but their reduction bases differ numerically. Hintz CMM's reduction basis consists of interface constraint modes, inertia-relief modes and zero free-interface normal modes. Since no normal modes are included in order to obtain six internal modes after the transformation, Hintz CMM's reduction basis is the same as Herting's reduction basis.

For comparison purposes, the normalised perpendicular distance from the midpoint of the flexible connector to its neutral line, indicated by d in Figure 16, has been plotted against the crank angle for each simulation. The results are presented in Figure 17. The results for two beams and a Guyan reduction basis represent those obtained in [1] using the original superelement formulation and are equal to those obtained with Spacar [1]. These results are thus considered as the benchmark results.

It can be seen in Figure 17a that the results are inaccurate when the flexible connector is modelled as a single flexible beam and no internal modes are included. Including internal modes improves the accuracy considerably, but the results still deviate significantly from the benchmark results. It has been verified that this also holds when 18 internal modes are included, such that the total number of generalised coordinates describing the flexible connector is equal to that in the simulations that model the flexible connector as two flexible beams. The deviation might be caused by the effect of geometric stiffening that is not included when the flexible connector is modelled as a single flexible body.

It can also be seen in Figure 17a that the results only deviate slightly from the benchmark results when the flexible connector is modelled as two connected flexible bodies and internal modes are included. Since the results are similar for all reduction bases, it is expected that these results are more accurate than those obtained when no internal modes are included. However, since the exact solution is not available, this cannot be verified.

Based on Figure 17a, it seems that the results obtained with different types of reduction bases do not differ significantly. However, Figure 17b reveals that there are some slight differences. When the

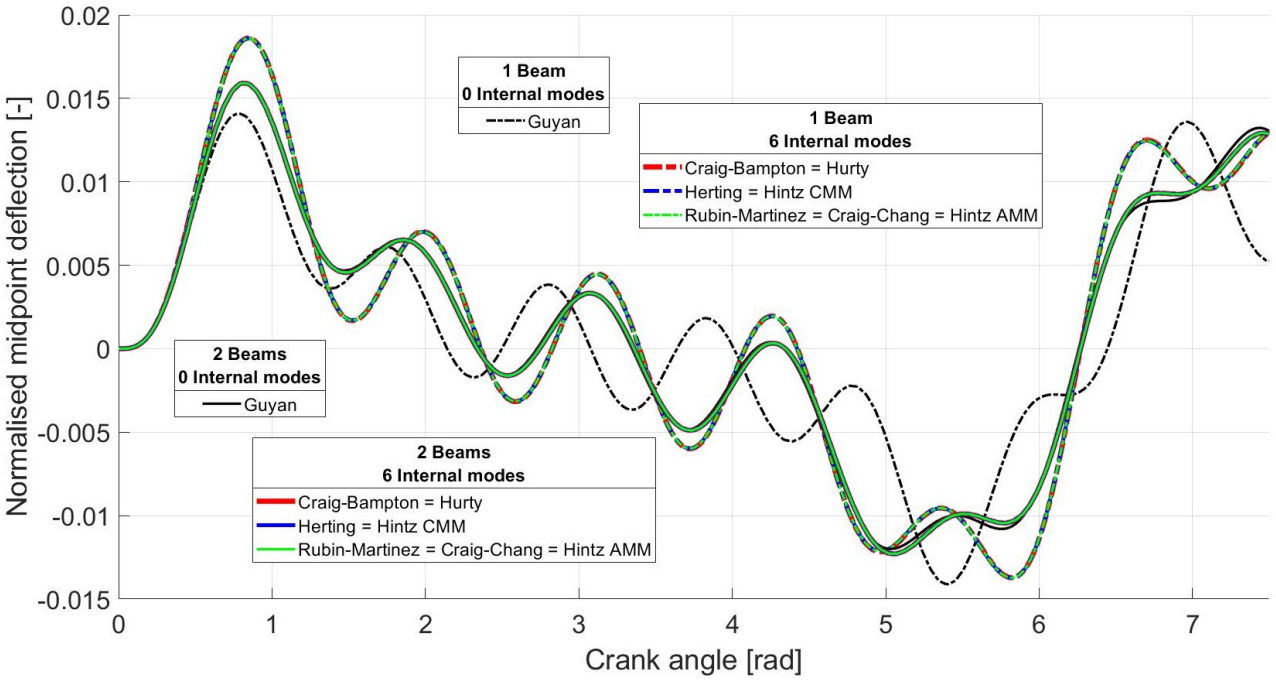

(a) Comparison of (1) flexible connector modelled as one or two flexible beams and (2) inclusion or exclusion of six internal modes

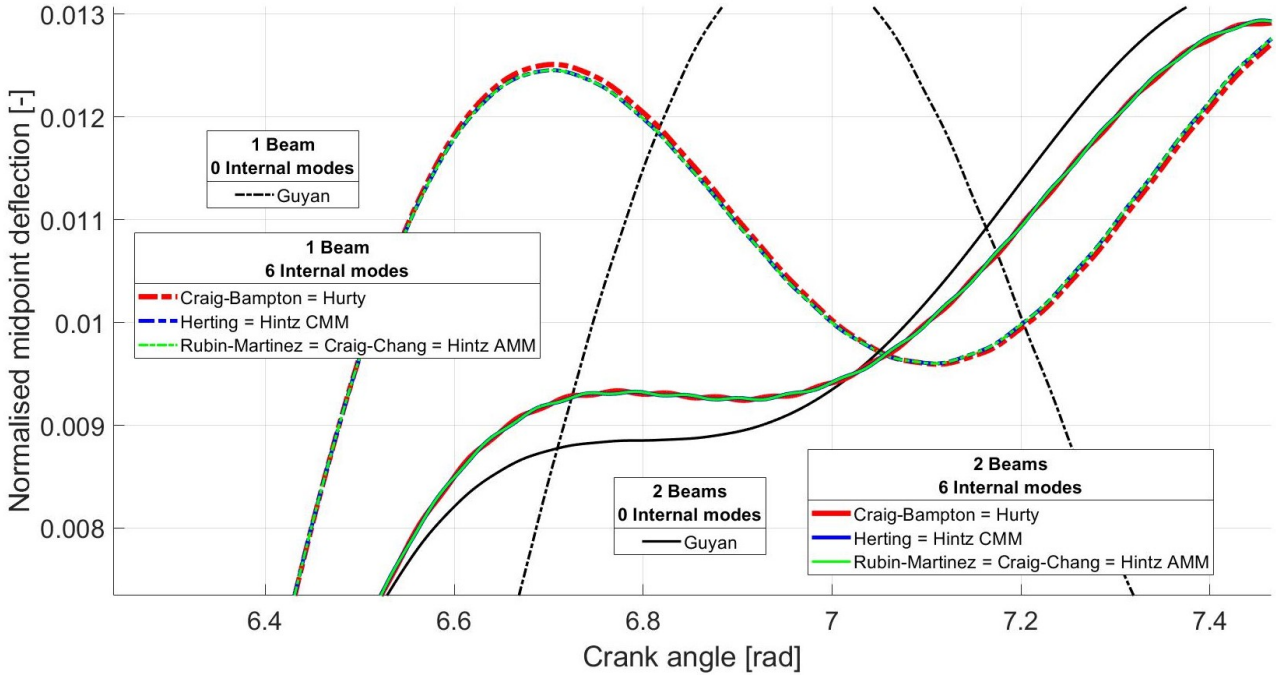

(b) Comparison of reduction bases

Figure 17: Validation results for two-dimensional slider-crank mechanism: *Normalised midpoint deflection against crank angle*

flexible connector is modelled as a single flexible body, the results obtained with Craig-Bampton's reduction basis show a slight offset to those obtained with Herting's or Rubin-Martinez's reduction basis. When the flexible connector is modelled as two connected flexible bodies, the high-frequent vibrations in the results obtained with Craig-Bampton's reduction basis are out of phase compared to those in the results obtained with Herting's or Rubin-Martinez's reduction basis. The simulations with Herting's and Rubin-Martinez's reduction bases do yield the same results, which is expected, since both methods are equivalent.

To further compare the accuracy of results obtained with the different types of reduction bases, the model with two flexible bodies has also been simulated using twelve internal modes for each reduction basis. For Craig-Bampton's and Hurty's reduction bases this means that twelve fixed-interface normal modes are included. The boundary and internal reduction basis obtained with Hurty's method remain the same as those obtained with Craig-Bampton's method. For Rubin-Martinez's, Craig-Chang's and Hintz AMM's reduction bases it means that six (manipulated) free-interface normal modes are included. The boundary and internal reduction basis obtained with Craig-Chang's method remain the same as those obtained with Rubin-Martinez's method if the preliminary boundary reduction basis is composed of the residual-flexibility attachment modes. Since normal modes are now included, the inertia-relief attachment modes are no longer the same as the residual-flexibility attachment modes, such that Hintz AMM's reduction basis is distinct from Craig-Chang's and different boundary and internal reduction bases are obtained after the transformation. However, Hintz's attachment mode method remains equivalent to Rubin-Martinez's and Craig-Chang's methods. Also for Herting's and Hintz CMM's reduction bases it means that six (manipulated) free-interface normal modes are included. Even though Hintz CMM's reduction basis is then no longer the same as Herting's, the boundary and internal reduction basis obtained after the transformation are identical. The results of these simulations are presented in Figure 18.

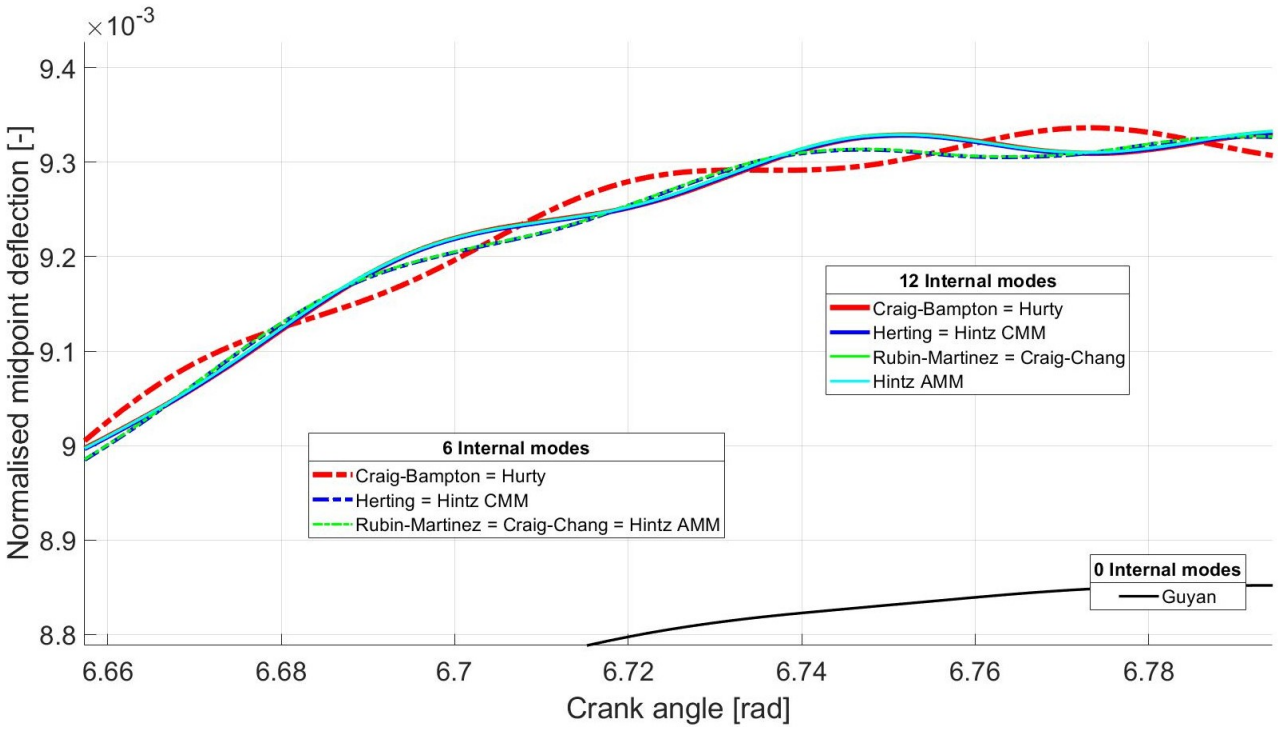

Figure 18: Validation results for two-dimensional slider-crank mechanism [with the flexible connector modelled as two flexible beams]: *Normalised midpoint deflection against crank angle* – Comparison of reduction bases with six or twelve internal modes

It can be seen that the results obtained with all different reduction bases nearly coincide when twelve internal modes are used. These results thus seem to have converged. The high-frequent vibrations in the results obtained with six internal Craig-Bampton modes are almost entirely out of phase with the converged solution, whereas those in the results obtained with six internal Rubin-Martinez or Herting modes only exhibit a relatively small phase difference. This difference suggests that the simulation results converge faster when Rubin-Martinez's or Herting's reduction basis is used, compared to when Craig-Bampton's reduction basis is used.

In addition to the accuracy of the results obtained with the different types of reduction bases, the required computation times have also been compared. The blue bars in Figure 19 represent the number of steps required by the integrator to compute the results for the model with two flexible beams and six internal modes. It can be seen that the simulation using Herting's reduction basis takes significantly longer than the simulation using Rubin-Martinez's reduction basis, which again takes significantly longer than the simulation using Craig-Bampton's reduction basis.

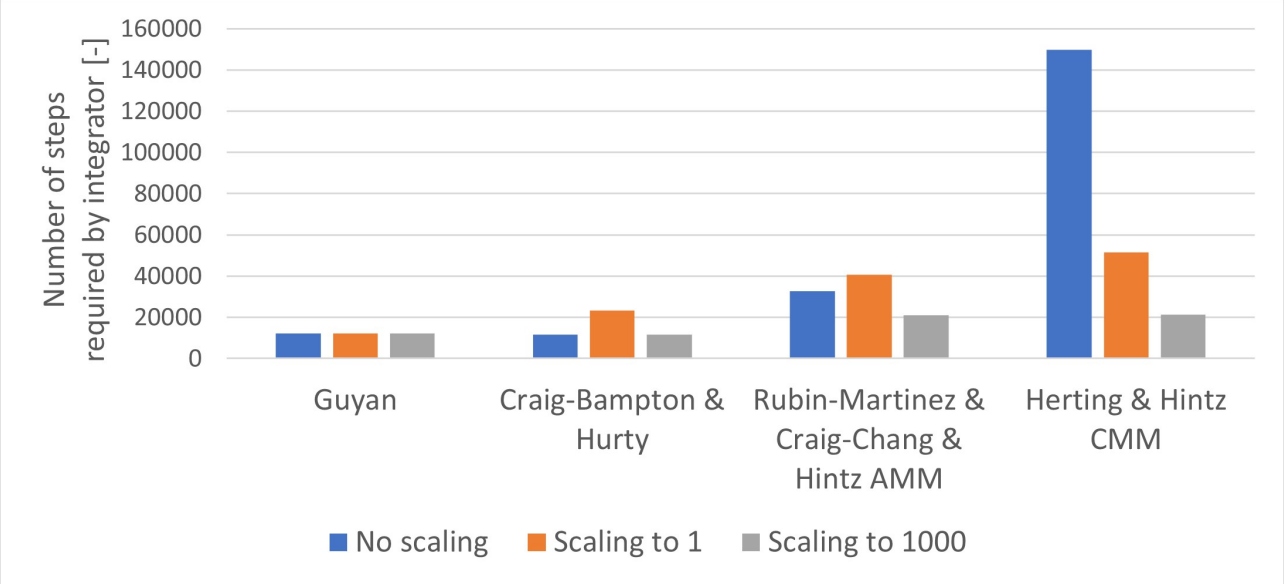

Figure 19: Validation results for two-dimensional slider-crank mechanism [with the flexible connector modelled as two flexible beams and the internal reduction basis consisting of six modes]: *Number of steps required by integrator* – Comparison of reduction bases

The differences in computation times are caused by differences in the orders of magnitude of the internal modes and the corresponding internal flexible coordinates. To ensure that the order of magnitude of the internal modes approximately equals the order of magnitude of the boundary modes, the internal modes have been scaled in such a way that the largest value in each internal mode equals one. The simulations with these scaled modes yield the same results, while the computation times as represented by the orange bars in Figure 19 are influenced. It can be seen that the computation time for the simulation using Herting's reduction basis is significantly reduced, whereas it is (slightly) increased for the simulations using Craig-Bampton's or Rubin-Martinez's reduction basis. This is caused by the fact that the magnitude of the internal flexible coordinates is (slightly) increased for the latter two due to the scaling, whereas the magnitude is significantly reduced for the former.

The grey bars in Figure 19 represent the number of steps required by the integrator when the modes are scaled in such a way that their largest value equals 1000. It can be seen that for each type of

reduction basis the computation time is again reduced. It has been verified that a further increase in the order of magnitude of the internal modes does not influence the required number of steps. Also scaling the entire internal reduction basis or scaling all individual modes before the transformation does not further reduce the computation time. The number of steps required by the integrator when Herting's reduction basis is used thus remains equal to that required when Rubin-Martinez's reduction basis is used and approximately twice as large as that required when Craig-Bampton's method is used.

5.3 Implementation and validation of the nonlinear floating frame formulation

For verification purposes, both the nonlinear finite element method and the nonlinear floating frame formulation as presented in Chapter 4 have been implemented in Python for (1) one-dimensional uniaxial stress 2-node bar elements, (2) two-dimensional plane stress rectangular 4-node quadrilateral elements and (3) three-dimensional rectangular 8-node hexahedral elements. The corresponding interpolation functions are presented in Appendix E. In each case isotropic material properties were considered, for which the corresponding elasticity matrices are presented in Appendix F.

The global nodal degrees of freedom of the elements have then been prescribed for specific types of motion and deformation: (1) rigid-body motion, (2) stretching deformation, (3) shear deformation in the case of two- and three-dimensional elements, (4) a combination of rigid-body motion and small local deformations and (5) arbitrary motion. This has been used to verify that for each element type and deformation case the global internal load vector and tangent stiffness matrix obtained with the nonlinear floating frame formulation are identical to those obtained with the nonlinear finite element method. It has also been verified that the symmetry properties of the stiffness matrices, as presented in Equations 130 and 133, are satisfied in all cases. Moreover, it has been verified that the global internal load vector is zero in the case of rigid-body motion and that the results for stretch and shear in different dimensions and directions are in agreement with each other.

For illustration purposes, the nonlinear finite element (NFE) method and the nonlinear floating frame (NFF) formulation have additionally been implemented in Python for bodies with isotropic material properties consisting of two-dimensional plane stress rectangular 8-node quadrilateral elements. A distinction is made here between the body-level nonlinear floating frame formulation that applies both transformations at the level of the entire body (NFFb) and the element-level nonlinear floating frame formulation that applies both transformations at the element level (NFFe). Prescribed stretching, shear and bending deformations have been modelled with each method as illustrated in Figures 20, 21 and 22.

The dashed grey and solid black lines represent the original undeformed and current deformed configuration respectively. The solid grey lines represent the undeformed reference configuration with respect to which the deformations are expressed. In the nonlinear finite element method, the undeformed reference configuration coincides with the original undeformed configuration. In the body-level nonlinear floating frame formulation, a single undeformed reference configuration is used for the body as a whole and it is positioned and oriented such that its center of mass remains rigidly attached to that of the deformed configuration. In the element-level nonlinear floating frame formulation, an undeformed reference configuration is used for each element individually and each is again positioned and oriented such that its center of mass remains rigidly attached to that of the deformed configuration.

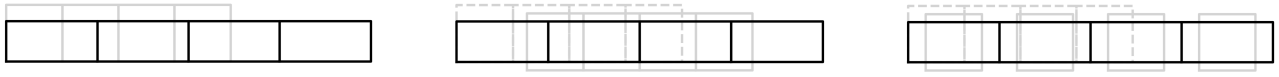

(a) NFE (b) NFFb (c) NFFe

Figure 20: Illustration – Stretching deformation

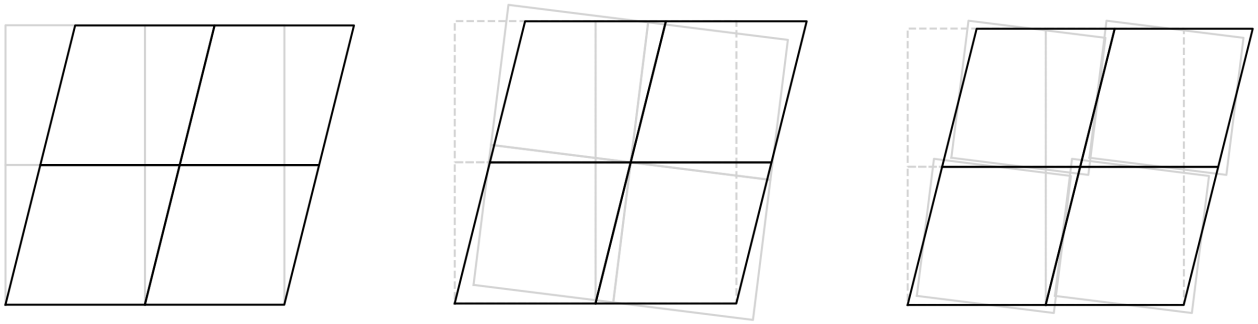

(a) NFE (b) NFFb (c) NFFe

Figure 21: Illustration – Shear deformation

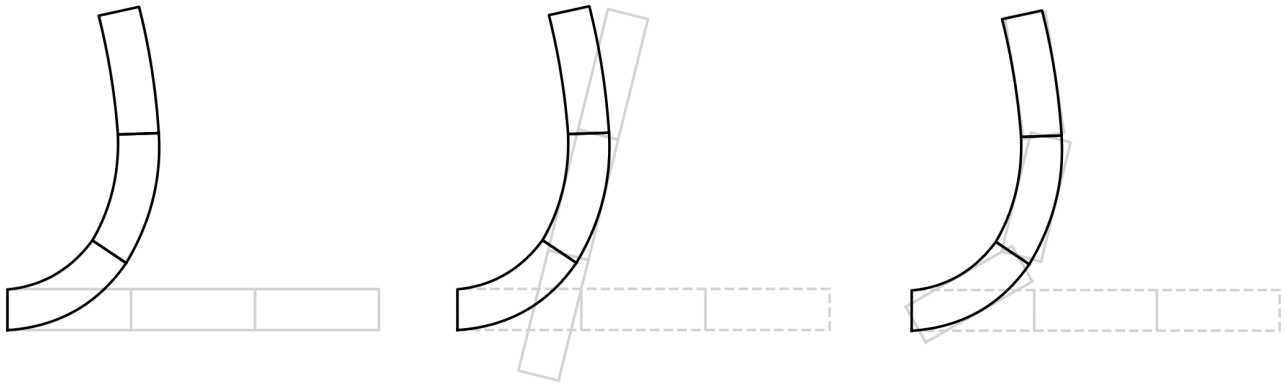

(a) NFE (b) NFFb (c) NFFe

Figure 22: Illustration – Bending deformation

The implementation of each method has additionally been applied in an incremental solution procedure for the computation of the static response due to externally applied forces and/or prescribed displacements. The two-dimensional plane stress rectangular 8-node quadrilateral elements have been used in this to minimise the risk of shear locking. The solution procedure for one load increment is illustrated schematically in Figure 23.

A Newton-Raphson procedure is applied to iteratively compute the deformed configuration for which the global internal load vector approximately equals the global vector of externally applied loads. The global internal load vectors and tangent stiffness matrices obtained with all methods are identical and are thus used in this incremental solution procedure in the same manner. The methods differ in how the global internal load vector and tangent stiffness matrix are obtained from the global nodal degrees of freedom.

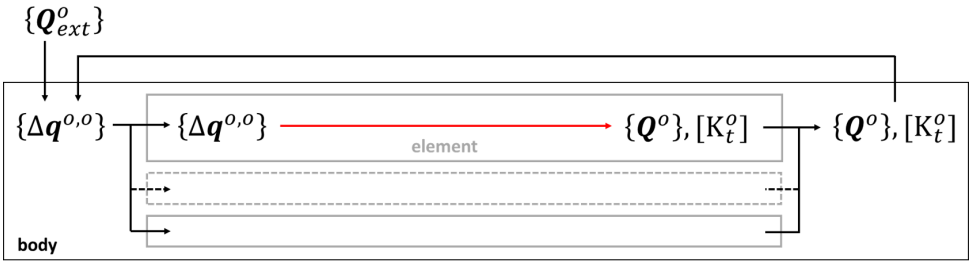

(a) NFE

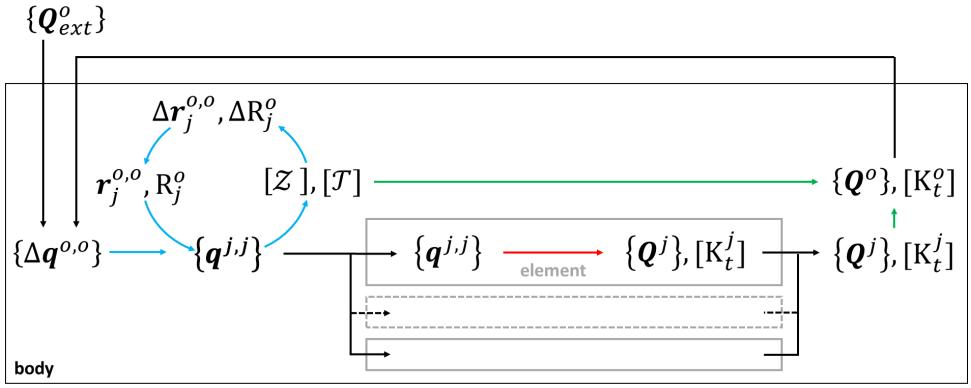

(b) NFFb

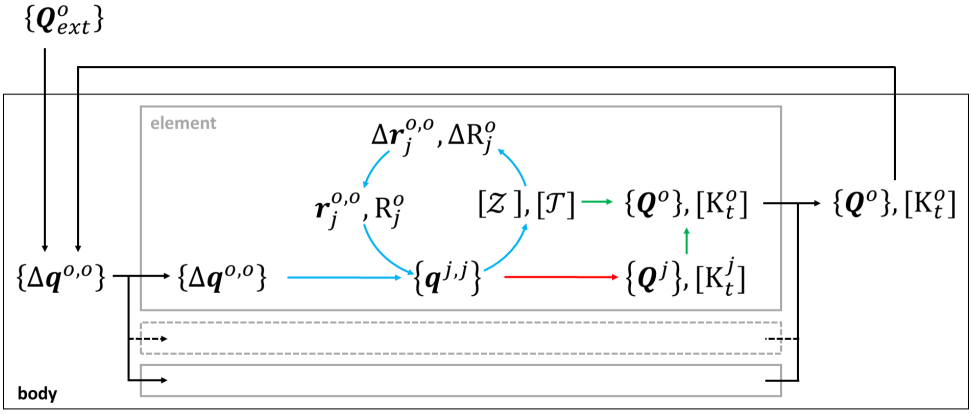

(c) NFFe

Figure 23: Implementation – Schematic illustration of incremental solution procedure

In the nonlinear finite element method, the global internal load vector and tangent stiffness matrix are computed directly from the global nodal degrees of freedom using the expressions in Section 4.2 (indicated in red). In the nonlinear floating frame formulation this is done by converting the global nodal degrees of freedom to the local frame using the expressions in Section 4.1 (indicated in blue), computing the local internal load vector and tangent stiffness matrix from the local nodal degrees of freedom using the expressions in Section 4.2 (indicated in red) and then transforming the local internal load vector and tangent stiffness matrix back to the global frame using the expressions in Section 4.3 (indicated in green). In the body-level nonlinear floating frame formulation, both transformations are applied at the level of the entire body. In the element-level nonlinear floating frame formulation, both transformations are applied at the element level.

The coordinate transformation given in Equation 118 is applied in incremental form and implemented in an iteration loop to ensure that it is satisfied in the current deformed configuration. In this

iteration loop, the local nodal degrees of freedom are not computed from the incremental form of Equation 119, but rather computed directly from the global nodal degrees of freedom and the global position and orientation of the floating frame to prevent the accumulation of numerical inaccuracies that originate from the incremental solution procedure. The transformation matrices obtained in the last iteration loop of the coordinate transformation are used in the transformation of the internal load vector and tangent stiffness matrix.

This implementation has been validated using two benchmark problems. The first is illustrated in Figure 24a. It comprises a cantilever beam that is clamped on one end and subjected to a transversal point force at the midpoint of the other end. It has a length of 1.0 m, a height of 5 cm and a thickness of 1 cm and is made of steel with a Young's modulus of 200 GPa and a Poisson ratio of 0.3. Its static response has been computed using the nonlinear finite element method and both versions of the nonlinear floating frame formulation. In Figure 24b, the resulting horizontal deflection u and vertical deflection v of the tip are plotted against the magnitude of the applied force and compared against the nonlinear analytical solution as formulated in [31] and evaluated and tabulated in [32]. It can be seen that the results obtained with all methods coincide with the analytical solution.

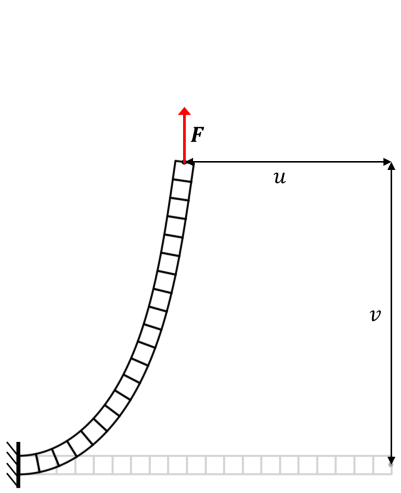

(a) Illustration

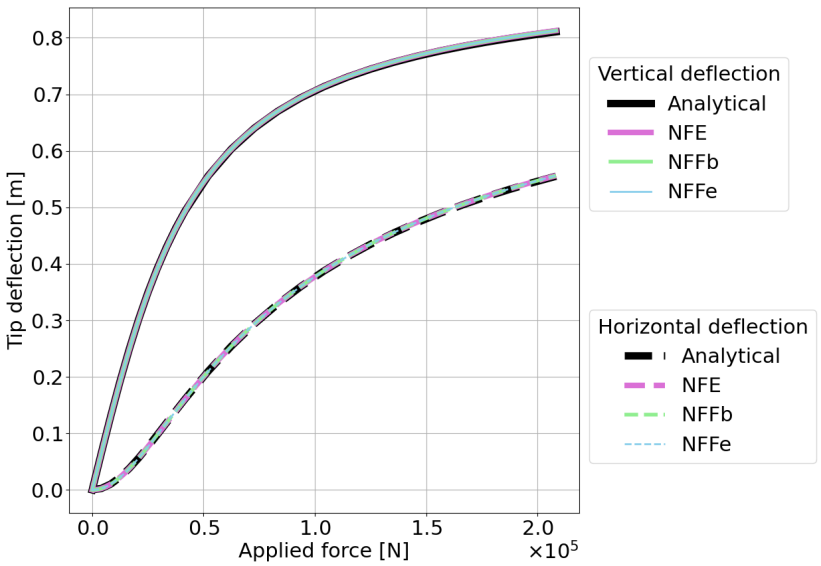

(b) Numerical results: *Horizontal and vertical tip deflection against applied force* – Comparison to analytical solution

Figure 24: Validation – Benchmark problem – Cantilever beam subjected to transversal force

The second benchmark problem is illustrated in Figure 25a. It comprises a cantilever beam that is clamped on one end and subjected to a bending moment on the other end. It has a length of 2.0 m, a height of 5 cm and a thickness of 1 cm and is made of steel with a Young's modulus of 200 GPa and a Poisson ratio of 0.3. The bending moment is applied in the form of a force couple. Its magnitude is gradually increased to 65,450 Nm. It can be derived analytically that a slender beam should then wind around once to form a circle [19]. The static response has been computed using the nonlinear finite element method and both versions of the nonlinear floating frame formulation. In Figure 25b, the resulting deformation is plotted, which is identical for all methods. It can be seen that the beam indeed winds around to a circle upon application of the full bending moment.

The correspondence of the numerical results to the analytical predictions in both benchmark prob-

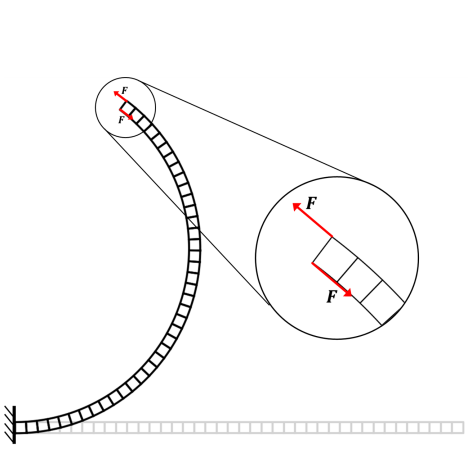

(a) Illustration

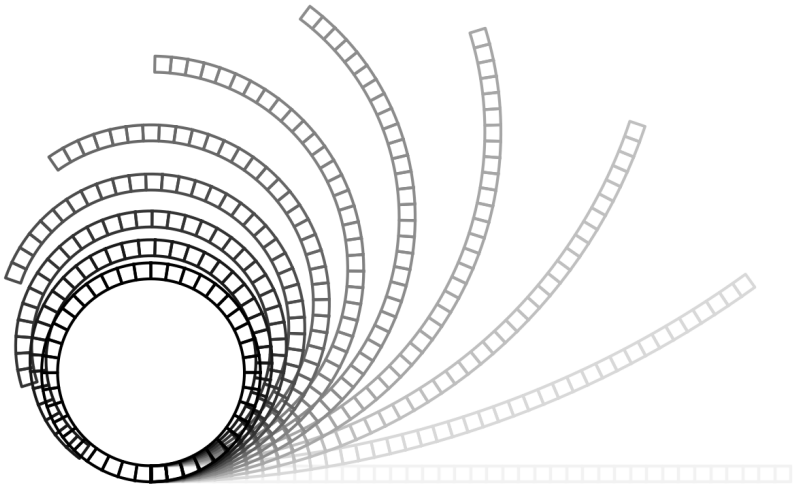

(b) Numerical results: *Deformation during gradual application of bending moment* – Identical results for NFE, NFFb and NFFe

Figure 25: Validation – Benchmark problem – Cantilever beam subjected to bending moment

lems indicates that the nonlinear finite element method and both versions of the nonlinear floating frame formulation have successfully been implemented in an incremental solution procedure for static problems and for bodies with isotropic material properties consisting of two-dimensional plane stress rectangular 8-node quadrilateral elements.

5.4 Simplifications of the nonlinear floating frame formulation

The internal load vector and tangent stiffness matrix as computed from Equations 130 and 133 consist of terms that are either constant or have a linear, quadratic or cubic dependence on the nodal degrees of freedom. In case the nodal degrees of freedom from which the internal load vector and tangent stiffness matrix are computed are small, the terms of lowest order are dominant and the higher order terms can be neglected when modelling the static or dynamic behaviour.

In the nonlinear finite element method, the global internal load vector and tangent stiffness matrix are computed from the global nodal degrees of freedom. The higher order terms can thus be neglected if the deformations relative to the original undeformed configuration remain small. This is the case if a body does not undergo rigid-body motion and is only subjected to small deformations. The method then reduces to the linear finite element method commonly used in structural mechanics.

In the body-level nonlinear floating frame formulation, the overall rigid-body motion of an entire body is captured by a single undeformed reference configuration and the local internal load vector and tangent stiffness matrix are computed from the local nodal degrees of freedom. The higher order terms can thus be neglected if the local deformations relative to the undeformed reference body remain small. This is the case if a body undergoes arbitrarily large rigid-body motions, while being subjected to small local deformations. This assumption is made in the (linear) floating frame formulation commonly used in flexible multibody dynamics. The nonlinear floating frame formulation then reduces to a form of the superelement formulation. This is elaborated in Section 5.4.1.

In the element-level nonlinear floating frame formulation, the overall rigid-body motion is captured by an undeformed reference configuration for each element individually and the local internal load

vector and tangent stiffness matrix are computed from the local nodal degrees of freedom. The higher order terms can thus be neglected if the local deformations relative to the undeformed reference elements remain small. This is the case if the individual elements undergo arbitrarily large rigid-body motions, while being subjected to small local deformations. This is the assumption that is made in the co-rotational nonlinear finite element formulation and it can generally be satisfied by refining the finite element mesh if the strains remain small [12]. The nonlinear floating frame formulation then reduces to a form of the co-rotational formulation. This is elaborated in Section 5.4.2.

5.4.1 Superelement formulation

To illustrate that in the body-level nonlinear floating frame formulation the terms of lowest order are dominant in case a body undergoes arbitrarily large rigid-body motions and small local deformations, the problem as illustrated in Figure 26a is considered. It consists of a beam that is subjected to a combination of prescribed displacements that result in rigid-body translation and rotation and prescribed transverse forces that result in small local deformations. The prescribed displacements and forces are gradually increased simultaneously. The beam has a length of 1.0 m, a height of 5 cm and a thickness of 1 cm and is made of steel with a Young's modulus of 200 GPa and a Poisson ratio of 0.3.

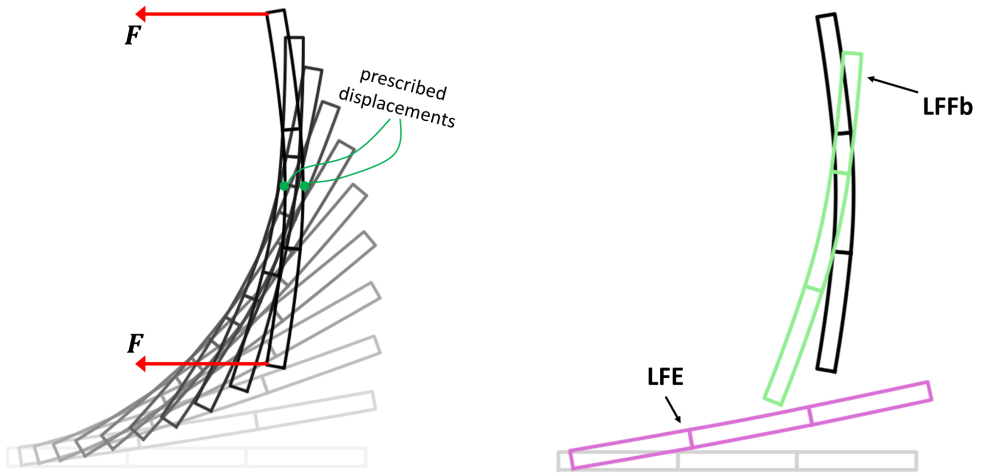

(a) Illustration (b) Maximum allowable deformation

Figure 26: Body undergoing rigid-body motion and small local deformations

The static response has been computed with the nonlinear finite element method and both versions of the nonlinear floating frame formulation. For each load increment, the average magnitude of each of the terms that constitute the (global or local) internal load vector and tangent stiffness matrix has been computed. The results are presented in Figure 27.

It can first of all be seen that the average magnitude of each of the internal load vector and tangent stiffness matrix terms is in general largest for the nonlinear finite element method and smallest for the element-level nonlinear floating frame formulation. This is a direct consequence of the fact that the nodal degrees of freedom from which the internal load vector and tangent stiffness matrix are computed are largest for the nonlinear finite element method and smallest for the element-level nonlinear floating frame formulation. The global internal load vectors and tangent stiffness matrices obtained after the transformation are identical for all methods.

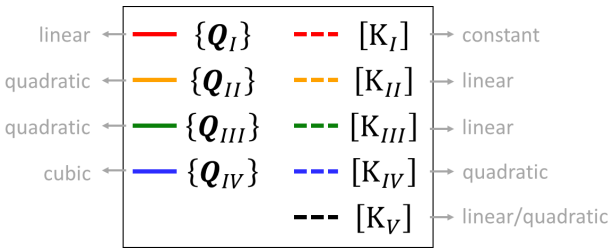

(a) Legend

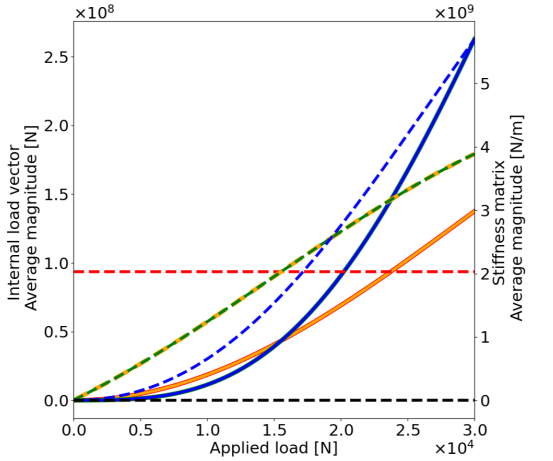

(b) NFE

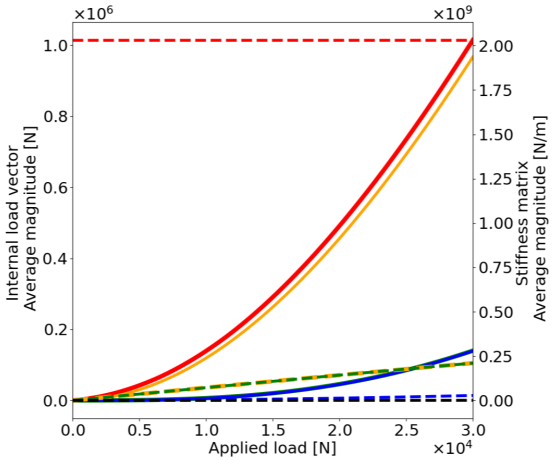

(c) NFFb

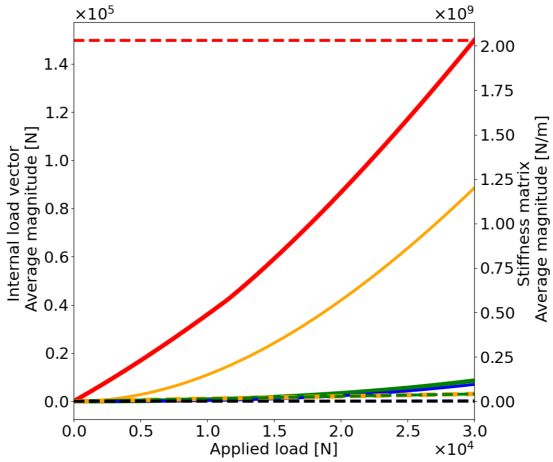

(d) NFFe

Figure 27: Body undergoing rigid-body motion and small local deformations – Average magnitude of internal load vector and tangent stiffness matrix terms

It can also be seen that the higher order terms in the nonlinear finite element method become dominant relatively rapidly in comparison to both versions of the nonlinear floating frame formulation. This is caused by the fact that the nodal degrees of freedom used in the nonlinear finite element method are considerably larger than those in both versions of the nonlinear floating frame formulation due to the large rigid-body motions in comparison to the local deformations. As the element-level nonlinear floating frame formulation separates the rigid-body motion from the local deformations at the element level rather than at the level of the entire body, its nodal degrees of freedom are smaller than those in the body-level nonlinear floating frame formulation and thus also its higher order terms become dominant less rapidly. The relatively rapid growth of the average magnitude of $\{Q_{II}\}$ is related to the fact that in the case of pure rigid-body motion it holds that $\{Q_I\} = -\{Q_{II}\}$ and $\{Q_{III}\} = -\{Q_{IV}\}$. Although the overall rigid-body motion of the entire body is separated from its local deformations, the local deformations can still be described as a combination of rigid-body motion and local deformations at the element level.

The dominance of the terms of lowest order in both versions of the nonlinear floating frame formulation suggests that the static response can be approximated by using linear models to describe the local flexible behaviour. To verify this, the static response has also been computed using a simplified

version of each of the methods in which only the terms of lowest order were included: the linear finite element method (LFE), the body-level linear floating frame formulation (LFFb) and the element-level linear floating frame formulation (LFFe). The maximum allowable deformation, defined as the configuration at which the average error in the global nodal degrees of freedom just exceeds 10%, was then determined for each of these methods. The results are presented in Figure 26b.

It can indeed be seen that the maximum allowable deformation is considerably larger for the body-level linear floating frame formulation than for the linear finite element method. The linear finite element method fails due to the rigid-body rotations. The body-level linear floating frame formulation eventually fails due to the local deformations becoming too large. The maximum allowable deformation for the element-level linear floating frame formulation is again considerably larger than that in both other methods and is not plotted here.

This example illustrates that in case a body undergoes arbitrarily large rigid-body motions and small local deformations, the body-level linear floating frame formulation can be used to approximate the static or dynamic behaviour. This simplified formulation can be considered to be a form of the superelement formulation [1] that does not reduce the linear finite element model describing the local flexible behaviour and thus expresses the equations of motion or equilibrium in terms of all global nodal degrees of freedom, rather than only those of the interface points. It is formulated for continuum elements that only have translational degrees of freedom, as opposed to the superelement formulation as formulated in [1] and the generalised superelement formulation as formulated in Chapter 3 that consider elements with both translational and rotational degrees of freedom.

5.4.2 Co-rotational formulation

To illustrate that in the element-level nonlinear floating frame formulation the terms of lowest order are dominant in case the elements within a body undergo arbitrarily large rigid-body motions and small local deformations, the problem as illustrated in Figure 28a is considered. It consists of a cantilever beam that is clamped on one end and subjected to a perpendicular follower force with gradually increasing magnitude on the other end. The beam has a length of 1.0 m, a height of 5 cm and a thickness of 1 cm and is made of steel with a Young's modulus of 200 GPa and a Poisson ratio of 0.3.

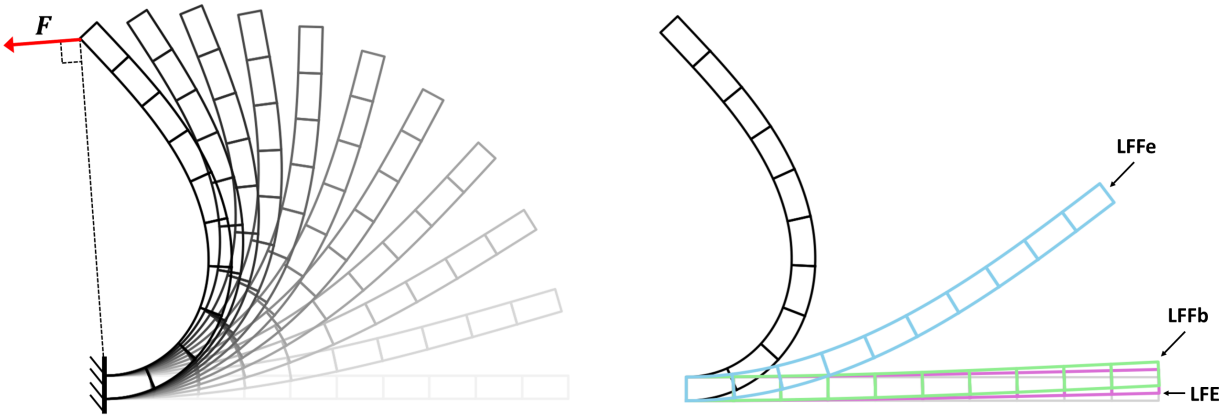

(a) Illustration (b) Maximum allowable deformation

Figure 28: Body with elements undergoing rigid-body motion and small local deformations

The static response has been computed with the nonlinear finite element method and both versions

of the nonlinear floating frame formulation. For each load increment, the average magnitude of each of the terms that constitute the (global or local) internal load vector and tangent stiffness matrix has again been computed. The results are presented in Figure 29.

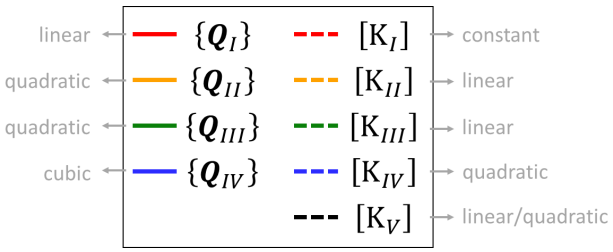

(a) Legend

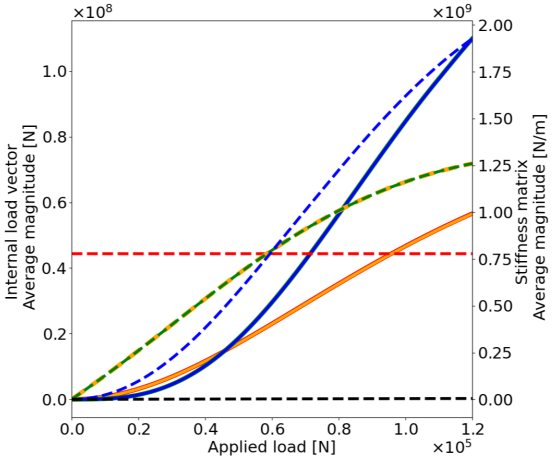

(b) NFE

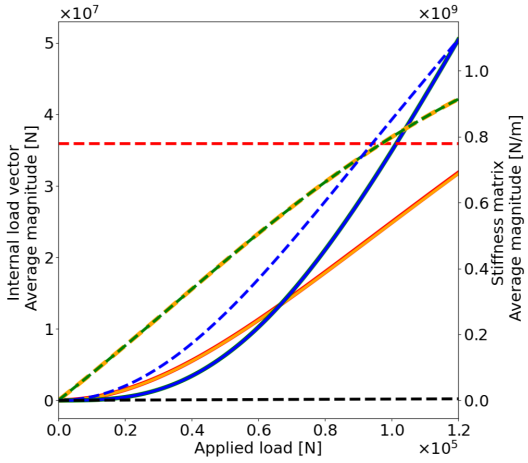

(c) NFFb

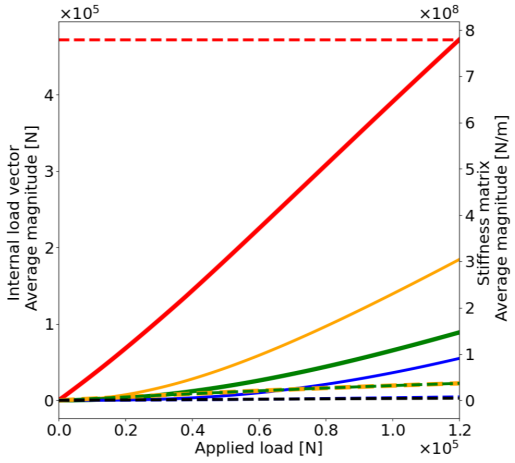

(d) NFFe

Figure 29: Body with elements undergoing rigid-body motion and small local deformations – Average magnitude of internal load vector and tangent stiffness matrix terms

It can first of all again be seen that the average magnitude of each of the internal load vector and tangent stiffness matrix terms is in general largest for the nonlinear finite element method and smallest for the element-level nonlinear floating frame formulation due to the fact that the nodal degrees of freedom are largest and smallest in the nonlinear finite element method and element-level nonlinear floating frame formulation respectively.

It can also be seen that the terms of lowest order in the element-level nonlinear floating frame formulation remain dominant for relatively large deformations in comparison to the nonlinear finite element method and the body-level nonlinear floating frame formulation. This is caused by the fact that the nodal degrees of freedom used in the element-level nonlinear floating frame formulation are considerably smaller than those in the other methods due to the separation of rigid-body motion and local deformations at the element level. The separation of rigid-body motion and local deformations at the level of the entire body causes the higher order terms to increase slightly less rapidly in the

body-level nonlinear floating frame formulation than in the nonlinear finite element method, but this difference is only small due to the fact that the overall rigid-body motion of the body as a whole remains small.

The dominance of the terms of lowest order in the element-level nonlinear floating frame formulation suggests that the static response can be approximated by using a linear model to describe the local flexible behaviour. To verify this, the static response has again also been computed using the simplified versions of each of the methods in which only the terms of lowest order were included and the maximum allowable deformation was determined for each method. The results are presented in Figure 28b.

It can indeed be seen that the maximum allowable deformation is considerably larger for the element-level linear floating frame formulation than for the body-level linear floating frame formulation or the linear finite element method. All methods eventually fail due to the deformations becoming too large. Refining the mesh in the element-level linear floating frame formulation increases the maximum allowable deformation.

This example illustrates that in case the elements within a body undergo arbitrarily large rigid-body motions and small local deformations, the element-level linear floating frame formulation can be used to approximate the static or dynamic behaviour. This simplified formulation can be considered to be a form of the co-rotational nonlinear finite element formulation. Whereas most forms of the co-rotational formulation determine the position and orientation of the floating frame using a best-fit approach [12], [29], the element-level linear floating frame formulation determines its position and orientation by requiring the floating frame to remain rigidly attached to a single material point. Moreover, the element-level linear floating frame formulation is formulated for continuum elements that only have translational degrees of freedom, as opposed to most forms of the co-rotational formulation that consider elements with both translational and rotational degrees of freedom [12]–[14], [16]. The element-level linear floating frame formulation is most comparable to the form of the co-rotational formulation as formulated in [13], [14] and [15] for continuum elements. This formulation also orients the floating frame by requiring the local rotations at the center of the element to be zero, but it positions the floating frame differently and consequently formulates alternative transformations in which one term is erroneously assumed to vanish [33]. The form of the expressions for the internal load vector and tangent stiffness matrix transformation obtained with the element-level linear floating frame formulation is furthermore similar to that in [18]. This formulation also positions the floating frame in the centroid, but orients it using a nodal averaging and geometric fit procedure rather than requiring the local rotations to be zero.

6 Conclusions

Two generalisations of the superelement floating frame formulation have been formulated, implemented and validated: the generalised superelement formulation and the nonlinear floating frame formulation.

The generalised superelement formulation models the motion of a flexible body by making a distinction between its overall rigid-body motion and its local deformations. The local deformations are assumed to be small and the local flexible behaviour is modelled using a linear finite element model that is reduced using an arbitrary reduction basis that is able to (1) describe rigid-body motion and (2) describe the local nodal degrees of freedom of the interface points independently. This allows the generalised superelement formulation to be implemented using any of the commonly used reduction bases as presented in this text, whereas the original superelement formulation can only be implemented using Guyan's reduction basis. The generalised superelement formulation expresses the equations of motion of a single flexible body in terms of the global nodal degrees of freedom of its interface points and a set of internal flexible coordinates. This allows for a primal coupling method to obtain the constrained equations of motion of a flexible multibody system that are expressed only in terms of the independent generalised coordinates, whereas the traditional floating frame formulation requires a dual coupling method to obtain the constrained equations of motion that are expressed in terms of all generalised coordinates and all constraint loads. The applicability of the generalised superelement formulation remains limited to problems in which the local deformations remain small and it requires the linear finite element model describing the local flexible behaviour to be reduced using a reduction basis that satisfies the imposed restrictions.

The reduction bases obtained with the most commonly used component mode synthesis methods found in literature have been presented. The equations of motion of a single flexible body in the generalised superelement formulation have been derived from the equations of motion of a single flexible body in the traditional floating frame formulation using a coordinate transformation, the required transformation of the reduction basis has been formulated and the coupling method to obtain the constrained equations of motion has been outlined. The generalised superelement formulation has been implemented in a generic Python program and the implementation has been validated using simulations of a benchmark problem consisting of a two-dimensional slider-crank mechanism. The validation results indicate that the generalised superelement formulation has been implemented successfully.

Also some conclusions that are specific to the two-dimensional slider-crank mechanism can be drawn from the validation results. First of all, the results reveal that the flexible behaviour of the flexible connector cannot be accurately described if it is modelled as a single flexible body, even though the results are considerably more accurate when internal modes are included. Secondly, since Rubin-Martinez's and Herting's reduction bases are equivalent when free-interface normal modes are used, the results obtained with both reduction bases coincide. Moreover, the results seem to be more accurate when internal modes are included and seem to converge faster when Rubin-Martinez's or Herting's reduction basis is used, compared to when Craig-Bampton's reduction basis is used. Lastly, the required computation time is related to the order of magnitude of the internal flexible coordinates, but after scaling the modes the computation time required by the simulation when using Rubin-Martinez's or Herting's reduction basis remains approximately twice as large as the computation time when Craig-Bampton's reduction basis is used.

The nonlinear floating frame formulation models the motion of a flexible body by making a dis-

tinction between the overall rigid-body motion and local deformations of the body or its individual elements. It expresses the internal load vector and tangent stiffness matrix in terms of all global nodal degrees of freedom and can thus be considered an alternative to the total and updated Lagrangian formulations of the nonlinear finite element method that do not make a distinction between overall rigid-body motion and local deformations. The nonlinear floating frame formulation describes the local flexible behaviour using a geometrically nonlinear model. This allows the nonlinear floating frame formulation to model arbitrarily large local deformations, whereas the applicability of both the superelement formulation and the co-rotational formulation is limited to problems in which the local deformations remain small. The applicability of the nonlinear floating frame formulation remains limited to problems in which only geometric nonlinearities occur.

The coordinate transformation by which the nonlinear floating frame formulation separates the local deformations from the overall rigid-body motion has been expressed in variational form, expressions for the computation of the internal load vector and tangent stiffness matrix have been derived and the transformations by which the local internal load vector and tangent stiffness matrix are transformed back to the global frame have been formulated. The nonlinear floating frame formulation has been implemented for various types of continuum elements and the implementation of the method using two-dimensional plane stress rectangular 8-node quadrilateral elements in an incremental solution procedure for static problems has been validated using a benchmark problem consisting of a cantilever beam. The validation results indicate that the nonlinear floating frame formulation has been implemented successfully.

The body-level linear floating frame formulation and the element-level linear floating frame formulation have been presented as simplifications of the nonlinear floating frame formulation through two illustrative problems. The first illustrative problem reveals that the body-level linear floating frame formulation is suitable for problems in which a body undergoes arbitrarily large rigid-body motions and small local deformations. It is a form of the superelement formulation. The second illustrative problem reveals that the element-level linear floating frame formulation is suitable for problems in which the elements within a body undergo arbitrarily large rigid-body motions and small local deformations. It is a form of the co-rotational formulation.

7 Recommendations

Recommendations for further research as well as recommendations for improvements and extensions of the generalised superelement formulation and nonlinear floating frame formulation can be proposed on the basis of the current research. The recommendations concerning the generalised superelement formulation are provided in Section 7.1. The recommendations concerning the nonlinear floating frame formulation are provided in Section 7.2.

7.1 Generalised superelement formulation

Implementation of three-dimensional constraints: For the further investigations concerning the generalised superelement formulation it can be desirable to extend the adaptability of the generic Python program by implementing the constraints for three-dimensional flexible multibody systems. This implementation should then be validated using simulations of one or more three-dimensional benchmark problems. These simulations can then also be used to investigate whether the specific conclusions drawn for the two-dimensional slider-crank mechanism are also more generally applicable.

Comparison of computational efficiency: A first recommendation for further research is to compare the computational efficiency of the generalised superelement formulation to that of the traditional floating frame formulation. Whereas the coupled equations of motion in the traditional floating frame formulation are expressed in terms of all generalised coordinates and all constraint loads, the coupled equations of motion in the generalised superelement formulation are expressed only in terms of the independent generalised coordinates. This reduction in the number of generalised coordinates in terms of which the coupled equations of motion are expressed might render the generalised superelement formulation more computationally efficient than the traditional floating frame formulation. On the other hand, the system matrices obtained in the generalised superelement formulation are generally more dense than those obtained in the traditional floating frame formulation and the generalised superelement formulation requires additional computations to separate the overall rigid-body motion from the local deformations. This might render the generalised superelement formulation less computationally efficient than the traditional floating frame formulation.

Analysis of problems with more complex geometries: Another relevant research could concern the analysis of problems with more complex geometries. It can be investigated whether for such problems it also holds that the results are inaccurate if each component is modelled as a single flexible body. In such problems it might not be straightforward how to split a component into multiple bodies and their connection might require a large number of constraints.

Investigation of required computation times: A further recommendation for future research is to investigate the required computation times more elaborately. It has been shown that the required computation time depends on the order of magnitude of the internal flexible coordinates and thus the order of magnitude of the internal modes. A more thorough investigation of the methods by which the modes can be scaled can lead to an optimisation of the required computation time. There are several scaling aspects to be considered. First of all, the modes can be scaled by setting either their maximum value or their norm. Secondly, either the individual modes or the entire internal reduction basis can be scaled. Lastly, the scaling can be done before or after the transformation of the reduction basis.

Formulation of reduction basis selection guidelines: Since the generalised superelement formulation allows the linear finite element model describing the local flexible behaviour to be reduced using any arbitrary reduction basis that satisfies the imposed restrictions, it would be valuable if selection guidelines could be formulated that indicate which type of reduction basis is suitable for which type of problem. Some rough guidelines can already be proposed on the basis of the current research.

A first rough guideline is that it is advisable to use a reduction basis in which the physical boundary is retained, as such a reduction basis can directly be separated into a boundary and internal reduction basis. When considering the reduction bases presented in Chapter 2 on component mode synthesis, this means that Craig-Bampton's, Rubin-Martinez's and Herting's reduction bases are the reduction bases of choice. All the other presented reduction bases are either equivalent to or special cases of one of these three reduction bases and in some cases even yield the same boundary and internal reduction basis after the transformation.

It can also be considered that the most suitable reduction basis for a specific component might depend on its connectivity to the other components. For the two-dimensional slider-crank mechanism it seems that the most accurate results with the least number of modes are obtained with Rubin-Martinez's or Herting's reduction basis. For components of which the boundary connectivity can best be approximated by fixed-interface normal modes, Craig-Bampton's reduction basis might yield more accurate results. Alternatively, if it is desirable to use mixed-interface normal modes, Herting's reduction basis can be used.

Another rough guideline is to consider the differences in computation times when selecting a suitable reduction basis. For the two-dimensional slider-crank mechanism the computation time with Rubin-Martinez's or Herting's reduction basis is at least twice as large as with Craig-Bampton's reduction basis, even if the internal modes are scaled. Further investigation is required on how the computation times differ for different types of problems.

A further consideration is that the choice of reduction basis might depend on the objective of the simulation. If one is mainly interested in the global coordinates of the interface points, a reduction basis that only accurately captures the deformations of the boundary and not the interior might fulfill the needs. If one is interested in the internal stresses, a reduction basis is required that accurately describes both the boundary and internal deformations. For the two-dimensional slider-crank mechanism it has briefly been examined whether Guyan's reduction basis, which better captures the local degrees of freedom of the boundary points than those of the interior points in structural dynamics problems, yields more accurate results for the global coordinates of the interface points than for the internal deformations. However, no such result was found. In fact, the global coordinates of the floating frame are inaccurate when using reduction bases that do not accurately describe the local degrees of freedom of the interior, which possibly leads to even larger inaccuracies in the global coordinates of the interface points.

Further generalisation for the use of any arbitrary reduction basis: The generalised superelement formulation as proposed in this text has the limitation that it requires the linear finite element model describing the local flexible behaviour to be reduced using a reduction basis that is able to (1) describe rigid-body motion and (2) describe the local nodal degrees of freedom of the interface points independently. Although the most commonly used reduction bases as presented in Chapter 2 satisfy these criteria, it is possible to formulate two further generalisations, such that the superelement formulation can be implemented using any arbitrary reduction basis.

If certain modes of deformation, such as elongation modes, are excluded from the analysis, the reduction basis is not able to describe all local nodal degrees of freedom of the interface points independently. Appendix G briefly outlines how the generalised superelement formulation can be further generalised to allow for the use of reduction bases with which an arbitrary number of local nodal degrees of freedom of the interface points can be described independently. The generalised superelement formulation as outlined in Chapter 3 is the special case of this further generalisation for which all local nodal degrees of freedom of the interface points can be described independently.

If the reduction basis in unable to describe rigid-body motion, it does not represent the modes of deformation with respect to a floating frame rigidly attached to a point on the body and thus the generalised superelement formulation cannot be implemented. This can for example occur if the reduction basis consists only of free-interface normal modes or if the rigid-body modes are excluded from Rubin-Martinez's reduction basis. Making the superelement formulation suitable for reduction bases that are unable to describe rigid-body motion requires the formulation of an alternative coordinate transformation that positions the floating frame in the center of mass of the deformed body.

Non-consistent formulation: Another alternative superelement formulation that could be worth investigating is a non-consistent formulation. For structural dynamics problems, non-consistent variations to several reduction methods exist that result in reduced computational time due to a sparser reduced finite element mass matrix at the cost of a slight reduction in accuracy [10], [11], [21], [23], [24]. These non-consistent formulations neglect the residual mass terms that originate from the reduction of the finite element mass matrix using the part of the reduction basis that contains residual-flexibility attachment modes. Also for flexible multibody dynamics problems a non-consistent formulation might be beneficial in terms of computational efficiency. Such a formulation reduces the finite element mass matrix using a simplified reduction basis that does not capture the residual flexibility effects, while the reduction of the finite element stiffness matrix and the formulation of the coordinate transformation do require the complete reduction basis.

Formulation for continuum elements: The generalised superelement formulation as proposed in this text has been formulated for elements that have both translational and rotational degrees of freedom. The method can also be formulated for continuum elements that only have translational degrees of freedom, as is done for the nonlinear floating frame formulation. This requires the global and local vectors of nodal degrees of freedom to be redefined and the linear finite element model describing the local flexible behaviour to be modified accordingly. Also the kinematic relations and the floating frame constraints from which the coordinate transformation is derived require some modifications.

7.2 Nonlinear floating frame formulation

Direct coordinate transformation at the position level: The nonlinear floating frame formulation as proposed in this text formulates the coordinate transformation in variational form and implements it partly in incremental form to obtain the position and orientation of the floating frame. Due to this incremental procedure, the floating frame constraints are in general not satisfied exactly. Although this does not result in inaccuracies in the global internal load vector and tangent stiffness matrix due to the direct determination of the local nodal degrees of freedom at the position level, the rigid-body motion is in general not entirely separated from the local deformations. The nonlinear floating frame formulation can be improved by formulating the direct coordinate transformation at the position level in such a way that the floating frame constraints are satisfied exactly. This can be done

by positioning the floating frame at the global position of the material point to which it is connected and describing its orientation by the rotation matrix that is obtained from a polar decomposition of the global deformation gradient at the location of the floating frame [13], [16], [17]. The polar decomposition can be performed using different algorithms, but the resulting formulation is independent of the selected method [33]. This alternative definition of the floating frame is equivalent to the floating frame constraints as formulated in this text and thus the coordinate transformation in variational form that is used in the derivation of the transformation of the internal load vector and tangent stiffness matrix remains valid.

Implementation using different types of continuum elements: The nonlinear floating frame formulation as proposed in this text is in principle valid for all types of continuum elements. However, it has only been implemented for a few specific types for validation and illustration purposes. The implementation of the method using different types of continuum elements would allow for a broader applicability. Other types of elements that can be used in the formulation include tetrahedral elements and hexahedral elements with higher order interpolation functions. Moreover, the method has only been implemented for rectangular elements, but also arbitrarily shaped quadrilateral or hexahedral elements can be used, in which case a mapping of the integrals to natural coordinates is required.

Nonlinear floating frame formulation for beam and shell elements: The nonlinear floating frame formulation as proposed in this text has been formulated for continuum elements that only have translational degrees of freedom. The method can also be formulated for beam and shell elements that have both translational and rotational degrees of freedom, as is done for the generalised superelement formulation. This requires the global and local vectors of nodal degrees of freedom to be redefined and the geometrically nonlinear model describing the local flexible behaviour to be modified accordingly. Also the kinematic relations and floating frame constraints from which the coordinate transformation is derived as well as the transformation of the tangent stiffness matrix require some modifications.

Co-rotational formulation for continuum elements: The co-rotational formulation has most frequently been formulated for elements that have both translational and rotational degrees of freedom [12]–[14], [16]. The existing co-rotational formulations using continuum elements show some slight differences with the element-level linear floating frame formulation as presented in this text [13]–[17]. The element-level linear floating frame formulation can thus be implemented as an alternative co-rotational formulation using continuum elements.

Implementation for dynamic analysis: The applicability of the nonlinear floating frame formulation can be extended by implementing it in incremental solution procedures for modelling the dynamic behaviour of flexible bodies. This requires the discretisation of the virtual work by inertia forces, which can be obtained by making a distinction between overall rigid-body motion and local deformations and transforming the expressions back to the global frame, as is done in the superelement formulation [1]. However, since the local model is not reduced, the virtual work by inertia forces can also be discretised directly in the global frame, as is done in the nonlinear finite element method [19], [20]. The discretisation of the internal virtual work is outlined in this text and the computation of the internal load vector is identical in static and dynamic problems. Also the virtual work by external loads can be more generally discretised to allow for distributed loads.

Inclusion of alternative material models: Another possible extension of the nonlinear floating frame formulation is the inclusion of linear anisotropic material behaviour or nonlinear material

behaviour. Modelling linear anisotropic material behaviour only requires the use of a different elasticity matrix in the implementation. Modelling material nonlinearities requires a reformulation of the method using an alternative material model. Rather than using the total Lagrangian formulation as in this text, it might then be necessary to use an updated Lagrangian formulation in which the stress and strain measures are expressed in terms of the deformed configuration and the integration is performed over the deformed volume [19], [20].

Investigation of higher order terms: It has been shown that the inclusion of only the terms of lowest order in the nonlinear floating frame formulation suffices for problems in which the local deformations remain small, as is done in the superelement formulation and the co-rotational formulation. The nonlinear floating frame formulation is a generalisation of these methods that allows for arbitrarily large local deformations, but in some situations it might not be required to use a fully nonlinear model even though the local deformations are too large for all higher order terms to be neglected. A more thorough examination of the composition of the internal load vector and tangent stiffness matrix can reveal which terms need to be included in which (types of) situations. Such a study can concern either (1) the constant, linear, quadratic and cubic vector or matrix terms of which the internal load vector and tangent stiffness matrix are composed, or (2) the elements within these vectors and matrices that describe specific physical phenomena such as the coupling between bending and elongation.

The first has already briefly been examined. The results in Section 5.4 reveal that the quadratic internal load vector term $\{\boldsymbol{Q}_{II}\}$ is more dominant than the quadratic term $\{\boldsymbol{Q}_{III}\}$, which is related to the fact that in the case of pure rigid-body motion it holds that $\{\boldsymbol{Q}_{I}\} = -\{\boldsymbol{Q}_{II}\}$ and $\{\boldsymbol{Q}_{III}\} = -\{\boldsymbol{Q}_{IV}\}$ due to the vanishing of the strain. This suggests that the inclusion of $\{\boldsymbol{Q}_{II}\}$ will have a larger effect on the accuracy than the inclusion of $\{\boldsymbol{Q}_{III}\}$. For the problem of the cantilever beam it has indeed been found that the maximum allowable deformation is considerably larger for the case in which $\{\boldsymbol{Q}_{I}\}$ and $\{\boldsymbol{Q}_{II}\}$ are included than for the case in which $\{\boldsymbol{Q}_{I}\}$ and $\{\boldsymbol{Q}_{III}\}$ are included. However, it has also been found that the inclusion of both quadratic terms again reduces the accuracy and that in other problems the inclusion of one or both of the quadratic terms can lead to instabilities. The inclusion of the higher order terms in the tangent stiffness matrix only influences the (rate of) convergence and has no effect on the accuracy in case a solution is found.

References

[1] J. P. Schilder, "Flexible multibody dynamics: Superelements using absolute interface coordinates in the floating frame formulation," Ph.D. dissertation, Nov. 2018.

[2] D. De Klerk, D. Rixen, and S. Voormeeren, "General framework for dynamic substructuring: History, review, and classification of techniques," *AIAA Journal*, vol. 46, no. 5, pp. 1169–1181, 2008.

[3] D. J. Rixen, "A dual craig-bampton method for dynamic substructuring," *Journal of Computational and Applied Mathematics*, vol. 168, no. 1-2, pp. 383–391, 2004.

[4] R. J. Guyan, "Reduction of stiffness and mass matrices," *AIAA Journal*, vol. 3, no. 2, p. 380, 1965.

[5] R. R. Craig and M. C. C. Bampton, "Coupling of substructures for dynamic analyses," *AIAA Journal*, vol. 6, no. 7, pp. 1313–1319, 1968.

[6] W. C. Hurty, "Dynamic analysis of structural systems using component modes," *AIAA Journal*, vol. 3, no. 4, pp. 678–685, 1965.

[7] D. Herting, "A general purpose, multi-stage, component modal synthesis method," *Finite Elements in Analysis and Design*, vol. 1, no. 2, pp. 153–164, 1985.

[8] R. M. Hintz, "Analytical methods in component modal synthesis," *AIAA Journal*, vol. 13, no. 8, pp. 1007–1016, 1975.

[9] R. R. Craig and C.-J. Chang, "Free-interface methods of substructure coupling for dynamic analysis," *AIAA Journal*, vol. 14, no. 11, pp. 1633–1635, 1976.

[10] S. Rubin, "Improved component-mode representation for structural dynamic analysis," *AIAA Journal*, vol. 13, no. 8, pp. 995–1006, 1975.

[11] D. R. Martinez, T. G. Carne, D. L. Gregory, and A. Miller, "Combined experimental/analytical modeling using component mode synthesis.," pt 2, 1984, pp. 140–152.

[12] C. A. Felippa and B. Haugen, "A unified formulation of small-strain corotational finite elements: I. theory," *Computer Methods in Applied Mechanics and Engineering*, vol. 194, no. 21-24 SPEC. ISS. Pp. 2285–2335, 2005.

[13] M. Crisfield and G. Moita, "A unified co-rotational framework for solids, shells and beams," *International Journal of Solids and Structures*, vol. 33, no. 20-22, pp. 2969–2992, 1996.

[14] M. Crisfield and G. Moita, "A co-rotational formulation for 2-d continua including incompatible modes," *International Journal for Numerical Methods in Engineering*, vol. 39, no. 15, pp. 2619–2633, 1996.

[15] G. Moita and M. Crisfield, "A finite element formulation for 3-d continua using the co-rotational technique," *International Journal for Numerical Methods in Engineering*, vol. 39, no. 22, pp. 3775–3792, 1996.

[16] Y. Rong, Q. Sun, and K. Liang, "Modified unified co-rotational framework with beam, shell and brick elements for geometrically nonlinear analysis," *Acta Mechanica Sinica/Lixue Xuebao*, vol. 38, no. 4, 2022.

[17] V. A. Nguyen, M. Zehn, and D. Marinković, "An efficient co-rotational fem formulation using a projector matrix," *Facta Universitatis, Series: Mechanical Engineering*, vol. 14, no. 2, pp. 227–240, 2016.

[18] H. Cho, S. Shin, and J. J. Yoh, "Geometrically nonlinear quadratic solid/solid-shell element based on consistent corotational approach for structural analysis under prescribed motion," *International Journal for Numerical Methods in Engineering*, vol. 112, no. 5, pp. 434–458, 2017.

[19] N.-H. Kim, *Introduction to nonlinear finite element analysis*. New York: Springer, 2014, ISBN: 9781441917461.

[20] T. Belytschko, W. K. Liu, and B. Moran, *Nonlinear finite elements for continua and structures*. New York: Wiley, 2000, ISBN: 9780471987734.

[21] R. R. Craig Jr., "Coupling of substructures for dynamic analyses: An overview," *41st Structures, Structural Dynamics, and Materials Conference and Exhibit*, 2000.

[22] Y. Sun, Y. Lu, and Z. Song, "Review on the theories and applications of dynamic condensation and component mode synthesis methods in solving fem-based structural dynamics," *Acta Mechanica Solida Sinica*, vol. 36, no. 3, pp. 361–389, 2023.

[23] R. R. Craig, *Structural Dynamics: An Introduction to Computer Methods*. Wiley, 1981.

[24] M. Géradin and D. J. Rixen, *Mechanical Vibrations: Theory and Application to Structural Dynamics*. Wiley, 2015.

[25] M. Géradin and D. J. Rixen, "A fresh look at the dynamics of a flexible body application to substructuring for flexible multibody dynamics," *International Journal for Numerical Methods in Engineering*, vol. 122, no. 14, pp. 3525–3582, 2021.

[26] VIBES.technology, *3 substructuring methods*, Mar. 2023. [Online]. Available: `https://www.vibestechnology.com/academy/methodology/substructuring-methods/`.

[27] V. Sonneville, M. Scapolan, M. Shan, and O. A. Bauchau, "Modal reduction procedures for flexible multibody dynamics," *Multibody System Dynamics*, vol. 51, no. 4, pp. 377–418, 2021.

[28] M. Ellenbroek, J. Schilder, and Q. Kilsdonk, "Merging nonlinear finite element models and the floating frame of reference formulation," in preparation.

[29] M. K. Nygård and P. G. Bergan, "Advances in treating large rotations for nonlinear problems," *State Of The Art Surveys On Computational Mechanics*, pp. 305–333, 1989.

[30] C. Andersson, C. Führer, and J. Åkesson, "Assimulo: A unified framework for {ode} solvers," *Mathematics and Computers in Simulation*, vol. 116, no. 0, pp. 26–43, 2015, ISSN: 0378-4754.

[31] K. E. Bisshopp and D. C. Drucker, "Large deflection of cantilever beams," *Quarterly of Applied Mathematics*, vol. 3, no. 3, pp. 272–275, 1945.

[32] K. Mattiasson, "Numerical results from large deflection beam and frame problems analysed by means of elliptic integrals," *International Journal for Numerical Methods in Engineering*, vol. 17, no. 1, pp. 145–153, 1981.

[33] H. Lesiv and B. Izzuddin, "Consistency and misconceptions in co-rotational 3d continuum finite elements: A zero-macrospin approach," *International Journal of Solids and Structures*, vol. 281, 2023.

Appendix A – Derivation of the coordinate transformation in the generalised superelement formulation

In Section 3.2, the coordinate transformation was derived that expresses the variations in the global coordinates of the floating frame, the variations in the local nodal degrees of freedom of the interface points and the variations of the internal flexible coordinates in terms of the variations of the global nodal degrees of freedom of the interface points and the variations of the internal flexible coordinates. It is derived from the kinematic relations in Equation 74:

$$\delta \boldsymbol{q}_{IP}^{o,o} = \left[\bar{\mathrm{R}}_j^o\right] \delta \boldsymbol{q}_{IP}^{j,j} + \left[\bar{\mathrm{R}}_j^o\right] \Phi_r \left[\mathrm{R}_o^j\right] \delta \boldsymbol{q}_j^{o,o} \tag{74}$$

and the floating frame constraints in Equation 77:

$$\Psi_{FF} \delta \boldsymbol{q}_{IP}^{j,j} + \Upsilon_{FF} \delta \boldsymbol{\eta} = \mathbf{0}. \tag{77}$$

Using Equation 77, Equation 74 can be inverted. From Equation 74 follows:

$$\delta \boldsymbol{q}_{IP}^{j,j} = \left[\bar{\mathrm{R}}_o^j\right] \delta \boldsymbol{q}_{IP}^{o,o} - \Phi_r \left[\mathrm{R}_o^j\right] \delta \boldsymbol{q}_j^{o,o}. \tag{146}$$

Substitution in Equation 77 yields:

$$\Psi_{FF} \left[\bar{\mathrm{R}}_o^j\right] \delta \boldsymbol{q}_{IP}^{o,o} - \Psi_{FF} \Phi_r \left[\mathrm{R}_o^j\right] \delta \boldsymbol{q}_j^{o,o} + \Upsilon_{FF} \delta \boldsymbol{\eta} = \mathbf{0}, \tag{147}$$

which can be solved for the variations of the global coordinates of the floating frame:

$$\begin{aligned} \delta \boldsymbol{q}_j^{o,o} &= \left[\mathrm{R}_j^o\right] \left(\Psi_{FF} \Phi_r\right)^{-1} \left(\Psi_{FF} \left[\bar{\mathrm{R}}_o^j\right] \delta \boldsymbol{q}_{IP}^{o,o} + \Upsilon_{FF} \delta \boldsymbol{\eta} \right) \\ &= \left[\mathrm{R}_j^o\right] \mathrm{Z} \left[\bar{\mathrm{R}}_o^j\right] \delta \boldsymbol{q}_{IP}^{o,o} + \left[\mathrm{R}_j^o\right] \mathrm{Z}_{int} \delta \boldsymbol{\eta}, \end{aligned} \tag{148}$$

with

$$\begin{aligned} \mathrm{Z} &= \left(\Psi_{FF} \Phi_r\right)^{-1} \Psi_{FF} \\ \mathrm{Z}_{int} &= \left(\Psi_{FF} \Phi_r\right)^{-1} \Upsilon_{FF}. \end{aligned} \tag{149}$$

Back substitution in Equation 146 yields a solution for the variations of the local nodal degrees of freedom of the interface points:

$$\begin{aligned} \delta \boldsymbol{q}_{IP}^{j,j} &= \left(\mathbf{1} - \Phi_r \mathrm{Z}\right) \left[\bar{\mathrm{R}}_o^j\right] \delta \boldsymbol{q}_{IP}^{o,o} - \Phi_r \mathrm{Z}_{int} \delta \boldsymbol{\eta} \\ &= \mathrm{T} \left[\bar{\mathrm{R}}_o^j\right] \delta \boldsymbol{q}_{IP}^{o,o} + \mathrm{T}_{int} \delta \boldsymbol{\eta}, \end{aligned} \tag{150}$$

with

$$\begin{aligned} \mathrm{T} &= \mathbf{1} - \Phi_r \mathrm{Z} \\ \mathrm{T}_{int} &= -\Phi_r \mathrm{Z}_{int}. \end{aligned} \tag{151}$$

Clearly, it holds that:

$$\delta \boldsymbol{\eta} = \mathbf{0} \delta \boldsymbol{q}_{IP}^{o,o} + \mathbf{1} \delta \boldsymbol{\eta}. \tag{152}$$

Combining Equations 148, 150 and 152 yields:

$$\begin{Bmatrix} \delta \boldsymbol{q}_j^{o,o} \\ \delta \boldsymbol{q}_{IP}^{j,j} \\ \delta \boldsymbol{\eta} \end{Bmatrix} = \begin{bmatrix} [\mathrm{R}_j^o]\,\mathrm{Z}\,[\bar{\mathrm{R}}_o^j] & [\mathrm{R}_j^o]\,\mathrm{Z}_{int} \\ \mathrm{T}\,[\bar{\mathrm{R}}_o^j] & \mathrm{T}_{int} \\ \mathbf{0} & \mathbf{1} \end{bmatrix} \begin{Bmatrix} \delta \boldsymbol{q}_{IP}^{o,o} \\ \delta \boldsymbol{\eta} \end{Bmatrix} = \begin{bmatrix} [\mathrm{R}_j^o] & \mathbf{0} & \mathbf{0} \\ \mathbf{0} & \mathbf{1} & \mathbf{0} \\ \mathbf{0} & \mathbf{0} & \mathbf{1} \end{bmatrix} \begin{bmatrix} \mathrm{Z} & \mathrm{Z}_{int} \\ \mathrm{T} & \mathrm{T}_{int} \\ \mathbf{0} & \mathbf{1} \end{bmatrix} \begin{bmatrix} [\bar{\mathrm{R}}_o^j] & \mathbf{0} \\ \mathbf{0} & \mathbf{1} \end{bmatrix} \begin{Bmatrix} \delta \boldsymbol{q}_{IP}^{o,o} \\ \delta \boldsymbol{\eta} \end{Bmatrix}, \quad (153)$$

which is the coordinate transformation as given in Equation 78.

Appendix B – Coordinate transformation in the nonlinear floating frame formulation

The coordinate transformation in variational form used in the nonlinear floating frame formulation is given by:

$$\boxed{\begin{aligned} \{\delta \boldsymbol{q}_j^{o,o}\} &= [\mathrm{R}_j^o][\mathcal{Z}][\overline{\mathrm{R}}_o^j]\{\delta \boldsymbol{q}^{o,o}\} \\ \{\delta \boldsymbol{q}^{j,j}\} &= \quad [\mathcal{T}][\overline{\mathrm{R}}_o^j]\{\delta \boldsymbol{q}^{o,o}\} \end{aligned}} \qquad \begin{aligned} [\mathcal{Z}] &\equiv \left([\Xi_{FF}][\Phi_R]\right)^{-1}[\Xi_{FF}] \\ [\mathcal{T}] &\equiv \mathbf{1} - [\Phi_R][\mathcal{Z}] \end{aligned} \tag{154}$$

1D

In one-dimensional problems, the degree of freedom of each node is its displacement u in x-direction and the position of the floating frame is fully defined by its x-coordinate:

$$\{\delta \boldsymbol{q}^{o,o}\} = \begin{Bmatrix} \delta u_1^o \\ \vdots \\ \delta u_N^o \end{Bmatrix} \qquad \{\delta \boldsymbol{q}^{j,j}\} = \begin{Bmatrix} \delta u_1^j \\ \vdots \\ \delta u_N^j \end{Bmatrix} \qquad \{\delta \boldsymbol{q}_j^{o,o}\} = \delta x_j^o. \tag{155}$$

The rotation matrices are given by:

$$[\mathrm{R}_j^o] = 1 = [\mathrm{R}_o^j]^{\mathrm{T}} \qquad [\overline{\mathrm{R}}_j^o] = \mathbf{1} = [\overline{\mathrm{R}}_o^j]^{\mathrm{T}} \tag{156}$$

or can alternatively be left out of the formulation.

The rigid-body mode and floating frame constraint matrix are given by:

$$[\Phi_R] = \begin{bmatrix} 1 \\ \vdots \\ 1 \end{bmatrix} \qquad [\Xi_{FF}] = \begin{bmatrix} N_1^{FF} & \dots & N_N^{FF} \end{bmatrix}. \tag{157}$$

2D

In two-dimensional problems, the degrees of freedom of each node are its displacements u and v in x- and y-direction and the position and orientation of the floating frame are defined by its x- and y-coordinates and its angle θ respectively:

$$\{\delta \boldsymbol{q}^{o,o}\} = \begin{Bmatrix} \delta u_1^{o,o} \\ \delta v_1^{o,o} \\ \vdots \\ \delta u_N^{o,o} \\ \delta v_N^{o,o} \end{Bmatrix} \qquad \{\delta \boldsymbol{q}^{j,j}\} = \begin{Bmatrix} \delta u_1^{j,j} \\ \delta v_1^{j,j} \\ \vdots \\ \delta u_N^{j,j} \\ \delta v_N^{j,j} \end{Bmatrix} \qquad \{\delta \boldsymbol{q}_j^{o,o}\} = \begin{Bmatrix} \delta x_j^{o,o} \\ \delta y_j^{o,o} \\ \delta \theta_j^o \end{Bmatrix}. \tag{158}$$

The rotation matrices are given by:

$$[\mathrm{R}_j^o] = \begin{bmatrix} c & -s & 0 \\ s & c & 0 \\ 0 & 0 & 1 \end{bmatrix} = [\mathrm{R}_o^j]^{\mathrm{T}} \qquad [\overline{\mathrm{R}}_j^o] = \begin{bmatrix} \begin{bmatrix} c & -s \\ s & c \end{bmatrix} & & \\ & \ddots & \\ & & \begin{bmatrix} c & -s \\ s & c \end{bmatrix} \end{bmatrix} = [\overline{\mathrm{R}}_o^j]^{\mathrm{T}} \tag{159}$$

with $c = \cos\left(\theta_j^o\right)$ and $s = \sin\left(\theta_j^o\right)$.

The rigid-body modes and floating frame constraint matrix are given by:

$$[\Phi_R] = \begin{bmatrix} 1 & 0 & -y_1^{j,j} \\ 0 & 1 & x_1^{j,j} \\ & \vdots & \\ 1 & 0 & -y_N^{j,j} \\ 0 & 1 & x_N^{j,j} \end{bmatrix} \qquad [\Xi_{FF}] = \begin{bmatrix} N_1^{FF} & 0 & & N_N^{FF} & 0 \\ 0 & N_1^{FF} & \dots & 0 & N_N^{FF} \\ -\frac{1}{2}\frac{\partial N_1^{FF}}{\partial y} & \frac{1}{2}\frac{\partial N_1^{FF}}{\partial x} & & -\frac{1}{2}\frac{\partial N_N^{FF}}{\partial y} & \frac{1}{2}\frac{\partial N_N^{FF}}{\partial x} \end{bmatrix}. \tag{160}$$

3D

In three-dimensional problems, the degrees of freedom of each node are its displacements in x-, y- and z-direction and the position and orientation of the floating frame are defined by its position vector $\boldsymbol{r}_j^{o,o}$ and its rotation matrix R_j^o respectively:

$$\{\delta \boldsymbol{q}^{o,o}\} = \begin{Bmatrix} \delta \boldsymbol{u}_1^{o,o} \\ \vdots \\ \delta \boldsymbol{u}_N^{o,o} \end{Bmatrix} \qquad \{\delta \boldsymbol{q}^{j,j}\} = \begin{Bmatrix} \delta \boldsymbol{u}_1^{j,j} \\ \vdots \\ \delta \boldsymbol{u}_N^{j,j} \end{Bmatrix} \qquad \{\delta \boldsymbol{q}_j^{o,o}\} = \begin{Bmatrix} \delta \boldsymbol{r}_j^{o,o} \\ \delta \boldsymbol{\theta}_j^{o,o} \end{Bmatrix}. \tag{161}$$

The rotation matrices are given by:

$$[\mathrm{R}_j^o] = \begin{bmatrix} \mathrm{R}_j^o & \mathbf{0} \\ \mathbf{0} & \mathrm{R}_j^o \end{bmatrix} = [\mathrm{R}_o^j]^{\mathrm{T}} \qquad [\overline{\mathrm{R}}_j^o] = \begin{bmatrix} \mathrm{R}_j^o & & \\ & \ddots & \\ & & \mathrm{R}_j^o \end{bmatrix} = [\overline{\mathrm{R}}_o^j]^{\mathrm{T}}. \tag{162}$$

The rigid-body modes and floating frame constraint matrix are given by:

$$[\Phi_R] = \begin{bmatrix} \mathbf{1} & -\widetilde{\boldsymbol{r}}_1^{j,j} \\ & \vdots \\ \mathbf{1} & -\widetilde{\boldsymbol{r}}_N^{j,j} \end{bmatrix} \qquad [\Xi_{FF}] = \begin{bmatrix} \mathbf{1}\mathrm{N}_1^{FF} & \dots & \mathbf{1}\mathrm{N}_N^{FF} \\ \frac{1}{2}\widetilde{\nabla \mathrm{N}}_1^{FF} & & \frac{1}{2}\widetilde{\nabla \mathrm{N}}_N^{FF} \end{bmatrix}. \tag{163}$$

Appendix C – Computation of internal load vector and tangent stiffness matrix in the nonlinear floating frame formulation

The internal load vector and tangent stiffness matrix are computed from the nodal degrees of freedom as:

$$\boxed{\begin{aligned} \{Q\} &= \{Q_I\} + \{Q_{II}\} + \{Q_{III}\} + \{Q_{IV}\} \\ [\mathrm{K}_t] &= [\mathrm{K}_I] + [\mathrm{K}_{II}] + [\mathrm{K}_{III}] + [\mathrm{K}_{IV}] + [\mathrm{K}_V] \end{aligned}}$$

$$\begin{aligned} \{Q_I\} &\equiv [\mathrm{K}_I]\{q\}; & [\mathrm{K}_I] &\equiv E_{ab}\int_V [\mathbf{B}_a]^{\mathrm{T}}[\mathbf{B}_b]\,\mathrm{d}V & &= [\mathrm{K}_I]^{\mathrm{T}} \\ \{Q_{II}\} &\equiv \frac{1}{2}[\mathrm{K}_{II}]\{q\}; & [\mathrm{K}_{II}] &\equiv E_{ab}\int_V [\mathbf{B}_a]^{\mathrm{T}}\{q\}^{\mathrm{T}}[\mathrm{D}_b]\,\mathrm{d}V & &= [\mathrm{K}_{III}]^{\mathrm{T}} \\ \{Q_{III}\} &\equiv [\mathrm{K}_{III}]\{q\}; & [\mathrm{K}_{III}] &\equiv E_{ab}\int_V [\mathrm{D}_a]\{q\}[\mathbf{B}_b]\,\mathrm{d}V & &= [\mathrm{K}_{II}]^{\mathrm{T}} \\ \{Q_{IV}\} &\equiv \frac{1}{2}[\mathrm{K}_{IV}]\{q\}; & [\mathrm{K}_{IV}] &\equiv E_{ab}\int_V [\mathrm{D}_a]\{q\}\{q\}^{\mathrm{T}}[\mathrm{D}_b]\,\mathrm{d}V & &= [\mathrm{K}_{IV}]^{\mathrm{T}} \\ & & [\mathrm{K}_V] &\equiv E_{ab}\int_V [\mathrm{D}_a]\left(\left([\mathbf{B}_b] + \frac{1}{2}\{q\}^{\mathrm{T}}[\mathrm{D}_b]\right)\{q\}\right)\mathrm{d}V & &= [\mathrm{K}_V]^{\mathrm{T}} \end{aligned} \tag{164}$$

where the global internal load vector and tangent stiffness matrix are obtained if the global nodal degrees of freedom are used and the local internal load vector and tangent stiffness matrix are obtained if the local nodal degrees of freedom are used.

1D

In one-dimensional problems, the Green-Lagrange strain tensor reduces to a scalar value, such that $a, b = 1$ and:

$$[\mathbf{B}_1] \equiv \frac{\mathrm{d}\,[\mathrm{N}]}{\mathrm{d}x} \qquad\qquad [\mathrm{D}_1] \equiv \frac{\mathrm{d}\,[\mathrm{N}]^{\mathrm{T}}}{\mathrm{d}x}\frac{\mathrm{d}\,[\mathrm{N}]}{\mathrm{d}x} = [\mathrm{D}_1]^{\mathrm{T}}. \tag{165}$$

Integration over the undeformed volume reduces to:

$$\int_V \ldots \mathrm{d}V = A\int_x \ldots \mathrm{d}x \tag{166}$$

with A the cross-sectional area in the undeformed configuration and where the integration takes place over the undeformed length.

2D

In two-dimensional problems, the Green-Lagrange strain tensor consists of three independent components, such that $a, b = 1, 2, 3$ and:

$$
\begin{aligned}
[\mathbf{B}_1] &\equiv [\mathbf{N}_{1,1}] & [\mathrm{D}_1] &\equiv [\mathbf{N}_{m,1}]^{\mathrm{T}} [\mathbf{N}_{m,1}] & &= [\mathrm{D}_1]^{\mathrm{T}} \\
[\mathbf{B}_2] &\equiv [\mathbf{N}_{2,2}] & [\mathrm{D}_2] &\equiv [\mathbf{N}_{m,2}]^{\mathrm{T}} [\mathbf{N}_{m,2}] & &= [\mathrm{D}_2]^{\mathrm{T}} \\
[\mathbf{B}_3] &\equiv [\mathbf{N}_{1,2}] + [\mathbf{N}_{2,1}] & [\mathrm{D}_3] &\equiv [\mathbf{N}_{m,1}]^{\mathrm{T}} [\mathbf{N}_{m,2}] + [\mathbf{N}_{m,2}]^{\mathrm{T}} [\mathbf{N}_{m,1}] &&= [\mathrm{D}_3]^{\mathrm{T}}.
\end{aligned} \tag{167}
$$

Integration over the undeformed volume reduces to:

$$
\int_V \ldots \mathrm{d}V = d \int_A \ldots \mathrm{d}A \tag{168}
$$

with d the thickness in the undeformed configuration and where the integration takes place over the undeformed area.

3D

In three-dimensional problems, the Green-Lagrange strain tensor consists of six independent components, such that $a, b = 1, 2, ..., 6$ and:

$$
\begin{aligned}
[\mathbf{B}_1] &\equiv [\mathbf{N}_{1,1}] & [\mathrm{D}_1] &\equiv [\mathbf{N}_{m,1}]^{\mathrm{T}} [\mathbf{N}_{m,1}] & &= [\mathrm{D}_1]^{\mathrm{T}} \\
[\mathbf{B}_2] &\equiv [\mathbf{N}_{2,2}] & [\mathrm{D}_2] &\equiv [\mathbf{N}_{m,2}]^{\mathrm{T}} [\mathbf{N}_{m,2}] & &= [\mathrm{D}_2]^{\mathrm{T}} \\
[\mathbf{B}_3] &\equiv [\mathbf{N}_{3,3}] & [\mathrm{D}_3] &\equiv [\mathbf{N}_{m,3}]^{\mathrm{T}} [\mathbf{N}_{m,3}] & &= [\mathrm{D}_3]^{\mathrm{T}} \\
[\mathbf{B}_4] &\equiv [\mathbf{N}_{2,3}] + [\mathbf{N}_{3,2}] & [\mathrm{D}_4] &\equiv [\mathbf{N}_{m,2}]^{\mathrm{T}} [\mathbf{N}_{m,3}] + [\mathbf{N}_{m,3}]^{\mathrm{T}} [\mathbf{N}_{m,2}] &&= [\mathrm{D}_4]^{\mathrm{T}} \\
[\mathbf{B}_5] &\equiv [\mathbf{N}_{3,1}] + [\mathbf{N}_{1,3}] & [\mathrm{D}_5] &\equiv [\mathbf{N}_{m,3}]^{\mathrm{T}} [\mathbf{N}_{m,1}] + [\mathbf{N}_{m,1}]^{\mathrm{T}} [\mathbf{N}_{m,3}] &&= [\mathrm{D}_5]^{\mathrm{T}} \\
[\mathbf{B}_6] &\equiv [\mathbf{N}_{1,2}] + [\mathbf{N}_{2,1}] & [\mathrm{D}_6] &\equiv [\mathbf{N}_{m,1}]^{\mathrm{T}} [\mathbf{N}_{m,2}] + [\mathbf{N}_{m,2}]^{\mathrm{T}} [\mathbf{N}_{m,1}] &&= [\mathrm{D}_6]^{\mathrm{T}}.
\end{aligned} \tag{169}
$$

Appendix D – Internal load vector and tangent stiffness matrix transformation in the nonlinear floating frame formulation

The internal load vector and stiffness matrix transformation used in the nonlinear floating frame formulation is given by:

$$\boxed{\begin{array}{l}\boxed{\begin{array}{l}\{Q^o\} = [\overline{\mathrm{R}}_j^o][\mathcal{T}]^{\mathrm{T}}\{Q^j\} \\ [\mathrm{K}_t^o] = [\overline{\mathrm{R}}_j^o]\left([\mathrm{K}_1^j] + [\mathrm{K}_2^j] + [\mathrm{K}_3^j]\right)[\overline{\mathrm{R}}_o^j]\end{array}} \\ [\mathrm{K}_1^j] \equiv [\mathcal{T}]^{\mathrm{T}}[\mathrm{K}_t^j][\mathcal{T}]; \qquad [\mathrm{K}_2^j] \equiv -[\mathcal{Z}]^{\mathrm{T}}[\widehat{\mathrm{F}}^j]^{\mathrm{T}}[\mathcal{T}]; \qquad [\mathrm{K}_3^j] \equiv -[\widehat{\mathrm{F}}^j][\mathcal{Z}]\end{array}} \tag{170}$$

1D

In one-dimensional problems, the projected internal load matrix is given by:

$$[\widehat{\mathrm{F}}^j] = \begin{bmatrix} 0 \\ \vdots \\ 0 \end{bmatrix}. \tag{171}$$

2D

In two-dimensional problems, the projected internal load matrix is given by:

$$[\widehat{\mathrm{F}}^j] = \begin{bmatrix} 0 & 0 & \widehat{\mathrm{F}}_{1y}^j \\ 0 & 0 & -\widehat{\mathrm{F}}_{1x}^j \\ & \vdots & \\ 0 & 0 & \widehat{\mathrm{F}}_{Ny}^j \\ 0 & 0 & -\widehat{\mathrm{F}}_{Nx}^j \end{bmatrix} \qquad \{\widehat{Q}^j\} \equiv [\mathcal{T}]^{\mathrm{T}}\{Q^j\} \equiv \begin{Bmatrix} \widehat{F}_{1x}^j \\ \widehat{F}_{1y}^j \\ \vdots \\ \widehat{F}_{Nx}^j \\ \widehat{F}_{Ny}^j \end{Bmatrix}. \tag{172}$$

3D

In three-dimensional problems, the projected internal load matrix is given by:

$$[\widehat{\mathrm{F}}^j] = \begin{bmatrix} \mathbf{0} & \widetilde{\widehat{\boldsymbol{F}}}_1^j \\ & \vdots \\ \mathbf{0} & \widetilde{\widehat{\boldsymbol{F}}}_N^j \end{bmatrix} \qquad \{\widehat{Q}^j\} \equiv [\mathcal{T}]^{\mathrm{T}}\{Q^j\} \equiv \begin{Bmatrix} \widehat{\boldsymbol{F}}_1^j \\ \vdots \\ \widehat{\boldsymbol{F}}_N^j \end{Bmatrix}. \tag{173}$$

Appendix E – Interpolation functions

1D – 2-node bar element

For a 2-node bar element, the interpolation functions are given by:

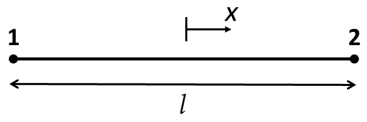

$$N_1(x) = \frac{1}{2}\left(1 - \frac{2x}{l}\right)$$
$$N_2(x) = \frac{1}{2}\left(1 + \frac{2x}{l}\right)$$

2D – Rectangular 4-node quadrilateral element

For a rectangular 4-node quadrilateral element, the interpolation functions are given by:

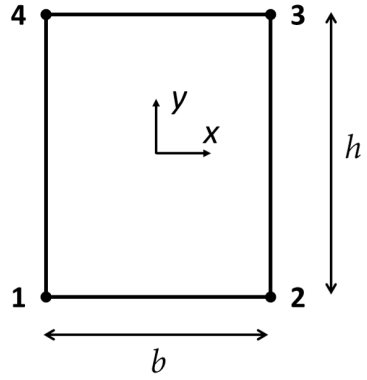

$$N_1(x,y) = \frac{1}{4}\left(1 - \frac{2x}{b}\right)\left(1 - \frac{2y}{h}\right)$$
$$N_2(x,y) = \frac{1}{4}\left(1 + \frac{2x}{b}\right)\left(1 - \frac{2y}{h}\right)$$
$$N_3(x,y) = \frac{1}{4}\left(1 + \frac{2x}{b}\right)\left(1 + \frac{2y}{h}\right)$$
$$N_4(x,y) = \frac{1}{4}\left(1 - \frac{2x}{b}\right)\left(1 + \frac{2y}{h}\right)$$

2D – Rectangular 8-node quadrilateral element

For a rectangular 4-node quadrilateral element, the interpolation functions are given by:

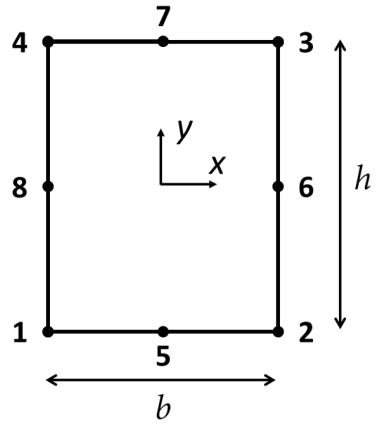

$$N_1(x,y) = \frac{1}{4}\left(1 - \frac{2x}{b}\right)\left(1 - \frac{2y}{h}\right)\left(-\frac{2x}{b} - \frac{2y}{h} - 1\right)$$
$$N_2(x,y) = \frac{1}{4}\left(1 + \frac{2x}{b}\right)\left(1 - \frac{2y}{h}\right)\left(\frac{2x}{b} - \frac{2y}{h} - 1\right)$$
$$N_3(x,y) = \frac{1}{4}\left(1 + \frac{2x}{b}\right)\left(1 + \frac{2y}{h}\right)\left(\frac{2x}{b} + \frac{2y}{h} - 1\right)$$
$$N_4(x,y) = \frac{1}{4}\left(1 - \frac{2x}{b}\right)\left(1 + \frac{2y}{h}\right)\left(-\frac{2x}{b} + \frac{2y}{h} - 1\right)$$
$$N_5(x,y) = \frac{1}{2}\left(1 - \frac{2y}{h}\right)\left(1 + \frac{2x}{b}\right)\left(1 - \frac{2x}{b}\right)$$
$$N_6(x,y) = \frac{1}{2}\left(1 + \frac{2x}{b}\right)\left(1 + \frac{2y}{h}\right)\left(1 - \frac{2y}{h}\right)$$
$$N_7(x,y) = \frac{1}{2}\left(1 + \frac{2y}{h}\right)\left(1 + \frac{2x}{b}\right)\left(1 - \frac{2x}{b}\right)$$
$$N_8(x,y) = \frac{1}{2}\left(1 - \frac{2x}{b}\right)\left(1 + \frac{2y}{h}\right)\left(1 - \frac{2y}{h}\right)$$

3D – Rectangular 8-node hexahedral element

For a rectangular 8-node hexahedral element, the interpolation functions are given by:

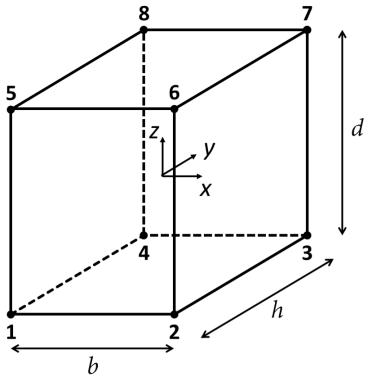

$$N_1(x,y,z) = \frac{1}{8}\left(1-\frac{2x}{b}\right)\left(1-\frac{2y}{h}\right)\left(1-\frac{2z}{d}\right)$$
$$N_2(x,y,z) = \frac{1}{8}\left(1+\frac{2x}{b}\right)\left(1-\frac{2y}{h}\right)\left(1-\frac{2z}{d}\right)$$
$$N_3(x,y,z) = \frac{1}{8}\left(1+\frac{2x}{b}\right)\left(1+\frac{2y}{h}\right)\left(1-\frac{2z}{d}\right)$$
$$N_4(x,y,z) = \frac{1}{8}\left(1-\frac{2x}{b}\right)\left(1+\frac{2y}{h}\right)\left(1-\frac{2z}{d}\right)$$
$$N_5(x,y,z) = \frac{1}{8}\left(1-\frac{2x}{b}\right)\left(1-\frac{2y}{h}\right)\left(1+\frac{2z}{d}\right)$$
$$N_6(x,y,z) = \frac{1}{8}\left(1+\frac{2x}{b}\right)\left(1-\frac{2y}{h}\right)\left(1+\frac{2z}{d}\right)$$
$$N_7(x,y,z) = \frac{1}{8}\left(1+\frac{2x}{b}\right)\left(1+\frac{2y}{h}\right)\left(1+\frac{2z}{d}\right)$$
$$N_8(x,y,z) = \frac{1}{8}\left(1-\frac{2x}{b}\right)\left(1+\frac{2y}{h}\right)\left(1+\frac{2z}{d}\right)$$

Appendix F – Elasticity marix for isotropic material behaviour

1D – Uniaxial stress

In one-dimensional uniaxial stress situations, the elasticity matrix reduces to the scalar Young's modulus E.

2D – Plane stress

In two-dimensional plane stress situations, the elasticity matrix for isotropic material behaviour is given by:

$$[\mathrm{E}] = \frac{E}{1-\nu^2}\begin{bmatrix} 1 & \nu & 0 \\ \nu & 1 & 0 \\ 0 & 0 & \frac{1-\nu}{2} \end{bmatrix} \tag{174}$$

with E the Young's modulus and ν the Poisson ratio.

3D

In three-dimensional situations, the elasticity matrix for isotropic material behaviour is given by:

$$[\mathrm{E}] = \begin{bmatrix} 2\mu+\lambda & \lambda & \lambda & 0 & 0 & 0 \\ \lambda & 2\mu+\lambda & \lambda & 0 & 0 & 0 \\ \lambda & \lambda & 2\mu+\lambda & 0 & 0 & 0 \\ 0 & 0 & 0 & \mu & 0 & 0 \\ 0 & 0 & 0 & 0 & \mu & 0 \\ 0 & 0 & 0 & 0 & 0 & \mu \end{bmatrix} \tag{175}$$

with

$$\begin{aligned} \mu &= \frac{E}{2\,(1+\nu)} = G \\ \lambda &= \frac{\nu E}{(1+\nu)\,(1-2\nu)} \end{aligned} \tag{176}$$

Lamé's constants and E, G and ν the Young's modulus, shear modulus and Poisson ratio respectively.

Appendix G – Further generalisation of the superelement formulation

The generalised superelement formulation as presented in Chapter 3 requires the reduction basis to be able to describe the local nodal degrees of freedom of the interface points independently. The superelement formulation can be further generalised to make it suitable for reduction bases with which an arbitrary number of local nodal degrees of freedom of the interface points can be described independently. This requires the formulation of the equations of motion in terms of only the independent global nodal degrees of freedom of the interface points and a set of internal flexible coordinates, as well as the formulation of constraints that relate the dependent global nodal degrees of freedom of the interface points to the independent global nodal degrees of freedom of the interface points. A brief account of how this formulation can be obtained is provided here.

First of all, a distinction is made between the independent and dependent local nodal degrees of freedom of the interface points. The independent local nodal degrees of freedom of the interface points $\boldsymbol{q}_{IPi}^{j,j}$ correspond to the subspace of local nodal degrees of freedom of the interface points that is spanned by the reduction basis and the number of independent local nodal degrees of freedom of the interface points equals the rank of the interface partitioning of the reduction basis. The dependent local nodal degrees of freedom of the interface points $\boldsymbol{q}_{IPd}^{j,j}$ are the remaining local nodal degrees of freedom of the interface points. Similarly, a distinction is made between the independent global nodal degrees of freedom of the interface points $\boldsymbol{q}_{IPi}^{o,o}$ and the dependent global nodal degrees of freedom of the interface points $\boldsymbol{q}_{IPd}^{o,o}$.

The reduction basis is then transformed to an independent boundary reduction basis Ψ and internal reduction basis Υ in a manner analogous to that outlined in Section 3.4, such that the local nodal degrees of freedom are related to the independent local nodal degrees of freedom of the interface points and the internal flexible coordinates as:

$$\boldsymbol{q}^{j,j} = \Psi \boldsymbol{q}_{IPi}^{j,j} + \Upsilon \boldsymbol{\eta}. \tag{177}$$

With this, the equations of motion of a single flexible body in the floating frame formulation can be expressed in terms of the global coordinates of the floating frame, the independent local nodal degrees of freedom of the interface points and the internal flexible coordinates in a manner analogous to that outlined in Section 3.1.

The coordinate transformation can then be derived in a manner similar to that outlined in Section 3.2. To this end, Equation 74 is partitioned as:

$$\begin{Bmatrix} \delta \boldsymbol{q}_{IPd}^{o,o} \\ \delta \boldsymbol{q}_{IPi}^{o,o} \end{Bmatrix} = \begin{bmatrix} \left[\bar{\mathrm{R}}_j^o\right]_{dd} & \left[\bar{\mathrm{R}}_j^o\right]_{di} \\ \left[\bar{\mathrm{R}}_j^o\right]_{id} & \left[\bar{\mathrm{R}}_j^o\right]_{ii} \end{bmatrix} \begin{Bmatrix} \delta \boldsymbol{q}_{IPd}^{j,j} \\ \delta \boldsymbol{q}_{IPi}^{j,j} \end{Bmatrix} + \begin{bmatrix} \left[\bar{\mathrm{R}}_j^o\right]_d \\ \left[\bar{\mathrm{R}}_j^o\right]_i \end{bmatrix} \Phi_r \left[\mathrm{R}_o^j\right] \delta \boldsymbol{q}_j^{o,o}, \tag{178}$$

where the subscripts d and i denote the dependent and independent partitioning of the relevant matrices. The requirement of zero elastic deformation at the location of the floating frame results in:

$$\Psi_{FF} \delta \boldsymbol{q}_{IPi}^{j,j} + \Upsilon_{FF} \delta \boldsymbol{\eta} = \mathbf{0}. \tag{179}$$

The constraints that relate variations in the dependent local nodal degrees of freedom of the interface points to variations in the independent local nodal degrees of freedom of the interface points and variations in the internal flexible coordinates are obtained from Equation 177 as:

$$\delta \boldsymbol{q}_{IPd}^{j,j} = \Psi_d \delta \boldsymbol{q}_{IPi}^{j,j} + \Upsilon_d \delta \boldsymbol{\eta}. \tag{180}$$

Equations 178, 179 and 180 allow the coordinate transformation to be formulated in the form:

$$\boxed{\begin{Bmatrix} \delta \boldsymbol{q}_j^{o,o} \\ \delta \boldsymbol{q}_{IPi}^{j,j} \\ \delta \boldsymbol{\eta} \end{Bmatrix} = \begin{bmatrix} ... & ... \\ ... & ... \\ \mathbf{0} & \mathbf{1} \end{bmatrix} \begin{Bmatrix} \delta \boldsymbol{q}_{IPi}^{o,o} \\ \delta \boldsymbol{\eta} \end{Bmatrix}} \tag{181}$$

and the constraints to be formulated in the form:

$$\boxed{\delta \boldsymbol{q}_{IPd}^{o,o} = ... \delta \boldsymbol{q}_{IPi}^{o,o} + ... \delta \boldsymbol{\eta}}. \tag{182}$$

The coordinate transformation can then be used to derive the equations of motion of a single flexible body in the generalised superelement formulation expressed in terms of the independent global nodal degrees of freedom of the interface points and the internal flexible coordinates, in a manner similar to that outlined in Section 3.3. The constraints can be used to obtain the coupled equations of motion.

Appendix H – Generic Python program for two-dimensional rigid multibody dynamics simulations

A generic Python program for two-dimensional rigid multibody dynamics simulations has been developed. It allows the user to define an arbitrary two-dimensional rigid multibody system and analyse its motion using a graphical user interface.

The coupled equations of motion of a rigid multibody system that are solved by the generic program and the graphical user interface are presented.

Coupled equations of motion of a rigid multibody system

In the traditional floating frame formulation, the coupled equations of motion of a rigid multibody system are given by:

$$\boxed{\begin{bmatrix} \mathrm{M} & C_{\boldsymbol{q}}^{\mathrm{T}} \\ C_{\boldsymbol{q}} & \mathbf{0} \end{bmatrix} \begin{Bmatrix} \ddot{\boldsymbol{q}} \\ \boldsymbol{\lambda} \end{Bmatrix} = \begin{Bmatrix} \boldsymbol{Q}_a \\ \boldsymbol{\gamma} \end{Bmatrix}} \tag{183}$$

The generalised coordinate vector $\boldsymbol{q}$ is assembled from the generalised coordinate vector of the individual bodies as:

$$\boldsymbol{q} = \begin{Bmatrix} \boldsymbol{q}_1 \\ \vdots \\ \boldsymbol{q}_N \end{Bmatrix}, \qquad \boldsymbol{q}_i = \begin{Bmatrix} x_i \\ y_i \\ \theta_i \end{Bmatrix}, \tag{184}$$

with x_i and y_i the absolute horizontal and vertical position of the center of mass of the i^{th} body, θ_i its absolute orientation and N the total number of bodies. The mass matrix M is assembled from the mass matrices of the individual bodies as:

$$\mathrm{M} = \begin{bmatrix} \mathrm{M}_1 & & \\ & \ddots & \\ & & \mathrm{M}_N \end{bmatrix}, \qquad \mathrm{M}_i = \begin{bmatrix} m_i & 0 & 0 \\ 0 & m_i & 0 \\ 0 & 0 & I_i \end{bmatrix}, \tag{185}$$

with m_i the mass of the i^{th} body and I_i the second moment of mass about its center of mass. The external load vector $\boldsymbol{Q}_a$ of externally applied loads is assembled from those of the individual bodies as:

$$\boldsymbol{Q}_a = \begin{Bmatrix} \boldsymbol{Q}_1 \\ \vdots \\ \boldsymbol{Q}_N \end{Bmatrix}, \qquad \boldsymbol{Q}_i = \begin{Bmatrix} F_{xi} \\ F_{yi} \\ M_i \end{Bmatrix}, \tag{186}$$

with F_{xi} and F_{yi} the resultant externally applied force on the i^{th} body in x- and y-direction respectively and M_i the resultant externally applied moment about its center of mass.

The constraint equations that define how the rigid multibody system is constrained are expressed in terms of all generalised coordinates as:

$$C(\boldsymbol{q}) = \mathbf{0} \tag{187}$$

and it holds that:

$$\begin{aligned} C_q \dot{\boldsymbol{q}} &= \boldsymbol{\nu} & \boldsymbol{\nu} &= -C_t \\ C_q \ddot{\boldsymbol{q}} &= \boldsymbol{\gamma} & \boldsymbol{\gamma} &= -\left(\left[C_q \dot{\boldsymbol{q}} \right]_q \dot{\boldsymbol{q}} + 2 C_{qt} \dot{\boldsymbol{q}} + C_{tt} \right), \end{aligned} \tag{188}$$

where the subscripts $\boldsymbol{q}$ and t denote differentiation with respect to the generalised coordinate vector and time respectively.

The vector of Lagrange multipliers $\boldsymbol{\lambda}$ is related to the generalised constraint force vector $\boldsymbol{Q}_c$ as:

$$\boldsymbol{Q}_c = -C_q^{\mathrm{T}} \boldsymbol{\lambda} \tag{189}$$

and the constraint loads at a point A on body i can be obtained from the Lagrange multipliers as:

$$\begin{aligned} F_{Ax} &= -C_{A,x_i}^{\mathrm{T}} \boldsymbol{\lambda}_A \\ F_{Ay} &= -C_{A,y_i}^{\mathrm{T}} \boldsymbol{\lambda}_A \\ M_A &= \left(-y_A^i C_{A,x_i}^{\mathrm{T}} + x_A^i C_{A,y_i}^{\mathrm{T}} - C_{A,\theta_i}^{\mathrm{T}} \right) \boldsymbol{\lambda}_A, \end{aligned} \tag{190}$$

where C_A and $\boldsymbol{\lambda}_A$ denote the constraint equations and Lagrange multipliers that are related to the constraints at point A, the subscripts $,x_i$, $,y_i$ and $,\theta_i$ denote differentiation with respect to the generalised coordinates of body i and x_A^i and y_A^i denote the absolute horizontal and vertical position of point A relative to the center of mass of body i.

Graphical User Interface

The graphical user interface for defining the rigid multibody system is presented in Figure 30. It allows the user to create bodies, define constraints and apply loads using the buttons in the control panel. Additionally, gravity can be turned on or off and the independent generalised coordinates and desired simulation time can be specified. The visualisation window allows the user to (automatically) zoom and pan.

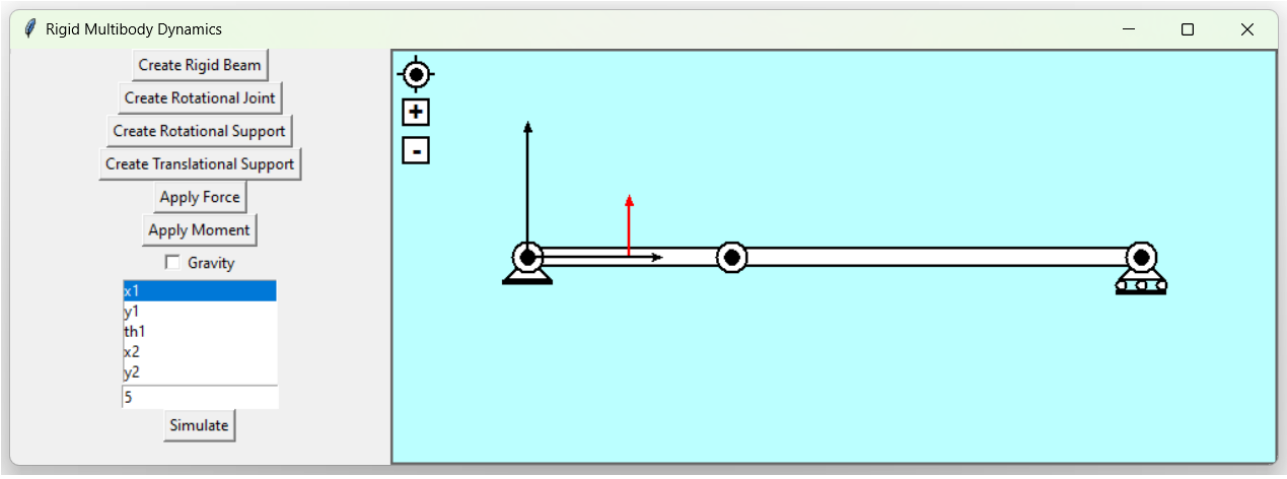

Figure 30: Graphical user interface – Defining the rigid multibody system

The properties of the bodies, constraints and loads can be specified in the settings window that is opened by double clicking the component. Several settings windows are presented in Figure 31.

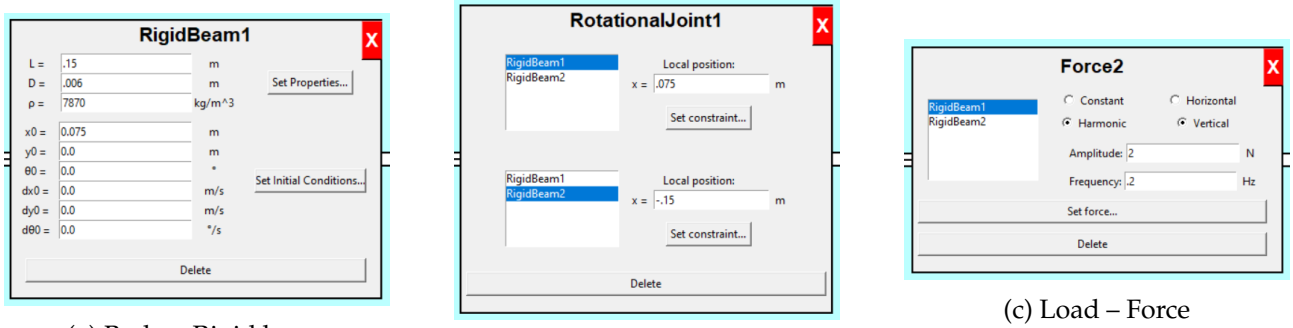

(a) Body – Rigid beam

(b) Constraint – Rotational joint

(c) Load – Force

Figure 31: Settings windows

Once the rigid multibody system has been defined, its motion can be simulated by clicking the *Simulate* button in the control panel. The coupled equations of motion of the defined rigid multibody system are then solved by the program.

After the simulation is completed, the graphical user interface for analysing the motion of the rigid multibody system appears. This is illustrated in Figure 32. The motion of the rigid multibody system over time can be visualised by clicking the *Play* button in the control panel. The motion can also be paused and resumed and the playback rate can be specified to speed up or slow down the animation. The motion can be analysed in more detail using the slider or the + or - button that switches to the next or previous time increment.

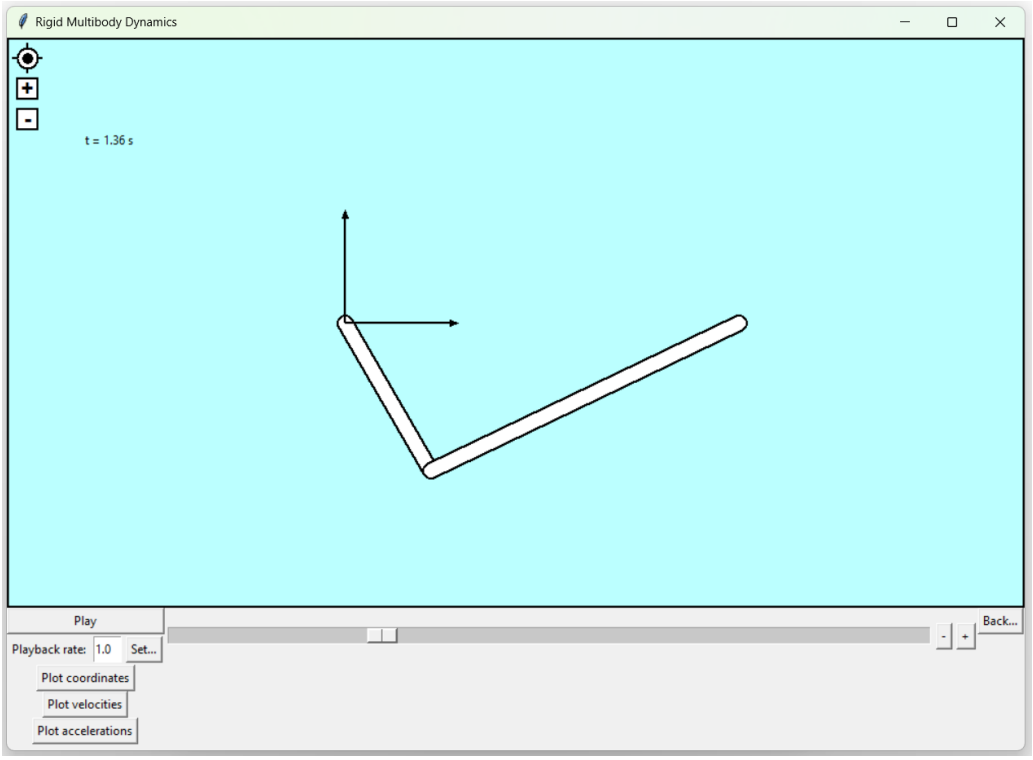

Figure 32: Graphical user interface – Analysing the motion of the rigid multibody system

The generalised coordinates, velocities and accelerations can be plotted as a function of time by clicking the corresponding buttons. The window that appears for plotting the coordinates is presented in

Figure 33.

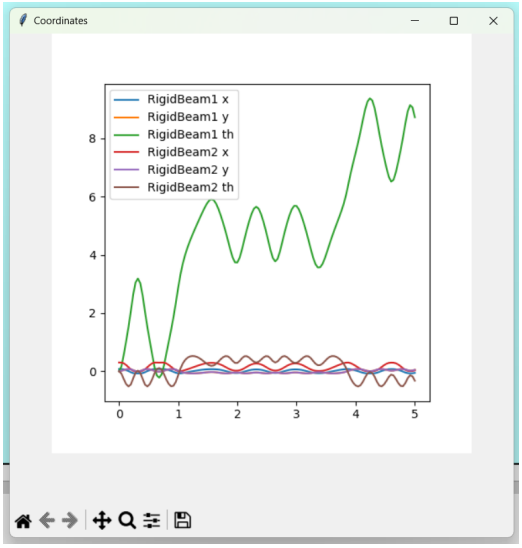

Figure 33: Plotting window – Coordinates